The Dissertation Committee for Arian Vistamehr Certifies that this is the approved version of the following dissertation:

Understanding Dynamic Balance during Walking Using Whole-body Angular Momentum

Committee:

Richard R. Neptune, Supervisor

Ronald E. Barr

Lawrence D. Abraham

Ashish D. Deshpande

Steven A. Kautz

Understanding Dynamic Balance during Walking Using Whole-body Angular Momentum

by

Arian Vistamehr, B.S.; M.S.

Dissertation

Presented to the Faculty of the Graduate School of

The University of Texas at Austin

in Partial Fulfillment

of the Requirements

for the Degree of

Doctor of Philosophy

The University of Texas at Austin

August 2014

Dedication

I dedicate my dissertation to Dr. Ganjavian, M.D.,
who has been my source of inspiration throughout my Ph.D. training. I would also like to dedicate this dissertation to all the interested readers in the biomechanics community.
May this work be a step towards balanced walking.

Acknowledgements

I would like to thank Dr. Rick Neptune for being my adviser and guiding me patiently as I grew throughout the years of my Ph.D. training. I thank him for believing in me and for pushing me beyond my limits. I cannot be more grateful for the opportunity of working on many challenging projects and for his constructive feedback throughout. Finally, I thank him for creating a collaborative environment. I thank all the members of the Neuromuscular Biomechanics Lab for their constant support and encouragement in critical times.

I would like to thank Dr. Steve Kautz for his insightful comments, which have always improved the quality of my work. I also thank all the members of the Locomotor Energetics and Assessment Lab in the Center for Rehabilitation Research in Neurological Conditions at the Medical University of South Carolina for their assistance with data collection.

I thank Dr. Larry Abraham, Dr. Ronald Barr, and Dr. Ashish Deshpande for serving on my dissertation committee. I also acknowledge the American Heart Association for the Southwest Affiliated Pre-doctoral Fellowship, which partially supported this research.

I would like to acknowledge my family for their unconditional love, support, encouragement and for always cheering for me regardless of the situation. Finally, I would like to thank my best friend and fiancé, John Kimla for his patience, understanding, love and continuous support throughout my education.

Understanding Dynamic Balance during Walking Using Whole-body Angular Momentum

Arian Vistamehr, Ph.D.

The University of Texas at Austin, 2014

Supervisor: Richard R. Neptune

Maintaining dynamic balance during walking is a major challenge in many patient populations including older adults and post-stroke hemiparetic subjects. To maintain dynamic balance, whole-body angular-momentum has to be regulated through proper foot placement and generation of the ground-reaction-forces. Thus, the overall goal of this research was to understand the mechanisms and adaptations used to maintain dynamic balance during walking by analyzing whole-body angular-momentum, foot placement and ground-reaction-forces in older adults and post-stroke subjects.

The analysis of healthy older adults showed that they regulated their frontal-plane angular-momentum poorly compared to the younger adults. This was mainly related to the increased step width, which when combined with the dominant vertical ground-reaction-force, created a higher destabilizing external moment during single-leg stance. The results also suggested that exercise programs targeting appropriate foot placement and lower extremity muscle strengthening, particularly of the ankle plantarflexors and hip abductors, may enhance balance control in older adults.

During post-stroke hemiparetic walking, ankle-foot-orthosis and locomotor therapy are used in an effort to improve the overall mobility. However, the analyses of healthy subjects walking with and without a solid ankle-foot-orthosis showed that they

can restrict ankle plantarflexor output and limit the successful regulation of angular-momentum and generation of forward propulsion. Thus, the prescription of solid ankle-foot-orthosis should be carefully considered. The analysis of hemiparetic subjects walking pre- and post-therapy showed that locomotor training did not improve dynamic balance. However, for those subjects who achieved a clinically meaningful improvement in their self-selected walking speed, their change in speed was correlated with improved dynamic balance. Also, improved balance was associated with narrower mediolateral paretic foot placement, longer anterior nonparetic steps, higher braking ground-reaction-force peaks and impulses, higher (lower) propulsive ground-reaction-force peaks and impulses from the paretic (nonparetic) leg, and higher vertical ground-reaction-force impulses from both legs during the late stance. Further, simulation analyses of hemiparetic walking highlighted the importance of ankle plantarflexors, knee extensors and hip abductors in maintaining balance and revealed the existence of compensatory mechanisms due to the paretic leg muscle weakness. Collectively, these studies showed the importance of ankle plantarflexors and hip abductors in maintaining dynamic balance.

Table of Contents

List of Tables

List of Figures

Chapter 1: Introduction

Maintaining dynamic balance during walking is a major challenge in many patient populations including older adults and post-stroke hemiparetic subjects. Approximately one third of the older adults fall each year (Centers for Disease Control & Prevention, 2008) and at least 50% of stroke survivors experience falls within one year post-stroke (e.g., Ashburn et al., 2008; Sackley et al., 2008). Falls can lead to serious musculoskeletal injuries and reduced physical activity (e.g., Schmid et al., 2009). Therefore, it is important to assess dynamic balance using quantitative methods to detect and treat balance disorders.

Previous studies have used whole-body angular momentum to investigate dynamic balance during human movement, which is thought to be highly regulated by the central nervous system (Robert et al., 2009). This mechanics-based measure of body rotation about the center-of-mass (CoM) is obtained using the sum of all body segments angular momenta with respect to the CoM. Although each segment can have a large angular momentum, the sum is kept low through segment-to-segment cancellations (e.g., Herr and Popovic, 2008). However, in the presence of perturbations, the range (minimum to maximum) of angular momentum increases (e.g., Martelli et al., 2013). In order to maintain balance, angular momentum has to be regulated by proper foot placement and generation of ground-reaction-forces (GRFs) (e.g., Pijnappels et al., 2005a). The regulation of angular momentum is often quantified using the time rate of change of angular momentum, which is equal to the net external moment created by the GRFs about the body CoM. The net external moment is calculated using the cross product of the moment arm vector (from the CoM to each foot center-of-pressure, CoP) and the GRF vector. This quantity can provide insight into how adaptations in the GRFs and foot placement influence dynamic balance. A recent study has shown that the time rate of change of angular momentum in the frontal plane was negatively correlated with

commonly used clinical balance measures such as the Berg Balance Scale and Dynamic Gait Index in post-stroke subjects (Nott et al., 2013). Thus, a high rate of change of angular momentum was associated with a poor balance score. Although clinical balance scores can provide some insight into balance disorders, they do not provide insight into mechanisms used to regulate angular momentum (e.g., adaptations in the GRFs and foot placement).

Previous studies have analyzed angular momentum to understand dynamic balance in lower-limb amputees (Silverman and Neptune, 2011), children with cerebral palsy (Bruijn et al., 2011), post-stoke hemiparetic subjects (Nott et al., 2013) and subjects with bilateral vestibular hypofunction (Kaya et al., 1998) during walking. Other studies have investigated angular momentum in older adults during recovery after tripping (e.g., Pijnappels et al., 2005b) and in younger healthy adults during unexpected unilateral perturbations (Martelli et al., 2013) and during stair ascent and descent (Silverman et al., 2014). In addition, muscle-driven forward dynamic simulation studies of healthy adults during walking have identified individual muscle contributions to the regulation of angular momentum (Neptune and McGowan, 2011; Neptune and McGowan, 2013). However, no study has analyzed angular momentum to assess dynamic balance in healthy older adults during steady-state walking. Thus, it is not clear whether older adults regulate their angular momentum differently than younger adults. This information may assist in understanding the high rate of falls in older adults and may suggest preventative measures. Therefore, the goal of the study in Chapter 2 was to compare the angular momentum profiles and external moment components in the frontal and sagittal planes between healthy younger and older adults walking at similar steady-state speeds.

Post-stroke subjects are also susceptible to falling, with a gait pattern that is characterized by a slow walking speed, gait asymmetry and foot drop (Olney, 1996).

Thus, therapeutic interventions (e.g., orthotic devices and locomotor rehabilitation therapy) aim to improve overall mobility post-stroke. The most commonly prescribed orthotic devices in post-stroke subjects are ankle foot orthoses (AFOs), primarily to correct foot drop during swing. However, it is not clear how AFOs influence the execution of fundamental walking tasks such as body support and forward propulsion as well as maintaining dynamic balance. Given the wide spread use of AFOs, it is important to understand if AFOs enhance or hinder overall mobility. Thus, the goal of the study in Chapter 3 was to assess the influence of solid polypropylene AFOs on forward propulsion and dynamic balance in healthy subjects during steady-state, accelerated and decelerated walking conditions. Assessing the influence of AFOs on healthy subjects' walking mechanics will provide a baseline for comparison with hemiparetic subjects, which collectively can provide clinicians with quantitative rationale as to whether AFOs improve paretic leg impairments and overall walking mobility.

In addition to orthotic devices, locomotor therapy has also been a fundamental element of rehabilitation interventions aimed at improving walking speed, balance and overall mobility. Locomotor training is based on the task-specific repetitive treatment concept in post-stroke rehabilitation (Hesse et al., 1994) with a number of studies reporting improved walking speed in post-stroke patients (e.g., Hesse, 2008; Peurala et al., 2005; Visintin et al., 1998). However, to date no study has investigated angular momentum following locomotor therapy to assess whether the regulation of the whole-body angular momentum is improved. Also, it is not clear if clinically meaningful increases in walking speed after locomotor training are correlated with improved dynamic balance. Thus, the goal of the study in Chapter 4 was to assess the influence of a 12-week locomotor training program (Bowden et al., 2013) on dynamic balance in post-stroke hemiparetic subjects and to determine if clinically meaningful increases in self-

selected walking speed were correlated with improved dynamic balance. Further, angular momentum is primarily regulated by muscle forces through the generation of GRFs, which create an external moment about the body CoM and control the whole-body angular momentum. Although previous simulation analyses of walking have identified the primary muscle groups (e.g., the plantarflexors) regulating angular momentum in healthy adults (Neptune and McGowan, 2011; Neptune et al., 2011), it is still unclear which muscles are the primary regulators of whole-body angular momentum during post-stroke hemiparetic gait. Also, it is unknown if therapy alters the individual muscles used to regulate angular momentum post-therapy. Thus, the goal of the study in Chapter 5 was to identify the primary muscle contributors to the regulation of whole-body angular momentum in post-stroke subjects using simulation analyses of hemiparetic walking and to investigate if therapy influenced these contributions pre- to post-therapy.

Understanding the mechanisms used to maintain dynamic balance has important implications for improving the design of therapeutic interventions and ultimately decrease the rate of falls. Therefore, the overall goal of this research was to understand the walking mechanisms and adaptations used to maintain dynamic balance by analyzing whole-body angular momentum in populations that are susceptible to falls including older adults and post-stroke subjects.

Chapter 2: Differences in Whole-body Angular Momentum between Healthy Younger and Older Adults during Steady-State Walking

Introduction

Each year approximately one third of older adults fall, which leads to extensive musculoskeletal injuries and functional disabilities (Centers for Disease Control & Prevention, 2008). A major concern and cause of death in the elderly is hip fracture (Deprey, 2009; Kung et al., 2008), which is associated with the lack of balance control in the mediolateral direction (Greenspan et al., 1998). Previous work has shown that dynamic balance may be maintained passively in the sagittal-plane, but active control is needed to stabilize lateral motion (Bauby and Kuo, 2000). Foot placement is a common strategy for controlling lateral balance (e.g., Hof et al., 2010). Previous studies have suggested that wider steps are used to increase lateral stability (Bauby and Kuo, 2000; Dean et al., 2007; Donelan et al., 2004; Gabell and Nayak, 1984) and some have observed that elderly fallers take narrower steps (Guimaraes and Isaacs, 1980). Others have associated wider steps with increased step width variability and increased instability (McAndrew Young and Dingwell, 2012) while some have observed higher rate of falls in subjects with wider steps (Gehlsen and Whaley, 1990; Maki, 1997; Moe-Nilssen and Helbostad, 2005; Nelson et al., 1999). Thus, the underlying mechanics for maintaining dynamic balance during walking in older adults is not well understood.

Whole-body angular momentum (H), a mechanics-based measure, has been used to investigate balance control in younger and older healthy adults recovering from a trip (Pijnappels et al., 2005b), healthy subjects during incline/decline walking (Silverman et al., 2012), and lower-limb amputees (Silverman and Neptune, 2011) and children with cerebral palsy (Bruijn et al., 2011) walking overground. A recent study observed a negative correlation between the frontal-plane angular momentum and two commonly used clinical measures (Dynamic Gait Index and Berg Balance Scale) in post-stroke subjects (Nott et al., 2013). They found that higher clinical scores were associated with a

lower range of frontal-plane angular momentum. The same study compared the frontal-plane angular momentum between post-stroke and healthy subjects and found that healthy subjects showed a timely regulation of angular momentum at the beginning of single-leg stance, while the post-stroke subjects had a poor regulation of angular momentum during early paretic single-leg stance.

The appropriate regulation of whole-body angular momentum is essential for maintaining dynamic balance during walking (e.g., Herr and Popovic, 2008) and can be quantified by analyzing the time rate of change of angular momentum about the body's center-of-mass (*CoM*), which is equivalent to the net external moment (i.e., the cross-product of the ground reaction force (*GRF*) vector and moment arm vector from the body *CoM* to center-of-pressure (*CoP*)). Identifying the changes in *GRFs* and moment arms (i.e. foot placement) can provide insight into the underlying mechanisms for maintaining balance (e.g., Silverman and Neptune, 2011). However, no study has analyzed the external moment components (i.e., *GRFs* and moment arms) to identify potential mechanisms leading to dynamic balance disorders in older adults.

Thus, the purpose of this study was to compare the angular momentum profiles and external moment components (i.e., *GRFs* and moment arms) in the frontal- and sagittal-planes between healthy younger and older adults walking at similar steady-state speeds. Further, to help interpret any observed differences, changes in the net intersegmental joint moments were investigated. We analyzed these quantities at two different speeds (self-selected and fastest-comfortable walking speeds for the older adults) to highlight any differences in walking strategies (e.g., foot placement and *GRFs*) between age groups that may arise due to differences in walking speed. We hypothesized that the range of H would increase in older adults due to differences in foot placement and GRFs that may occur with age.

Methods

Ten healthy young subjects (age: 27.3 ± 2.8 years; mass: 72.6 ± 10.2 kg; height: 1.75 ± 0.1 m) walked on an instrumented treadmill at 0.6 m/s and 1.2 m/s. From an existing database, we identified ten healthy older subjects (age: 56.1 ± 8.8 years; mass: 85.6 ± 13.3 kg; height: 1.72 ± 0.1m) who walked at their self-selected (0.62 ± 0.15 m/s) and fastest-comfortable (1.4 ± 0.3 m/s) speeds. In both data sets, three 30-second trials were collected for each subject using the same equipment. The study protocol and consent form were approved by an Institutional Review Board and all participants provided written, informed consent prior to study participation.

A 12-camera optical motion capture system (PhaseSpace Inc., San Leandro, CA, USA) was used to record 3D kinematics at 120 Hz from a modified Helen Hayes marker set. 3D *GRF* data were collected at 2000 Hz using an instrumented treadmill (Bertec Corp., Columbus, OH). The kinematic and *GRF* data were smoothed using a fourth-order Savitzky-Golay (Savitzky and Golay, 1964) least-square polynomial smoothing filter and were resampled at 100 Hz before performing an inverse dynamics analysis. A 13-segment model including the head, torso, pelvis, upper arms, lower arms, thighs, shanks and feet was used to determine the joint moments, *CoM* position and velocity as well as the mass and inertial properties of the body segments. At each time step, whole-body angular momentum (*H*) about the *CoM* was calculated as:

$$\vec{H} = \sum_{i=1}^{n} [\ (\vec{r}_i^{COM} - \vec{r}_{body}^{COM}) \times m_i(\vec{v}_i^{COM} - \vec{v}_{body}^{COM}) + I_i\overrightarrow{\omega_i}\ ] \tag{2.1}$$

where $\vec{r}_i^{COM}$, $\vec{v}_i^{COM}$ and $\overrightarrow{\omega_i}$ are the position, velocity, and angular velocity vectors of the i^{th} segment's *CoM*, respectively. $\vec{r}_{body}^{COM}$ and $\vec{v}_{body}^{COM}$ are the position and velocity vectors of the whole-body *CoM*, m_i and I_i are the mass and moment of inertia of each segment and n is the number of segments. H was normalized by the product of body mass, height and $\sqrt{g \cdot l}$, where g = 9.81m/s^2 and l is the subject's height. The $\sqrt{g \cdot l}$ factor has units of m/s and is independent of walking speed. The range of H in each plane was defined as the difference between the maximum and minimum value of H over the entire gait cycle. At each time step, the net external moment (which is equal to the time rate of change of H) was calculated as:

$$\vec{M}_{ext} = \vec{r} \times \overrightarrow{GRF} \tag{2.2}$$

where $\vec{r}$ is the moment arm vector from body *CoM* to *CoP* and $\overrightarrow{GRF}$ is the vector of *GRFs* (Fig. 2.1). Step width was calculated as the difference between the average *CoP* values in the left and right legs in the mediolateral (*M/L*) direction during a successive step. Step length was calculated as the difference in the anterior-posterior (*A/P*) *CoP* values between the two legs at mid-stance, and stride length was obtained by adding two successive step lengths from each foot. Step width, stride length and moment arms were each normalized by subject height.

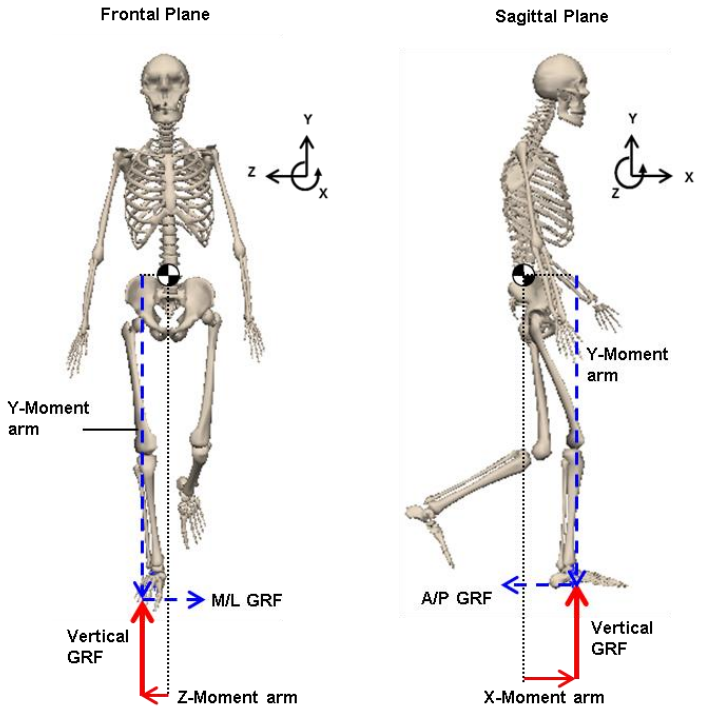

Figure 2.1. The components of net external moment in the frontal- and sagittal-planes during single-leg stance. Whole-body CoM is shown with '◓'. The GRF vectors and their corresponding moment arms appear in the same color. The higher magnitude of the vertical GRF compared to other components (after normalizing moment arms and GRFs by body height and weight, respectively) is highlighted by the line thickness.

To compare dynamic balance between the older and younger adults, the range of *H* and net external moment components (*GRFs* and peak moment arms) were compared within each walking speed using a two-sample t-test with equal variances. A two-way t-test was suitable for this study since the goal was to compare differences in the biomechanical quantities between the age groups at each walking speed. The equality of variances was confirmed using an F-test. Both the *GRF* peaks and impulses were calculated in early and late stance to capture the effects of instantaneous and average changes in the *GRFs* between the age groups. *GRF* impulses were calculated using the

time integral of *GRFs* in early (0-50%) and late (51-100%) stance. Peak hip, knee and ankle intersegmental joint moments were analyzed to further understand observed differences between age groups. *GRFs* and joint moments were normalized by body weight and mass, respectively. Pearson correlation analyses were performed between the range of *H* and the biomechanical quantities. Data for older and younger subjects were combined at each walking speed for the correlation analysis.

Results

Range of angular momentum

The range of frontal-plane *H* was significantly higher in older adults during both the self-selected and fastest-comfortable walking speeds (Fig. 2.2). However, in the sagittal-plane, the range of *H* was not significantly different between the two age groups at either speed.

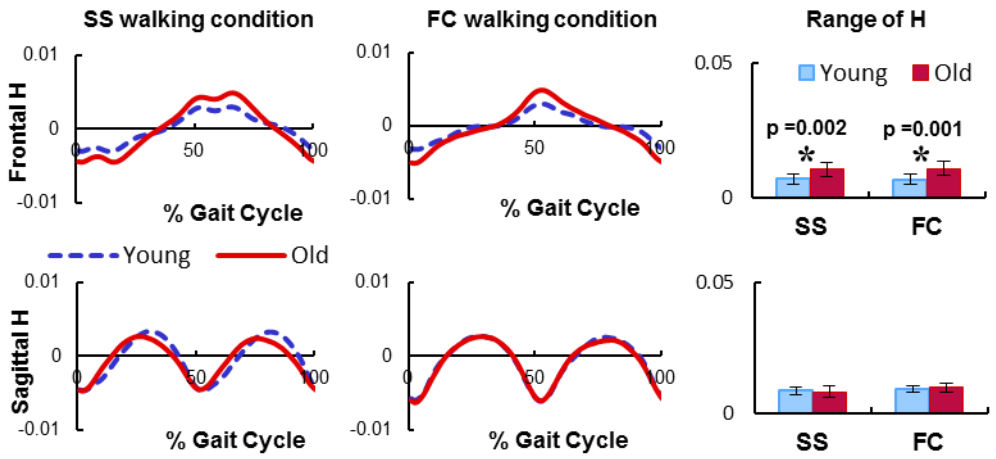

Figure 2.2. Normalized, mean angular momentum (H) in the frontal- and sagittal-planes during the self-selected (SS) and fastest-comfortable (FC) walking speed conditions. The mean (± SD) range of H is shown on the right. Statistically significant differences between the younger and older subjects are indicated with '*' ($p < 0.05$).

Biomechanical quantities - frontal-plane

During the self-selected walking condition, of the components that contribute to the frontal-plane net external moment (i.e., Y- and Z- moment arms, vertical and *M/L GRFs*), the peak *M/L GRF* and Z-moment arm (*M/L*) were significantly greater in the older adults (Fig. 2.3). In addition, the normalized step width in the older adults (0.15 ± 0.02) was significantly wider ($p = 0.001$) compared to the younger adults (0.11 ± 0.02). Although there were no differences in the peak vertical *GRF*, the vertical *GRF* impulses were significantly lower in the older adults (Fig. 2.3). The range of frontal-plane *H* was correlated with the first ($r = 0.57$, $p = 0.009$) and second ($r = 0.63$, $p = 0.003$) peak *M/L GRFs*, the peak Z-moment arm ($r = 0.44$, $p = 0.05$) and step width ($r = 0.70$, $p < 0.001$). Also, the range of frontal-plane *H* was inversely correlated with the vertical *GRF*

impulses in early (r = -0.64, p = 0.002) and late (r = -0.53, p = 0.02) stance. The range of *H* was also correlated with the *M/L GRF* impulses in early (r = 0.40, p = 0.08) and late (r = 0.52, p = 0.02) stance.

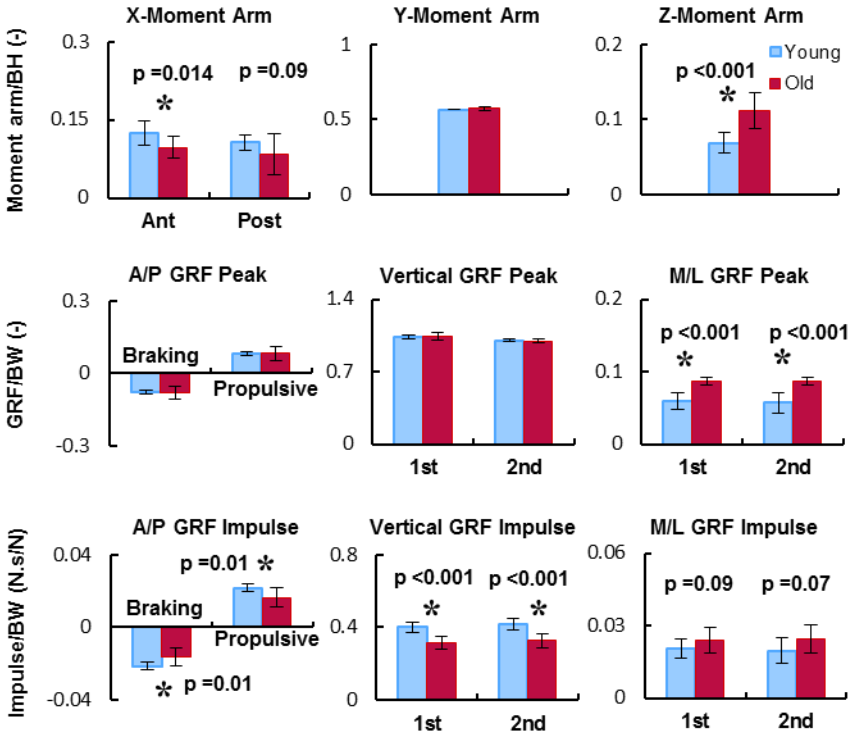

Figure 2.3. Biomechanical quantities during the self-selected walking speed condition. Top row shows the body-height (BH) normalized, mean (± SD) moment arms. The X-moment arm is decomposed into anterior (Ant) and posterior (Post) directions. The Y- and Z- moment arms are in the vertical and M/L directions, respectively. Middle row shows the body weight-normalized (BW), mean (± SD) first and second peak GRFs. Bottom row shows the BW-normalized, mean (± SD) GRF impulses during early and late stance. Significant differences between the two age groups are indicated with '*' ($p < 0.05$).

During the fastest-comfortable walking condition, there were similar trends between the age groups as in the self-selected walking condition (Fig. 2.4). The step width in older adults (0.14 ± 0.02) was significantly wider ($p < 0.001$) compared to the younger adults (0.10 ± 0.02). Also, both the peak Z-moment arm ($r = 0.47$, $p = 0.036$) and step width ($r = 0.47$, $p = 0.034$) were correlated with the range of frontal-plane *H* during the fastest-comfortable walking condition.

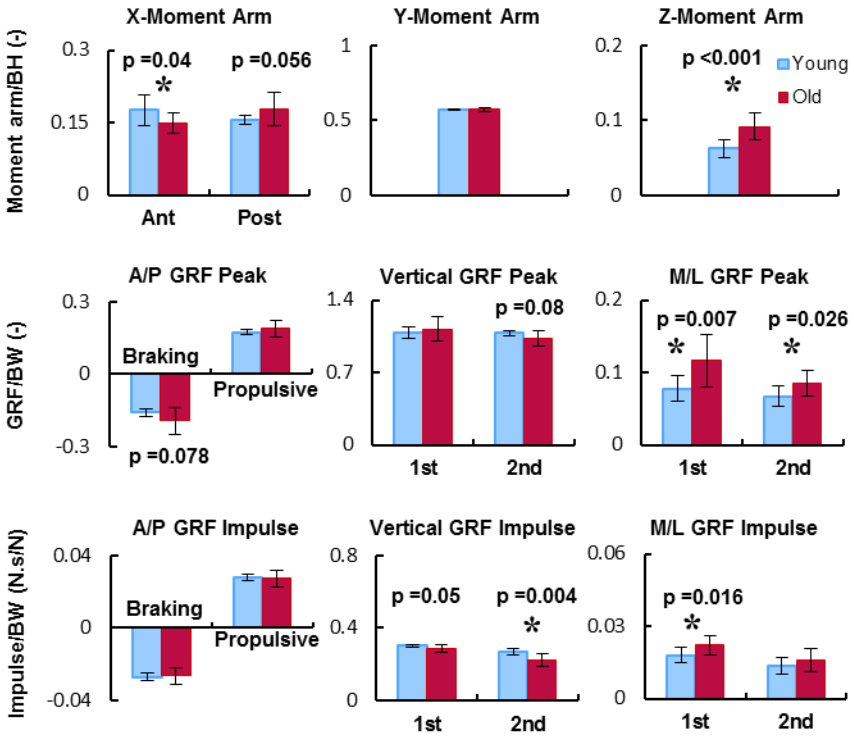

Figure 2.4. Biomechanical quantities during the fastest-comfortable walking speed condition. Top row shows the body-height (BH) normalized, mean (± SD) moment arms. The X-moment arm is decomposed into anterior (Ant) and posterior (Post) directions. The Y- and Z- moment arms are in the vertical and M/L directions, respectively. The middle row shows the body weight (BW)-normalized, mean (± SD) first and second peak GRFs. The bottom row shows the BW-normalized, mean (± SD) GRF impulses during early and late stance. Significant differences between the two age groups are indicated with '*' ($p < 0.05$).

In the frontal-plane joint moments, there were no significant differences in the peak hip abduction moment between the two age groups at the self-selected speed. However, during the fastest-comfortable speed, the second peak hip abduction moment was significantly lower in the older adults (Table 2.1). In addition, the second peak hip abduction moment was inversely correlated ($r = -0.44$, $p = 0.05$) with the range of frontal-plane *H*.

Table 2.1. Mean (±SD) peak intersegmental joint moments, normalized by body mass for old and young subjects. P-values from a two-way t-test between the younger and older subjects are shown within each speed. Significant differences ($p < 0.05$) between the age groups are highlighted in bold ($F_{critical} = 2.98$).

	Slow walking condition				Fast walking condition			
Joint moment	Younger	Older	p-value	F-test	Younger	Older	p-value	F-test
Hip abduction, 1st peak	0.82 (±0.07)	0.82 (±0.08)	0.920	0.81	0.88 (±0.11)	1.03 (±0.20)	0.058	0.89
Hip abduction, 2nd peak	0.75 (±0.07)	0.71 (±0.09)	0.184	0.49	**0.71 (±0.10)**	**0.58 (±0.11)**	**0.011**	0.89
Hip extension peak	0.31 (±0.08)	0.39 (±0.12)	0.092	0.29	**0.70 (±0.08)**	**0.92 (±0.23)**	**0.036**	0.00
Hip flexion peak	0.51 (±0.14)	0.64 (±0.21)	0.110	0.26	0.97 (±0.18)	1.07 (±0.28)	0.350	0.22
Knee extension peak	**0.21 (±0.13)**	**0.34 (±0.14)**	**0.044**	0.88	0.52 (±0.17)	0.75 (±0.33)	0.070	0.06
Knee flexion peak	0.30 (±0.11)	0.31 (±0.09)	0.840	0.54	0.40 (±0.09)	0.51 (±0.22)	0.170	0.01
Ankle plantarflexion peak	**1.32 (±0.15)**	**1.13 (±0.16)**	**0.011**	0.87	1.59 (±0.12)	1.46 (±0.22)	0.140	0.09

Biomechanical quantities - sagittal-plane

During the self-selected walking condition, of the components that contribute to the sagittal-plane net external moment (i.e., X-, Y-moment arms, *A/P* and vertical *GRFs*), the peak X-moment arm in the anterior direction was significantly lower in the older adults (Fig. 2.3). In addition, the normalized stride length was significantly shorter ($p = 0.02$) in the older adults (0.45 ± 0.12) compared to the younger adults (0.55 ± 0.03). There were no differences in the *A/P* or vertical *GRF* peaks. However, the older adults produced significantly lower braking and propulsive impulses as well as lower vertical *GRF* impulses in early and late stance (Fig. 2.3). The correlation between the range of sagittal-plane *H* and the vertical *GRF* impulse during early stance approached significance ($r = 0.42$, $p = 0.06$). There were no other correlations between the range of *H* and any of the external moment components.

During the fastest-comfortable walking condition, there were similar trends between the age groups as in the self-selected walking condition. However, only the peak X-moment arm in the anterior direction was significantly different between the two age groups (Fig. 2.4). The peak X-moment arm in the posterior direction approached significance ($p = 0.056$), while the normalized stride length in the older adults (0.79 ± 0.013) was not significantly different ($p = 0.70$) compared to the younger adults (0.77 ± 0.03). Although there were no significant differences in the peak *A/P GRFs*, sagittal-plane *H* had a negative correlation with the peak braking ($r = -0.56$, $p = 0.01$) and propulsive ($r = -0.41$, $p = 0.07$) *GRFs*.

In the sagittal-plane joint moments, there were significant differences during the self-selected speed, with the older adults having a higher peak knee extensor and a lower plantarflexor moment (Table 2.1). Also, the peak knee extensor moment was inversely correlated ($r = -0.43$, $p = 0.06$) with the range of sagittal-plane *H*. During the fastest-

comfortable speed, the older adults had a higher peak hip and knee extensor moments (Table 2.1). The range of sagittal-plane *H* was inversely correlated with the peak hip ($r = -0.66$, $p = 0.001$) and knee ($r = -0.40$, $p = 0.09$) extensor moments.

Discussion

The purpose of this study was to analyze frontal- and sagittal-plane whole-body angular momentum to gain insight into differences in the mechanics of maintaining dynamic balance between older and younger adults walking at two different speeds. Understanding these differences has the potential to help diagnose and treat balance disorders in older adults. We focused on the frontal- and sagittal-planes as previous studies have shown that the range of angular momentum in the transverse plane is much lower and requires little regulation (Bennett et al., 2010; Herr and Popovic, 2008; Silverman et al., 2012). The older adults had a significantly higher range of frontal-plane *H* than the younger adults at both walking speeds (Fig. 2.2). In the sagittal-plane, there were no differences in the range of *H* between the older and younger adults at either walking speed. Unlike previous studies that observed a decreased range of *H* with increasing walking speed (e.g., Bennett et al., 2010), we did not observe any differences related to speed. This is mainly due to the different normalization techniques. In previous studies, *H* was normalized by walking speed, whereas in this study it was normalized by a factor independent of walking speed and may be more suitable for studies comparing the range of *H* across various walking speeds.

The difference in the range of frontal-plane angular momentum was related to differences in the net external moment components (i.e., *GRFs* and moment arms), with the range being most affected by lateral foot placement. The older adults had a significantly wider step width, which along with the peak lateral (Z) moment arm, was

significantly correlated with the range of frontal-plane *H*. The wider step width combined with the dominant vertical *GRF* creates a higher external moment about the body *CoM*. During single-leg stance when there is no counteracting moment from the contralateral leg, the higher external moment acts to rotate the body towards the contralateral leg. This results in a higher rate of change and range in frontal-plane *H* (Fig. 2.2) that requires greater mediolateral balance control. Pijnappels et al. (2005) reported that during perturbed walking, older fallers showed insufficient reduction of angular momentum, improper placement of the recovery limb and inadequate joint moment generation of the support limb. Maki et al. (1997) have observed a positive correlation between wider steps and greater likelihood of falling in older adults. Others have shown that both old and young adults walk with narrower steps when external lateral stabilization is provided (Dean et al., 2007). However, lateral stability was also improved without external stabilization when young subjects voluntarily decreased their step width (McAndrew Young and Dingwell, 2012). Previous work has shown that falling in older adults is associated with decreased leg muscle strength (Pijnappels et al., 2008). Thus, it is possible that the external stabilization in Dean et al. (2007) compensated for the lack of muscle strength in older adults and resulted in the narrower steps.

Previous research has associated a higher range of frontal-plane *H* with a decrease in hip abduction moment (Silverman et al., 2012). During the self-selected walking condition, we did not observe any differences in the peak hip abduction moment between age groups. However, older adults had a significantly lower second peak hip abduction moment compared to the younger adults during the fastest-comfortable walking condition. In addition, we found an inverse correlation between the second peak hip abduction moment and the range of frontal-plane *H* during the self-selected ($r = -0.40$, $p = 0.09$) and fastest-comfortable ($r = -0.44$, $p = 0.05$) walking speeds, which suggests a

lower hip abduction moment is associated with a higher range of frontal-plane *H*. The hip abduction moment counteracts any destabilizing moments (e.g., from gravity) that act to rotate the body towards the contralateral leg during swing (MacKinnon and Winter, 1993). Thus, increasing the hip abductor moment of the ipsilateral leg during stance may be an effective way to reduce the range of frontal-plane *H*.

In addition to wider steps, the older adults also had lower vertical *GRF* impulses and higher *M/L GRF* peaks. However, during the self-selected walking condition, there were no significant differences in the vertical *GRF* peaks or in the *M/L GRF* impulses between the age groups (Fig. 2.3). The differences in the range of frontal-plane *H*, external moment components, and *GRF* impulses between the age groups were generally consistent across walking speeds for these older subjects who had a slow self-selected walking speed. This consistency suggests that age-related differences in the biomechanical quantities associated with balance control may be independent of walking speed, with older adults who prefer a slow self-selected walking speed being more challenged to maintain mediolateral balance. These results may relate to previous studies showing a strong association between elderly fallers and a slow self-selected walking speed (e.g., Luukinen et al., 1995; Nelson et al., 1999; Verghese et al., 2009). Future work is needed to investigate if similar differences exist in older adults who have a faster self-selected walking speed.

In the sagittal-plane, the range of *H* was not different between the older and younger adults at either walking speed despite the large difference in the range of frontal-plane *H*. This finding suggests that maintaining mediolateral balance may be more challenging than sagittal-plane balance for older adults. This would be consistent with previous studies showing that sagittal-plane balance control can be maintained passively while mediolateral balance requires active control (Bauby and Kuo, 2000; Kuo, 1999).

Although the older adults had a shorter stride length during the self-selected walking condition, and a lower peak anterior moment arm during both walking conditions, there were no correlations between the range of sagittal-plane *H* and these quantities. Since the treadmill speed was held constant, the shorter stride length during the self-selected walking condition led to a shorter stance time and lower braking, propulsive and vertical *GRF* impulses. Although there were no differences in the peak *A/P GRFs*, the peak braking and propulsive *GRFs* were negatively correlated with the range of sagittal-plane *H*. In addition, the older adults generated a lower peak ankle plantarflexor moment and higher peak knee extensor moment (Table 2.1). The decreased ankle plantarflexor moment has important implications for balance control, as previous studies have shown the plantarflexors play a critical role in maintaining dynamic balance by regulating whole-body angular momentum (Neptune and McGowan, 2011). In addition, fallers have been associated with lower plantarflexor moment generation compared to non-fallers (e.g., Barak et al., 2006) and older adults with a lower rate of support limb moment generation and ankle moment strength have a higher range of *H* following a forward trip and are more likely to fall (Pijnappels et al., 2005b). Thus, appropriate plantarflexor strength is an important element in regulating *H* and maintaining dynamic balance.

A potential limitation of this study is that the older adults were younger than what is typically considered elderly (e.g., greater than 65 years old). However, these individuals walked with similar gait characteristics as those reported in the elderly (e.g., slower preferred walking speed and shorter step lengths, McGibbon, 2003). Also, these subjects did not report any musculoskeletal or mobility impairments. Thus, we do not expect the lower age of our older subjects to affect the study findings. Another potential limitation is that the fastest-comfortable speed in the older adults (1.4 m/s) does not

match the walking speed in the younger adults (1.2 m/s). However, as shown in Fig. 2.2, the range of angular momentum is independent of walking speed. Therefore, the small difference in speeds is not expected to influence the study conclusions.

Conclusion

The successful regulation of angular momentum is critical in maintaining dynamic balance and preventing falls. The range of frontal-plane angular momentum in older adults was higher compared to younger adults. This difference was related to an increased step width in the older adults. This result may be counterintuitive, as wider step widths are often associated with increased stability due to increase in base of support. However, during single-leg stance, the wider step width combined with the dominant vertical *GRF* creates a greater destabilizing external moment that acts to rotate the body towards the contralateral leg and creates a greater range of angular momentum. Thus, in response to a perturbation, it may be more challenging to regulate the already increased angular momentum for older adults with muscle weakness and slow reaction times. Future perturbation studies are needed to test this premise. An interesting finding was that there were no differences in the range of sagittal-plane angular momentum between the age groups. These results suggest that maintaining mediolateral balance may be more challenging than maintaining sagittal-plane balance for older adults who prefer a slow self-selected walking speed. These results suggest that exercise programs that target appropriate foot placement and increasing lower extremity muscle strength, particularly of the ankle plantarflexors and hip abductors, may improve the regulation of angular momentum and enhance balance control in older adults.

Chapter 3: The Influence of Solid Ankle-Foot-Orthoses on Forward Propulsion and Dynamic Balance in Healthy Adults during Walking

Introduction

Ankle-foot-orthoses (AFOs) are frequently prescribed to assist with gait impairments in post-stroke hemiparetic subjects (Tyson and Thornton, 2001). The most commonly prescribed AFO is an L-shaped design made of polypropylene (Cakar et al., 2010; Nair et al., 2010), which holds the ankle in a near neutral position to assist in foot clearance during swing while bracing the ankle during stance. A number of studies have investigated the influence of these types of AFOs on post-stroke hemiparetic gait. Although these studies have found no improvement in step length symmetry when subjects walked with and without an AFO (Abe et al., 2009; Tyson and Thornton, 2001), most have reported an increase in walking speed and improved toe clearance when using some type of AFO (e.g., Abe et al., 2009; Bregman et al., 2010). However, a previous simulation analysis of healthy subjects showed that in order to generate adequate push-off during normal walking, significant plantarflexor strength was required to deform the AFO (Crabtree and Higginson, 2009). Thus, patients with weak plantarflexors may be hindered in generating adequate propulsion. In addition, recent studies have provided conflicting results as to whether AFOs reduce the risk of falling (Cakar et al., 2010; Guerra Padilla et al., 2011; Wang et al., 2007). Other studies have found no difference in clinical balance scores (Park et al., 2009; Wang et al., 2005) or in static or dynamic weight-bearing tasks when wearing an AFO (Simons et al., 2009). However, no study has used quantitative measures to assess the influence of AFOs on dynamic balance during walking.

Improving mobility (e.g., ability to change walking speed and direction) is a common rehabilitation goal. One aspect of mobility is to effectively accelerate or decelerate the body while maintaining dynamic balance. Previous studies have shown the ankle plantarflexors are primary contributors to regulating forward propulsion in healthy

subjects (e.g., Liu et al., 2008; Neptune et al., 2008; Peterson et al., 2011). In hemiparetic walkers, analysis of soleus and gastrocnemius electromyography data indicate they have reduced amplitude and altered timing of plantarflexor activity compared to healthy subjects (Knutsson and Richards, 1979). In addition, simulation analyses have identified the primary impairment in post-stroke limited community walkers as decreased paretic plantarflexor contributions to forward propulsion (Peterson et al., 2010b). Thus, with AFOs restricting ankle movement, the generation of forward propulsion may be further impaired.

Diminished balance control is another post-stroke complication. Greater than 50% of stroke survivors experience falls within one year post-stroke (e.g., Ashburn et al., 2008; Sackley et al., 2008). Studies have shown that whole-body angular momentum is highly regulated during normal walking to maintain dynamic balance (e.g., Herr and Popovic, 2008; Pijnappels et al., 2005b). Poor regulation of angular momentum has been associated with a higher range of angular momentum and is indicative of poor dynamic balance (e.g., Pijnappels et al., 2004). This is consistent with research showing that post-stoke hemiparetic subjects with lower clinical balance scores have difficulty regulating their frontal-plane angular momentum (Nott et al., 2013). Previous simulation analyses of healthy walking have shown that the plantarflexors are major contributors to the regulation of whole-body angular momentum (Neptune and McGowan, 2011). Thus, AFOs likely influence dynamic balance because they limit ankle motion and plantarflexor output.

Given the widespread use of AFOs in rehabilitation and the important role of the ankle plantarflexors in regulating propulsion and dynamic balance during walking, it is important to understand how AFOs influence the execution of these important biomechanical functions. As a first step, the purpose of this study was to assess the

influence of a commonly prescribed solid polypropylene AFO on forward propulsion and dynamic balance in healthy subjects across a range of walking conditions including steady-state, accelerated and decelerated walking. Further, to help interpret any observed differences, changes in the net intersegmental joint moments and powers with and without the AFO were investigated. We hypothesize that when walking with a unilateral AFO: 1) the generation of forward propulsion from the AFO leg will decrease, and 2) the range of whole-body angular momentum will increase. Assessing the influence of AFOs on healthy subjects' walking mechanics will provide a baseline for comparison with hemiparetic subjects, which collectively can provide clinicians with quantitative rationale as to whether AFOs improve paretic leg impairments and overall walking mobility.

Methods

Ten healthy subjects (age: 27.3, SD = 2.8 years; mass: 72.6, SD = 10.2 kg; height: 1.75, SD = 0.1 m) walked on an instrumented treadmill in randomized trials of steady-state (0.6 m/s and 1.2 m/s), accelerated (0-1.8 m/s at 0.06 m/s^2) and decelerated (1.8-0 m/s at -0.06 m/s^2) walking. For each walking speed condition, subjects walked with and without a common clinically prescribed unilateral solid polypropylene AFO (Fig. 3.1) on a randomly assigned leg while three 30-second trials were collected. The study protocol and consent form were approved by an Institutional Review Board and all participants provided informed, written consent prior to study participation.

A 12-camera optical motion capture system (PhaseSpace Inc., San Leandro, CA, USA) was used to record 3D kinematics at 120 Hz using a modified Helen Hayes marker set. 3D ground reaction force (GRF) data were collected at 2000 Hz using an instrumented treadmill (Bertec Corp., Columbus, OH, USA). The kinematic and GRF data were smoothed using a fourth-order Savitzky-Golay (Savitzky and Golay, 1964)

least-square polynomial smoothing filter and were resampled at 100 Hz before performing an inverse dynamics analysis. GRF data were normalized by body weight. A 13-segment whole-body model including the head, torso, pelvis, upper arms, lower arms, thighs, shanks and feet was used to determine the mass and inertial properties of the body segments, whole-body center-of-mass (CoM) position and velocity as well as the intersegmental joint moments and powers. The joint moments and powers were normalized by body-mass.

Figure 3.1. Solid polypropylene ankle-foot-orthosis (AFO) used in this study.

At each time step, whole-body angular momentum (*H*) about the CoM was calculated as:

$$\vec{H} = \sum_{i=1}^{n} [\ (\vec{r}_i^{COM} - \vec{r}_{body}^{COM}) \times m_i(\vec{v}_i^{COM} - \vec{v}_{body}^{COM}) + I_i\overrightarrow{\omega_i}\ ] \tag{3.1}$$

where $\vec{r}_i^{COM}$ and $\vec{v}_i^{COM}$ are respectively the position and velocity vectors of the *i*-th segment's CoM and $\overrightarrow{\omega_i}$ is the angular velocity of the *i*-th segment. $\vec{r}_{body}^{COM}$ and $\vec{v}_{body}^{COM}$ are the position and velocity vectors of the whole-body CoM, m_i and I_i are the mass and moment of inertia of the *i*-th segment and *n* is the number of segments. *H* was normalized by the product of subject mass, height and $\sqrt{g \cdot l}$, where g = 9.81 m/s^2 and l is the subject height. The term $\sqrt{g \cdot l}$ has units of m/s and is independent of walking speed. During the non-steady-state (i.e., accelerated and decelerated) walking conditions, four representative steps (S1-S4) were selected in each trial and each subject. For each step, the corresponding *H* was averaged across all trials and all subjects. The ranges of treadmill speed during the selected steps in the accelerated walking condition were approximately S1=0.40-0.49 m/s, S2=0.62-0.70 m/s, S3=1.20-1.26 m/s, S4=1.53-1.58 m/s. The ranges of treadmill speed during the selected steps in the decelerated walking condition were similar to those during the accelerated condition but with a descending speed order. Dynamic balance was assessed using the range of *H* in each plane, which was calculated as the difference between the maximum and minimum value of *H* over the entire gait cycle. Propulsion was assessed using the braking and propulsive GRF impulses, which were calculated using the time integral of the negative and positive anterior-posterior (A/P) GRFs, respectively. During the steady-state walking conditions the impulses were averaged across all steps and subjects. During the non-steady-state walking conditions, the impulses varied over each step due to A/P GRFs and stance time varying with walking speed (e.g., Peterson et al., 2011). Therefore, for comparison purposes, the propulsive and braking impulses were each summed over the entire trial before they were averaged across subjects. In addition, due to step symmetry in the no AFO condition (NAFO), the GRF impulses from both legs were averaged.

The range of *H* was compared between the AFO and NAFO conditions at each walking speed using a paired t-test. In the sagittal plane, the range of *H* was analyzed during the first (0-50%) and second (51-100%) halves of the gait cycle. Braking and propulsive impulses were compared using a one-factor (AFO condition) repeated measures ANOVA (α =0.05) with three levels (AFO leg, contralateral leg, and average of both legs during the NAFO condition). Mauchly's test of sphericity was used to verify equality of variances. If sphericity was violated, a Greenhouse-Geisser adjustment was applied. When significant effects were found, pairwise comparisons with a Bonferroni adjustment were used to determine which values were significantly different. Peak intersegmental joint moments and powers during early (0-50%) and late (51-100%) stance were compared using an ANOVA during steady-state walking speeds to further understand observed differences between the AFO and NAFO conditions. Pearson correlation analyses were performed between the range of *H* and the peak joint moments.

Results

Anterior-posterior GRF impulses

During steady-state slow (0.6 m/s) walking, there were no significant differences in the A/P GRF impulses with and without wearing the AFO (Fig. 3.2). Similarly, wearing the AFO had no influence on the peak ankle plantarflexor moment (Table 3.1). However, the peak plantarflexor power generation and absorption were significantly ($p < \alpha/3$, $\alpha = 0.05$) lower in the AFO leg compared to the contralateral leg and the NAFO condition (Table 3.2 and Fig. 3.3).

Table 3.1. Mean (SD) peak intersegmental joint moments normalized by body mass for the AFO leg (AFO_Leg), contralateral leg (AFO_Contra) and average of both legs during the no AFO condition (NAFO). A significant difference with the NAFO condition is indicated with '*'. A significant differences between the AFO leg and the contralateral leg is indicated with 'ψ'. ($p < \frac{\propto}{3}, \propto = 0.05$)

Peak joint moment (N.m/kg)	Slow steady-state speed			Moderate steady-state speed		
	AFO_Leg	AFO_Contra	NAFO	AFO_Leg	AFO_Contra	NAFO
Hip abduction, 1st peak	0.62 (0.16)*ψ	0.91 (0.19)	0.82 (0.07)	0.70 (0.19)*ψ	1.02 (0.18)*	0.88 (0.11)
Hip abduction, 2nd peak	0.55 (0.13)*	0.77 (0.19)	0.75 (0.07)	0.45 (0.14)*ψ	0.70 (0.20)	0.71 (0.10)
Hip extension	0.37 (0.12)	0.34 (0.14)	0.31 (0.08)	0.80 (0.14)*	0.79 (0.18)	0.70 (0.08)
Hip flexion	0.56 (0.22)	0.51 (0.23)	0.50 (0.14)	0.92 (0.21)	0.97 (0.27)	0.97 (0.18)
Ankle plantarflexion	1.32 (0.19)	1.23 (0.18)	1.32 (0.15)	1.49 (0.19)	1.53 (0.09)	1.59 (0.12)

Table 3.2. Mean (SD) peak joint power normalized by body mass for the AFO leg (AFO_Leg), contralateral leg (AFO_Contra) and average of both legs during the no AFO condition (NAFO). Positive and negative values indicate power generation and absorption, respectively. A significant difference with the NAFO condition is indicated with '*'. A significant difference between the AFO leg and the contralateral leg is indicated with 'ψ'. ($p < \frac{\propto}{3}, \propto = 0.05$)

	Slow steady-state speed			Moderate steady-state speed		
Peak joint power (W/kg)	AFO_Leg	AFO_Contra	NAFO	AFO_Leg	AFO_Contra	NAFO
Hip adduction (+)	0.04 (0.03)	0.03 (0.02)	0.04 (0.03)	0.11 (0.10)	0.14 (0.13)	0.13 (0.10)
Hip abduction (-)	-0.11 (0.09)*ψ	-0.26 (0.17)	-0.21 (0.10)	-0.29 (0.20)*ψ	-0.63 (0.22)	-0.54 (0.18)
Hip abduction 1st pk (+)	0.14 (0.06)	0.25 (0.17)*	0.16 (0.12)	0.21 (0.10)	0.31 (0.14)	0.27 (0.16)
Hip abduction 2nd pk (+)	0.10 (0.05)*	0.19 (0.13)	0.21 (0.09)	0.14 (0.11)*ψ	0.40 (0.15)	0.41 (0.14)
Hip extension (+)	0.35 (0.17)	0.31 (0.17)	0.27 (0.12)	0.94 (0.20)*	0.85 (0.35)	0.73 (0.18)
Hip flexion (-)	-0.38 (0.21)	-0.31(0.15)	-0.27 (0.10)	-0.79 (0.27)	-0.80 (0.23)	-0.67 (0.16)
Hip flexion (+)	0.38 (0.16)	0.42 (0.09)	0.36 (0.07)	1.04 (0.24)	1.03 (0.14)	1.03 (0.09)
Ankle plantarflexion (-)	-0.40 (0.10)*ψ	-0.51 (0.09)	-0.59 (0.18)	-0.75 (0.32)*	-0.85 (0.12)*	-1.21 (0.23)
Ankle plantarflexion (+)	0.50 (0.30)*ψ	1.10 (0.35)	1.19 (0.07)	1.22 (1.04)*ψ	3.41 (0.61)	3.69 (0.51)

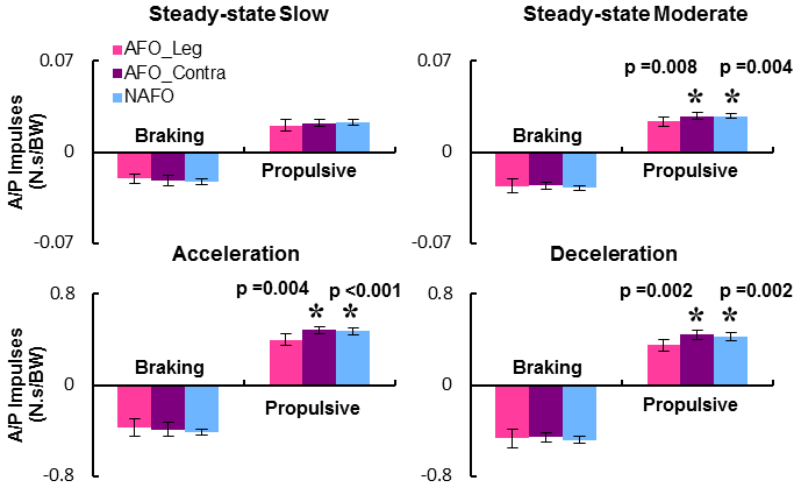

Figure 3.2. Mean braking and propulsive impulses (normalized by body weight) for the AFO leg (AFO_Leg), contralateral leg (AFO_Contra) and average of both legs in the no AFO condition (NAFO). A significant difference between the AFO leg and other conditions (contralateral leg and NAFO) is indicated with '*' ($p < \frac{\propto}{3}, \propto = 0.05$).

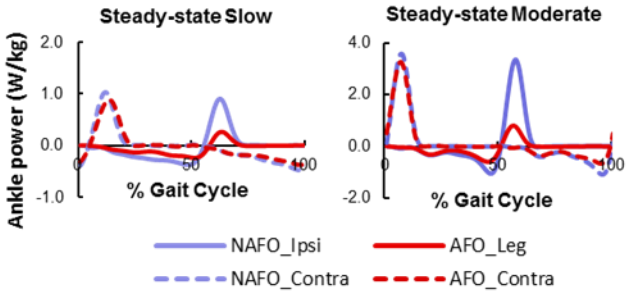

Figure 3.3. Mean ankle power (normalized by body mass) for each leg with and without a unilateral AFO during steady-state slow and moderate walking conditions. The AFO condition consists of the AFO leg (AFO_Leg) and contralateral leg (AFO_Contra). The no AFO condition consists of the ipsilateral leg (NAFO_Ipsi) and contralateral leg (NAFO_Contra).

During the steady-state moderate (1.2 m/s), and accelerated and decelerated walking conditions the propulsive impulse generated by the AFO leg was significantly lower than that from the contralateral leg and the NAFO condition (Fig. 3.2). There were no differences in the braking impulses. In addition, during steady-state moderate walking condition, the peak ankle plantarflexor moment (Table 3.1) and power (Table 3.2 and Fig. 3.3) were lower in the AFO leg although differences in the plantarflexor moment were not significant ($p > \alpha/3$, $\alpha = 0.05$). In addition, the peak hip extensor moment and power were significantly ($p < \alpha/3$, $\alpha = 0.05$) higher in the AFO leg (Tables 3.1 and 3.2).

Frontal-plane angular momentum

During steady-state walking, the range of frontal-plane *H* was significantly higher when wearing the AFO during slow ($p = 0.008$) and moderate ($p = 0.002$) walking speeds (Figs. 3.4-3.5). In addition, the first (early stance) and second (late stance) peak hip abduction moments were significantly ($p < 0.01$) lower in the AFO leg compared to the contralateral leg and the NAFO condition (Table 3.1). During steady-state slow walking, the range of *H* was negatively correlated with the peak hip abduction moment in the AFO leg in early ($r = -0.62$, $p = 0.003$) and late ($r = -0.56$, $p = 0.01$) stance. This correlation was also present during steady-state moderate walking in early ($r = -0.60$, $p = 0.004$) and late ($r = -0.59$, $p = 0.006$) stance. During accelerated walking, the range of *H* was significantly higher with the AFO during steps S2 ($p = 0.039$), S3 ($p = 0.017$) and approached significance in S4 ($p = 0.062$) (Fig. 3.6). During decelerated walking, the range of *H* was significantly higher with the AFO during steps S3 ($p = 0.046$), S2 ($p = 0.015$) and S1 ($p = 0.004$) (Fig. 3.6).

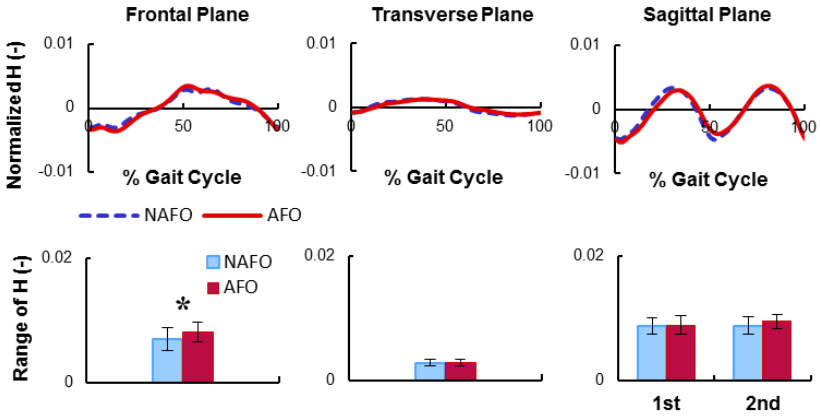

Figure 3.4. Normalized, mean 3D whole-body angular momentum (H) during the steady-state slow (0.6 m/s) walking condition with (AFO) and without (NAFO) an AFO. Figures are in the AFO leg reference frame. '1st' and '2nd' indicate the first and second halves of the gait cycle, respectively. The mean (SD) range of H is shown in the bottom row. A significant difference between the AFO and NAFO conditions is indicated with '*' ($p < 0.05$).

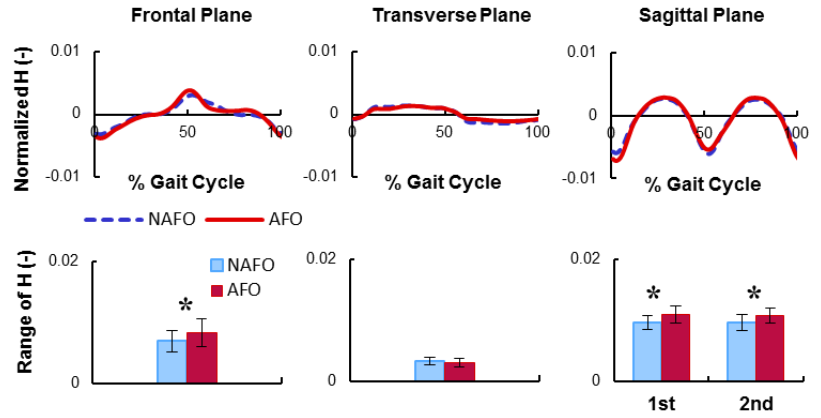

Figure 3.5. Normalized, mean 3D whole-body angular momentum (H) during the steady-state moderate (1.2 m/s) walking condition with (AFO) and without (NAFO) an AFO. Figures are in the AFO leg reference frame. '1st' and '2nd' indicate the first and second halves of the gait cycle, respectively. The mean (SD) range of H is shown in the bottom row. A significant difference between the AFO and NAFO conditions is indicated with '*' ($p < 0.05$).

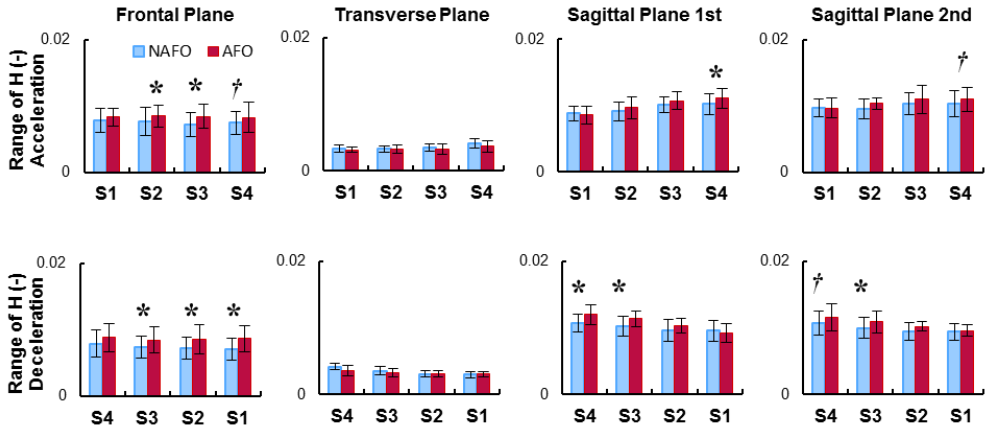

Figure 3.6. Normalized, mean (SD) range of whole-body angular momentum (H) in 3D with (AFO) and without (NAFO) an AFO. Top row shows the accelerated and bottom row shows the decelerated walking condition. '1st' and '2nd' indicate the first and second halves of the gait cycle, respectively. A significant difference between the AFO and NAFO conditions is indicated with '*' ($p < 0.05$). Marginal differences are shown with '†' ($0.05 < p < 0.1$). Treadmill speed values at the selected steps are S1=0.40-0.49 m/s, S2=0.62-0.70 m/s, S3=1.20-1.26 m/s, S4=1.53-1.58 m/s.

Transverse-plane angular momentum

There were no significant differences in the range of transverse-plane H during any of the walking conditions.

Sagittal-plane angular momentum

During steady-state slow walking, there were no significant ($p > 0.05$) differences in the sagittal-plane *H* (Fig. 3.4). However, during the moderate walking speed, the range of *H* in both the first ($p = 0.003$) and second ($p = 0.001$) halves of the gait cycle was significantly higher when wearing the AFO (Fig. 3.5). Also, the peak ankle plantarflexor moment in the AFO leg was negatively correlated with the range of *H* in the first ($r = -0.54$, $p = 0.01$) and second ($r = -0.44$, $p = 0.05$) halves of the gait cycle. During

accelerated walking, at the fastest speed (step S4), the range of *H* was significantly higher during the first ($p = 0.041$) and marginally higher during the second ($p = 0.09$) halves of the gait cycle when walking with the AFO (Fig. 3.6). During decelerated walking, in the first half of the gait cycle, the range of *H* was significantly higher with the AFO at the faster speeds S4 ($p = 0.004$) and S3 ($p = 0.006$). Also, during the second half of the gait cycle, the range of *H* was higher with the AFO at the faster speeds S4 ($p = 0.059$) and S3 ($p = 0.024$).

Discussion

The purpose of this study was to assess the influence of a commonly prescribed solid polypropylene AFO on forward propulsion and dynamic balance in healthy subjects across a range of walking conditions. During the steady-state slow walking condition, the AFO had no influence on the generation of propulsive and braking impulses and peak ankle plantarflexor moment. However, ankle plantarflexor power generation and absorption significantly decreased with the AFO (Fig. 3.3) due to the AFO limiting the ankle range of motion. Therefore, our first hypothesis that forward propulsion decreases with an AFO was not supported during the slow steady-state walking condition. However, during all other walking conditions (steady-state moderate, accelerated and decelerated walking), our first hypothesis was supported in that the propulsive impulses decreased in the AFO leg compared to the contralateral leg and NAFO condition (Fig. 3.2). In addition, during the moderate walking condition, the peak ankle moment and power also decreased in the AFO leg. These results were consistent with previous modeling work showing that significant plantarflexor strength is required to deform the AFO and generate needed propulsion (Crabtree and Higginson, 2009). Thus, the limited

ankle range of motion provided by AFOs appears to diminish plantarflexor output and the generation of forward propulsion.

An interesting finding was that the peak hip extensor moment and power increased during the moderate steady-state walking condition in the AFO leg (Tables 3.1 and 3.2). This is consistent with simulation analyses showing that the biarticular hamstrings contribute to forward propulsion in early and mid-stance in healthy walkers (Liu et al., 2006; Neptune et al., 2004) and the nonparetic leg rectus femoris and biarticular hamstrings contribute to forward propulsion in post-stroke subjects to compensate for the lack of plantarflexor output (Hall et al., 2011). In addition, previous studies have shown that both transtibial and transfemoral amputees also use similar strategies at the hip level to compensate for the loss of plantarflexor output (Prinsen et al., 2011). Thus, it is most likely that the peak hip extensor moment increased in the AFO leg to compensate for the decreased plantarflexor output. In contrast to a previous analysis of accelerated and decelerated walking that showed a higher hip extensor moment was associated with a higher braking impulse (Peterson et al., 2011), we did not observe any changes in the braking impulse. However, the variability in the AFO leg braking impulse increased in all conditions while the propulsive impulse in the AFO leg decreased (Fig. 3.2). With the generation of forward propulsion being a key factor for modulating walking speed (e.g., Shumway-Cook and Woollocott, 2001), the present results suggest that an AFO may hinder forward propulsion to a greater extent during non-steady-state walking (Fig. 3.2).

The AFO also influenced dynamic balance control, as wearing the AFO resulted in a higher range of H in both the frontal and sagittal planes, which supported our second hypothesis. Whole-body angular momentum has previously been found to be highly regulated during walking (Herr and Popovic, 2008) and that successful regulation of H is

needed in older adults to prevent a fall following a trip (Pijnappels et al., 2005b). Thus, poor regulation of *H* during walking results in higher magnitudes of *H*, which may lead to a decreased ability to recover dynamic balance following a perturbation.

In the frontal plane, the range of *H* was higher with the AFO during both steady-state and non-steady-state walking conditions, although differences were not significant at the lowest speed during the acceleration and at the highest speed during the deceleration conditions. During steady-state slow and moderate walking, the increased *H* corresponded to a lower peak hip abduction moment in the AFO leg during early and late stance. These findings are consistent with a previous study showing a correlation between a higher range of frontal-plane *H* and a lower peak hip abduction moment (Silverman et al., 2012). They also suggested increasing the hip abduction moment as a mechanism for reducing the range of frontal-plane *H*. Others have shown that the hip abduction moment is an important contributor to maintaining balance in the frontal plane by acting on the pelvis and moving the HAT (head, arms and trunk) CoM laterally towards the supporting foot and reducing the net external moment about the CoM (MacKinnon and Winter, 1993). In addition, simulation analyses of healthy walkers have shown that during late stance, the plantarflexors contribute to the frontal-plane *H* by rotating the body towards the contralateral leg, whereas the gluteus medius acts to rotate the body towards the ipsilateral leg (Neptune et al., 2011). The current study found that when wearing an AFO the peak hip abduction moment in the AFO leg decreased, which negatively affected the regulation of frontal-plane angular momentum. During the steady-state moderate walking condition, it is possible that the peak hip abduction moment decreased in the AFO leg due to a decreased ankle plantarflexion moment (Table 3.1). However, during steady-state slow walking, the peak hip abduction moment still decreased in the AFO leg even though

the peak plantarflexor moment was not affected by the AFO. Thus, the underlying reason for a decreased peak hip abduction moment in the AFO leg is not clear.

In the sagittal plane, the range of *H* was higher with an AFO during steady-state moderate walking (Fig. 3.5) and at the higher speeds during accelerated and decelerated walking (Fig. 3.6). Further, the peak ankle plantarflexor moment was lower in the AFO leg during steady-state moderate walking and negatively correlated with the range of *H* in both the first and second halves of the gait cycle (i.e., a lower ankle plantarflexor moment was associated with a higher range of *H*). Previous simulation analyses of healthy walkers have identified the ankle plantarflexors as the primary contributors to the regulation of *H* in the sagittal plane (Neptune and McGowan, 2011). Thus, AFOs restricting the ankle range of motion and hindering plantarflexor muscle force generation not only limit propulsion generation but also lead to a poor dynamic balance control. This has important implications for prescribing AFOs to post-stroke subjects as the influence of AFOs on propulsion and dynamic balance in those with post-stroke hemiparesis with different levels of plantarflexor impairment is unclear. Previous simulation analyses of unilateral below-knee amputees have shown that a foot-ankle prosthesis, which is functionally similar to an AFO, performs similarly as the uniarticular soleus muscle to provide forward propulsion (Silverman and Neptune, 2012). Thus, it is likely that those hemiparetic subjects with minimal plantarflexor output would benefit from the additional ankle stiffness provided by an AFO to generate needed stability and perhaps some levels of propulsion (e.g., the elastic energy stored in the AFO due to deformation is released and contributes to the net joint moment at the ankle). Future studies are needed to identify biomechanical markers that distinguish which subjects would benefit from an AFO from those that would not. Similarly, in cases where an AFO is needed to compensate for gait impairments such as foot drop, perhaps more advanced AFO designs that promote ankle

plantarflexion (e.g., Bartonek et al., 2007; Desloovere et al., 2006) or functional electrical stimulation systems (e.g., The WalkAide System, Austin, TX, USA) that promote dorsiflexion can improve rehabilitation outcomes.

In summary, common clinically prescribed solid polypropylene AFOs adversely influenced the generation of forward propulsion and dynamic balance in healthy adults during steady-state and non-steady-state walking. The ankle plantarflexors normally play an important role in the generation of propulsive impulses and regulation of whole-body angular momentum. However, the AFO restricted the ankle range of motion and was found to hinder the generation of propulsion and the regulation of angular momentum in both the frontal and sagittal planes. Thus, during mobility tasks when these important functions are needed, such as when changing walking speed and direction, AFOs limit their successful execution and suggest that the prescription of AFOs should be carefully considered.

Chapter 4: The Influence of Locomotor Training on Dynamic Balance and its Relation with Increased Walking Speed in Post-stroke Hemiparetic Subjects

Introduction

Post-stroke hemiparetic gait is characterized by slow walking speed, asymmetry (Olney, 1996) and balance disorders (Geurts et al., 2005). Thus, various methods of locomotor training are used to improve gait coordination (Hollands et al., 2012) and overall mobility. One common type is locomotor training which consists of treadmill walking with partial body weight support (Hesse, 2008). Locomotor training is based on the task-specific repetitive treatment concept in post-stroke rehabilitation (Hesse et al., 1994) with a number of studies reporting improved walking speed in post-stroke patients (e.g., Hesse, 2008; Peurala et al., 2005; Visintin et al., 1998). However, the effect of locomotor training on dynamic balance during walking remains unclear.

The effectiveness of locomotor training was investigated in its largest rehabilitation trial, Locomotor Experience Applied Post-stroke (LEAPS) (Duncan et al., 2011). This study suggested that receiving early locomotor training in patients with severe walking impairment were associated with falls. They also mentioned that locomotor training emphasized stepping and walking but did not include balance-specific training and therefore, it can lead to increased rate of falls. However, no biomechanical data were provided to support these findings. Recently, Bowden et al. (2013) performed locomotor training on post-stroke hemiparetic subjects, following a nearly identical protocol as that utilized in the LEAPS trial and found similar outcomes in walking speed. In addition, they have collected kinetic and kinematic biomechanical data from the subjects pre- and post-therapy to understand the underlying mechanisms for the increased walking speed. However, the influence of locomotor training on dynamic balance and its relation with changes in walking speed remain unclear. Given that at least 50% of stroke survivors experience falls within one year of their stroke (e.g., Ashburn et al.,

2008; Sackley et al., 2008), it is important to assess the effectiveness of locomotor training on dynamic balance using quantitative methods.

To maintain dynamic balance, angular-momentum needs to be regulated through proper foot placement and generation of appropriate ground-reaction-forces (GRFs) (e.g., Pijnappels et al., 2005a). Prior studies have shown that during walking, the range of whole-body angular-momentum is kept low through the cancellation of segmental angular momenta about the body center-of-mass (CoM) (e.g., Bennett et al., 2010; Herr and Popovic, 2008). However, in the presence of perturbations, the range of whole-body angular-momentum increases (e.g., Martelli et al., 2013). The regulation of angular-momentum can be quantified by the time rate of change of angular-momentum, which is equal to the net external moment created by the GRFs about the body CoM (Fig. 4.1).

A recent study investigated the relationships between the rate of change of frontal-plane angular-momentum and common clinical balance measures (e.g., BBS and DGI) in post-stroke subjects and found that the change in angular-momentum during paretic single-leg stance was negatively correlated with the clinical balance measures, indicating a greater change in angular-momentum was associated with poorer balance control (Nott et al., 2013). However, no study has assessed if locomotor training improves dynamic balance through improved regulation of whole-body angular-momentum. Also, it is not clear if clinically meaningful increases in walking speed after locomotor training are correlated with improved dynamic balance.

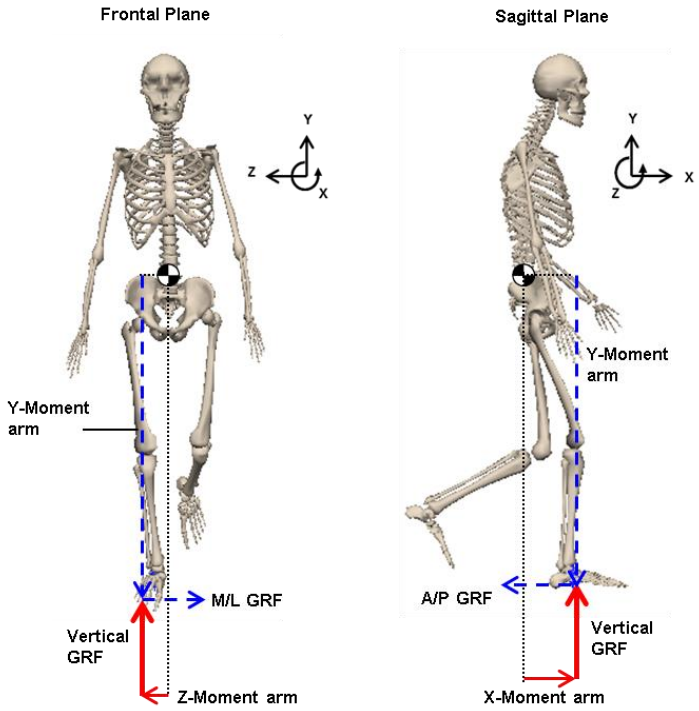

Figure 4.1. The components of net external moment in the frontal and sagittal planes during single-leg stance. Whole-body CoM is shown with '◓'. The GRF vectors and their corresponding moment arms appear in the same color. The higher magnitude of the vertical GRF compared to other components (after normalizing moment arms and GRFs by body height and weight, respectively) is highlighted by the line thickness.

Thus, the purpose of this study was to assess the influence of a 12-week locomotor training program (Bowden et al., 2013) on dynamic balance in post-stroke hemiparetic subjects and to determine if clinically meaningful increases in self-selected walking speed are correlated with improved dynamic balance. To further understand the underlying mechanisms for maintaining dynamic balance in post-stroke hemiparetic subjects, correlations between the range of angular-momentum and its external moment components were investigated. We hypothesized that locomotor training improves dynamic balance by decreasing the range of angular-momentum. We also hypothesized

that clinically meaningful improvements in walking speed are correlated with improved dynamic balance.

Methods

From a previous study (Bowden et al., 2013), a subgroup of 20 post-stroke subjects with hemiparesis (11 left hemiparesis; age: 56 ± 11.7 years; 15 men) and complete kinematic and GRF data sets pre- and post-therapy were selected. These subjects participated in a 12-week locomotor training program. Details regarding the therapy procedure and subject inclusion criteria were previously described in detail (Bowden et al., 2013) and were patterned after that used in the LEAPS clinical trial (Duncan et al., 2011). In short, the inclusion criteria consisted of subjects having experienced a stroke within the past 6 months to 5 years, with lower extremity hemiparesis (Fugl-Meyer lower extremity assessment score <34), ability to walk 10 m with maximum of one person assisting, and preferring a self-selected walking speed of less than 0.8 m/s. Also, Berg Balance Score (BBS) and Dynamic Gait Index (DGI) were assessed. Three subjects had a BBS<45 and 19 subjects had a DGI<19, which indicates a higher risk of falling (e.g., Berg et al., 1995; Shumway-Cook et al., 1997). The training sessions occurred 3 times per week, and each session included 20 minutes of walking on a treadmill with partial body weight support while physical therapists provided manual step and postural training. The training began with supporting 40% of the body weight and decreased body weight support to a minimal value as tolerated. The treadmill walking was followed by 10-20 minutes of overground training. The study protocol and consent form were approved by an Institutional Review Board and all participants provided informed, written consent prior to study participation.

Three-dimensional kinematics and GRFs were collected within one week of therapy initiation and completion. Subjects walked on a split-belt instrumented treadmill (Techmachine, Andrezieux Boutheon, France) for multiple 30-second trials at their self-selected and fastest-comfortable walking speeds pre-therapy (Table 4.1). During the post-therapy data collection, each subject walked at a speed matched to their pre-therapy self-selected and fastest-comfortable walking speeds. Also, overground self-selected speeds were determined post-therapy to allow the determination of speed increases from pre- to post-therapy (Table 4.1). In addition, three-dimensional kinematics and GRFs were collected from 10 healthy control subjects (age: 27.3 ± 2.8 years; 5 men) walking at a fixed speed of 0.6 m/s to provide a basis for comparison. Kinematic data were collected at 100 Hz using a 12-camera motion capture system (VICON, Los Angeles, USA) and GRFs were recorded at 2000 Hz. The kinematic and GRF data were low pass filtered using a fourth-order Butterworth filter with cutoff frequencies of 6 Hz and 20 Hz, respectively. A 13-segment inverse dynamics model (C-Motion, Inc., Germantown, MD) was used to calculate CoP, CoM position as well as the angular-momentum for each body segment. At each time step, whole-body angular-momentum (*H*) about the CoM was calculated as:

$$\vec{H} = \sum_{i=1}^{n} [(\vec{r}_i^{COM} - \vec{r}_{body}^{COM}) \times m_i(\vec{v}_i^{COM} - \vec{v}_{body}^{COM}) + I_i\overrightarrow{\omega_i}] \quad (4.1)$$

where $\vec{r}_i^{COM}$ and $\vec{v}_i^{COM}$ are the position and velocity vectors of the *i*-th segment's CoM, respectively. $\vec{r}_{body}^{COM}$ and $\vec{v}_{body}^{COM}$ are the position and velocity vectors of the whole-body CoM. $\overrightarrow{\omega_i}$, m_i and I_i are the angular velocity vector, and mass and moment of inertia of the *i*-th segment, respectively, and *n* is the number of segments. Angular momentum was

normalized by the product of subject mass, height and $\sqrt{g \cdot l}$, where g = 9.81 m/s^2 and l is the subject height. The term $\sqrt{g \cdot l}$ has units of m/s and is independent of walking speed.

Table 4.1. Self-selected (SS_{Pre}) and fastest-comfortable (FC_{Pre}) walking speeds pre-therapy for all post-stroke subjects. SS_{Post}-SS_{Pre} denotes the increase in the self-selected walking speed from pre- to post-therapy. Responders (i.e., SS_{Post}-SS_{Pre} > 0.16 m/s) are identified with '*'.

Subject	SS_{Pre} (m/s)	FC_{Pre} (m/s)	SS_{Post} - SS_{Pre}
1	0.71	1.11	0.08
2	0.51	0.90	0.21 *
3	0.79	1.15	0.26 *
4	0.76	0.99	0.32 *
5	0.54	0.74	0.09
6	0.76	1.06	0.17 *
7	0.43	0.53	0.16
8	0.48	0.85	0.49 *
9	0.22	0.24	0.02
10	0.39	1.06	0.61 *
11	0.50	0.73	0.25 *
12	0.33	0.73	0.14
13	0.44	0.57	0.15
14	0.63	0.90	0.19 *
15	0.20	0.31	0.13
16	0.60	0.82	0.36 *
17	0.70	1.01	0.29 *
18	0.05	0.05	0.15
19	0.43	0.77	0.16
20	0.37	0.56	0.30 *

Dynamic balance was assessed for each hemiparetic subject pre- and post-therapy using the range of angular-momentum in the frontal and sagittal planes, which was calculated as the difference between the maximum and minimum values of angular-momentum over the entire gait cycle. The range of angular-momentum in the sagittal

plane was calculated during the 1st and 2nd halves of the paretic gait cycle. Significant differences ($p<0.05$) in the range of angular-momentum between pre-therapy walking at self-selected speed and post-therapy walking at speed matched to their pre-therapy self-selected speed were identified for each subject using a paired t-test. Also, comparisons were conducted between pre-therapy walking at fastest-comfortable speed and post-therapy walking at speed matched to their pre-therapy fastest-comfortable speed. The range of angular-momentum for the healthy control data was averaged across all subjects for comparison with the hemiparetic data. For comparing angular-momentum with the clinical balance scores, BBS was determined pre- and post-therapy and was compared with the range of angular-momentum using spearman's correlation analyses. In addition, those with clinically meaningful improvements in walking speed (>0.16 m/s, (Bowden et al., 2013)) were identified as the responders and Pearson correlation analyses were performed to identify any relationships between changes in self-selected walking speed and changes in the range of angular-momentum. If significant correlations were found, the external moment components (i.e., 3D GRFs and moment arm vectors from the body CoM to CoP) were calculated and normalized by subject weight and height, respectively, to further understand the mechanisms used for maintaining balance and improving walking speed. At each time step, the net external moment (which is equal to the time rate of change of angular-momentum) was calculated in the frontal and sagittal planes as:

$$\vec{M}_{ext} = \vec{r} \times \overrightarrow{GRF} \tag{4.2}$$

where $\vec{r}$ is the moment arm vector from the body CoM to CoP and $\overrightarrow{GRF}$ is the vector of GRFs (Fig. 4.1). In each plane, two GRF components per leg create a moment about the

CoM (Fig. 4.1). Therefore, the location of each foot CoP, body CoM, and the magnitude of the GRFs determine the rate of change of angular-momentum. Both the GRF peaks and impulses were calculated in early (0-50%) and late (51-100%) stance to capture the effects of instantaneous and average changes in the GRFs between pre- and post-therapy. GRF impulses were calculated using the time integral of GRFs in early and late stance. To identify which quantities were most strongly correlated with angular-momentum, Pearson correlation analyses were performed between the range of angular-momentum in each plane and the peak external moment components. Data from pre-and post-therapy were combined for the correlation analyses among the responders.

Results

Angular momentum- all subjects

Overall, the range of angular-momentum over the gait cycle in the frontal plane and during the second half of the paretic gait cycle in the sagittal plane was higher in post-stroke subjects compared to the healthy control subjects. Generally, the range of angular-momentum was not improved post-therapy. Of the 20 subjects tested, five subjects decreased and seven subjects increased their range of angular-momentum post-therapy. However, these changes did not necessarily occur in both frontal and sagittal planes. In the remaining eight subjects, for each subject there was a combination of increases, decreases and no changes in the range of angular-momentum in different planes and walking speed conditions (Table 4.2 and Fig. 4.2).

Table 4.2. Significant changes ($p<0.05$) in the range of angular-momentum (H) between pre- and post-therapy are shown for each subject. Significant decreases in the range of H are shown with '✓' and significant increases are shown with 'X'. Subjects who **only** decreased their range of H are shown with '✓' and those who only increased their range of H are shown with '**X**'. Blank spaces indicate no significant changes. '1st' and '2nd' represent the 1st and 2nd halves of the paretic gait cycle.

	Self-selected walking speed			Fastest-comfortable walking speed		
Subject	Frontal	Sagittal 1st	Sagittal 2nd	Frontal	Sagittal 1st	Sagittal 2nd
1	✓	✓	✓	X		✓
2	✓		✓		✓	✓
3		**X**	**X**		**X**	**X**
4	✓		✓	✓		✓
5	**X**	**X**	**X**	**X**	**X**	**X**
6	✓			X	X	X
7			**X**		**X**	**X**
8			✓		✓	✓
9						
10	✓		X	✓		
11				✓	X	
12	**X**			**X**		
13	X	✓				
14			X	✓		X
15		✓				
16	✓			✓		
17		**X**	**X**	**X**	**X**	
18		**X**	**X**		**X**	**X**
19					**X**	**X**
20		✓	X	X	✓	✓

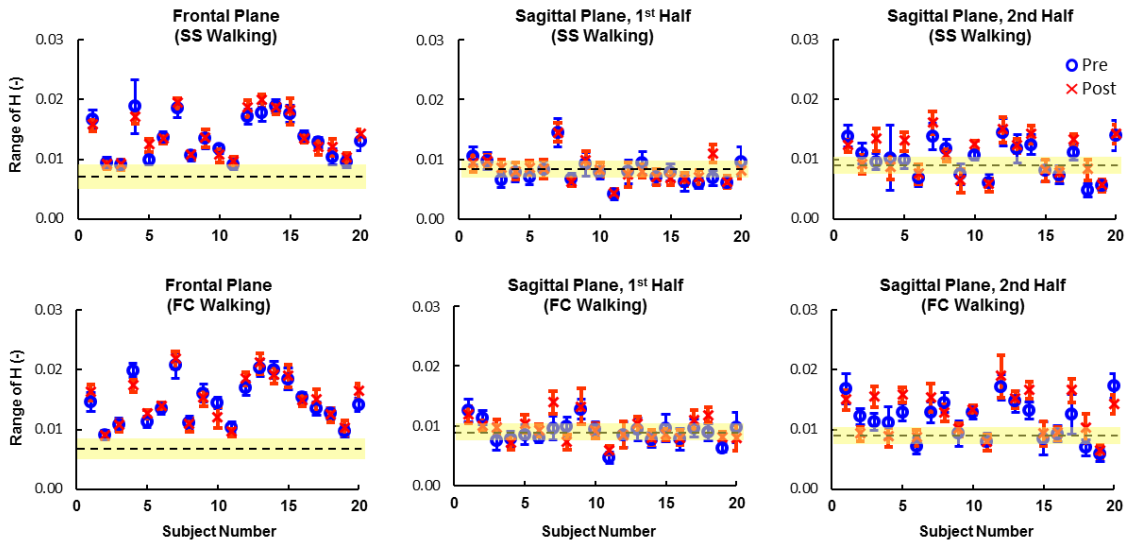

Figure 4.2. Normalized, mean (± SD) range of angular-momentum (*H*) for each hemiparetic subject pre- and post-therapy. Data is shown in the frontal and sagittal planes during the self-selected (SS) and fastest-comfortable (FC) walking speed conditions. The range of *H* in the sagittal plane is shown during the 1st and 2nd halves of the gait cycle. The dashed line (highlighted regions) depicts the average range of *H* (± SD) for the healthy control subjects.

Biomechanical analysis- responders

Of the 20 subjects tested, 11 subjects were identified as responders (i.e., those who improved their self-selected walking speed by more than 0.16 m/s) (Table 4.1). For these subjects, improvements in both self-selected and fastest-comfortable walking speeds were correlated with improvements (i.e., reductions) in the range of angular-momentum during the fastest-comfortable walking condition. Specifically, changes in self-selected walking speed were negatively correlated with changes in the range of angular-momentum in the frontal plane ($r = -0.48$, approaching significance at $P = 0.09$) and in the sagittal plane during the second half of the paretic gait cycle ($r = -0.55$, $P = 0.05$). Also, changes in the fastest-comfortable walking speed were negatively correlated

with changes in the range of angular-momentum in the sagittal plane during the paretic ($r = -0.86$, $P < 0.001$) and nonparetic ($r = -0.63$, $P = 0.02$) leg stance.

Discussion

The purpose of this study was to assess the influence of a 12-week locomotor training on dynamic balance in post-stoke hemiparetic subjects using whole-body angular-momentum. In addition, we investigated if clinically meaningful improvements in walking speed were correlated with improved dynamic balance. To further understand the underlying mechanisms for maintaining dynamic balance, peak external moment components and GRF impulses were analyzed.

Angular momentum- all subjects

Our hypothesis that locomotor training improves dynamic balance was not supported for the subjects as a group. The regulation of angular-momentum was improved in only 25% of the subjects and became worse in 35% of the subjects. The rest of the subjects did not have a clear pattern in regulating their angular-momentum, with each subject improving, becoming worse or showing no change in the different planes and walking conditions (Table 4.2). Overall, in the frontal plane, the range of angular-momentum was higher in the hemiparetic subjects than in the healthy control subjects, suggesting a poorer mediolateral balance control post stroke (Fig. 4.2). In the sagittal plane, the range of angular-momentum was generally higher during the second half of the paretic gait cycle than during the first half. This was mainly due to the longer duration of the nonparetic leg stance, leading to the generation of external moments over a longer time interval and a higher range of H.

BBS was negatively correlated with the range of angular-momentum in the frontal plane both during the self-selected ($r = -0.53$, $r < 0.001$) and fastest-comfortable ($r = -0.49$, $r < 0.001$) walking conditions, which was consistent with findings from Nott et al. (2013). That is, better clinical balance scores were associated with lower rang of angular-momentum. The reason for lack of a stronger correlation between the range of angular-momentum and BBS may be attributed to the differences between the two measures. BBS is based on score assignments while completing a series of movement tasks mainly during quiet standing, whereas angular-momentum is obtained using kinematic data and directly reflects the control of whole-body rotations in each plane during dynamic walking. The significant improvements in BBS observed after locomotor training (Bowden et al., 2013) may suggest an overall improvement in performing daily activities. However, it may not provide insight into controlling dynamic balance during walking. The movement tasks included in the DGI score include level ground walking and stair climbing. However, score assignments are based on visual observations. Nevertheless, overall there were no significant improvements in DGI scores after locomotor training (Bowden et al., 2013). In our subject set only four subjects improved their DGI scores above 19 (i.e., threshold for higher likelihood of falls) post-therapy. However, these four subjects did not improve their regulation of angular-momentum and there were no correlations between DGI and the range of angular-momentum.

Biomechanical analysis- responders

In the responder group, clinically meaningful improvements in self-selected walking speed post-therapy were correlated with the improvements in the range of angular-momentum in the frontal and sagittal planes during the fastest-comfortable walking condition. Improvements in the fastest-comfortable walking speed were also

correlated with the improvements in the range of angular-momentum in the sagittal plane. Thus, our hypothesis that improvements in walking speed post-therapy are correlated with improvements in the regulation of angular-momentum was supported. In contrast to the clinical balance scores that did not correlate with the improvements in walking speed (Bowden et al., 2013), the correlations between changes in walking speed and changes in the range of angular-momentum may provide insight into the underlying mechanisms for improvements in walking speed and dynamic balance. Further, the analyses of the peak external moment components within the responder group (pre- and post-therapy combined) revealed how certain characteristics in foot placement and GRFs in specific directions affect dynamic balance in the frontal and sagittal planes (Table 4.3).

Table 4.3. Significant Pearson correlations 'r (p-value)' between biomechanical quantities and the range of angular-momentum (*H*) in the frontal and sagittal planes during the fastest-comfortable walking speed condition. '1st' and '2nd' represent the 1st and 2nd halves of the gait cycle. Correlations are shown for biomechanical quantities from '*Paretic*' and '*Nonparetic*' legs. Data corresponds to the responders (i.e., subjects who increased their self-selected walking speed post-therapy by more than 0.16 m/s).

	H (frontal Plane)		H (sagittal plane 1st)		H (sagittal plane 2nd)	
	Paretic	***Nonparetic***	***Paretic***	***Nonparetic***	***Paretic***	***Nonparetic***
Biomechanical quantity						
Peak anterior moment arm			0.40 (0.06)	-0.41 (0.05)		
Peak posterior moment arm						
Peak vertical moment arm						
Peak M/L moment arm	0.46 (0.02)					
Peak braking GRF			-0.47 (0.02)		-0.57 (0.00)	
Peak propulsive GRF		0.41 (0.04)	-0.40 (0.05)			0.40 (0.05)
Peak vertical GRF (early stance)						
Peak vertical GRF (late stance)						
Peak M/L GRF (early stance)	0.44 (0.03)	0.62 (0.00)		0.64 (0.00)		0.43 (0.03)
Peak M/L GRF (late stance)				0.66 (0.00)		
Braking GRF impulse			-0.50 (0.01)		-0.41 (0.04)	
Propulsive GRF impulse			-0.52 (0.01)	0.59 (0.00)		
Vertical GRF impulse (early stance)			0.45 (0.02)	0.55 (0.00)	0.47 (0.02)	0.51 (0.01)
Vertical GRF impulse (late stance)	-0.79 (0.00)	-0.57 (0.00)			-0.55 (0.01)	-0.46 (0.02)
M/L GRF impulse (early stance)		0.47 (0.02)	0.78 (0.00)	0.73 (0.00)	0.53 (0.01)	0.55 (0.01)
M/L GRF impulse (late stance)		-0.50 (0.01)	0.47 (0.02)			

Foot placement

Placing the paretic foot farther away mediolaterally from the body CoM was associated with a higher range of angular-momentum in the frontal plane, which was negatively correlated ($r = -0.51$, $P = 0.01$) with BBS. Previous work has shown that wider paretic foot placement is strongly related to the lower weight-bearing of the paretic leg (Balasubramanian et al., 2010). Further, a wider mediolateral paretic foot placement along with the gravitational load creates a destabilizing moment about the body CoM, which acts to rotate the body towards the nonparetic leg. In order to maintain dynamic balance, the angular motion of the whole-body about the CoM must be regulated during the single-leg stance and this is achieved by the counteracting hip abductor moment generated by the stance leg (MacKinnon and Winter, 1993). However, previous studies have reported impaired paretic leg hip abductor muscle activity in post-stroke hemiparetic subjects (e.g., Kirker et al., 2000), which can lead to poor regulation of angular-momentum in the frontal plane and decreased balance control. This is consistent with previous studies suggesting hip abductor strengthening to improve lateral stability in post stroke subjects (Mercer et al., 2009).

The anterior foot placement influenced the regulation of angular-momentum in the sagittal plane during the first half of the paretic gait cycle (Table 4.3). Placing the paretic foot farther anteriorly from the body CoM was associated with a higher range of angular-momentum, whereas placing the nonparetic foot farther anteriorly was associated with a lower range of angular-momentum. A previous study has shown that the swing leg foot placement in the anterior-posterior direction is related to the forward propulsion generated by the stance leg (Balasubramanian et al., 2007). They showed that subjects with lower propulsion generated by the paretic leg had shorter nonparetic steps and they compensated by taking a longer paretic step. Thus, in the present study subjects with

longer nonparetic anterior foot placement may have had improved paretic leg ankle plantarflexor output compared to those with shorter nonparetic foot placement. Given the importance of plantarflexors in the regulation of angular-momentum in the sagittal plane (Neptune and McGowan, 2011), improved paretic leg plantarflexor output may lead to improved dynamic balance. This is further discussed below.

Ground reaction forces

Aside from foot placement, GRFs greatly influence the regulation of angular-momentum. Overall, higher mediolateral GRF peaks and impulses were associated with higher range of angular-momentum in both the frontal and sagittal planes. In the vertical direction, GRF impulses generated by both legs positively and negatively correlated with the range of angular-momentum in early and late stance, respectively (Table 4.3). This finding is similar to unilateral below-knee amputees where higher range of angular-momentum in the frontal plane was related to the reduced peak vertical GRFs in both the intact and residual legs during late stance (Silverman and Neptune, 2011). This similarity can be attributed to ankle plantarflexors being primary contributors to body support throughout the single-leg stance (e.g., Anderson and Pandy, 2003; Neptune et al., 2001) and that hemiparetic and unilateral below-knee amputee subjects have diminished plantarflexor output.

In the anterior-posterior direction, the braking (i.e., posterior) GRF peaks and impulses from the paretic leg were negatively correlated with the range of angular-momentum in the sagittal plane (Table 4.3). A similar correlation was reported in below-knee amputees due to reduced residual leg braking (Silverman and Neptune, 2011). More interestingly, higher propulsive (i.e., anterior) GRF peaks from the nonparetic leg were associated with higher range of angular-momentum in both the frontal and sagittal planes.

However, higher propulsive GRF peaks from the paretic leg were associated with lower range of angular-momentum in the sagittal plane. Similarly, the propulsive GRF impulses from the paretic and nonparetic legs negatively and positively correlated with the range of angular-momentum, respectively. Previous simulation analyses of healthy walking have shown that ankle plantarflexors are the primary contributors to forward propulsion (e.g., Liu et al., 2006; Neptune et al., 2001) and the regulation of angular-momentum in both the frontal (Neptune et al., 2011) and sagittal planes (Neptune and McGowan, 2011). Although increased propulsive peaks and impulses from the paretic leg can be achieved by increasing the paretic leg extension (Peterson et al., 2010a), they may also suggest improved plantarflexor activity, leading to improved regulation of angular-momentum and dynamic balance. In contrast, increased propulsive GRF peaks and impulses in the nonparetic leg may suggest impaired paretic leg output and increased reliance on the nonparetic leg compensations.

Conclusions

In summary, locomotor training did not improve dynamic balance for the group of post-stroke hemiparetic subjects. However, for those subjects who achieved a clinically meaningful improvement in their self-selected walking speed, changes in walking speed were correlated with improved dynamic balance as they were able to successfully regulate their whole-body angular-momentum in both the frontal and sagittal planes at their faster walking speeds. Further, the improved regulation of angular-momentum was correlated with changes in foot placement and generation of ground-reaction-forces. Specifically, better balance control was associated with narrower paretic mediolateral foot placement, longer nonparetic anterior foot placement, higher braking GRF peaks and impulses, higher (lower) propulsive GRF peaks and impulses from the paretic

(nonparetic) leg, and higher vertical GRF impulses from both legs in the late stance. Thus, targeting these biomechanical quantities may assist clinicians with designing effective locomotor training programs aimed at improving dynamic balance in post-stroke hemiparetic subjects.

Chapter 5: Individual Muscle Contributions to the Regulation of Whole-body Angular Momentum during Post-stroke Hemiparetic Walking: A Case Study

Introduction

Maintaining dynamic balance is a major challenge in post-stroke hemiparetic subjects (e.g., Czernuszenko, 2007). Previous studies have reported that over 50% of stroke survivors experience falls within one year of their stroke (e.g., Ashburn et al., 2008; Sackley et al., 2008), which can lead to serious injuries and reduced physical activity (e.g., Schmid et al., 2009).

The regulation of whole-body angular momentum is important for maintaining dynamic balance during walking (e.g., Herr and Popovic, 2008). Previous studies have shown that patient populations with balance disorders including amputees (Silverman and Neptune, 2011), children with Cerebral Palsy (Bruijn et al., 2011), and post-stroke hemiparetic subjects (Nott et al., 2013) regulate their whole-body angular momentum differently than healthy subjects. If angular momentum is poorly regulated, it may introduce a control challenge during perturbations (e.g., Pijnappels et al., 2004). Angular momentum is primarily regulated by muscle forces through the generation of ground-reaction-forces (GRFs), which create an external moment about the body center-of-mass (CoM) and control the whole-body angular momentum.

A previous simulation study of healthy subjects during walking used a two-dimensional (2D) musculoskeletal model to investigate the contributions of individual muscles and gravity to the net external moment, which is equal to the time rate of change of angular momentum (Neptune and McGowan, 2011). The primary contributors to the regulation of angular momentum in the sagittal plane were the uniarticular hip and knee extensors, biarticular hamstrings (HAMS), ankle dorsiflexors, soleus (SOL) and gastrocnemius (GAS). In a follow-up study, they extended this work and used a 3D musculoskeletal model to analyze the frontal and transverse planes (Neptune et al., 2011). The angular momentum was small in the transverse plane and almost all muscles had

small contributions to it. In the frontal plane, the vasti (VAS), adductor magnus (AM), gluteus medius (GMED), SOL, GAS and gravity were the primary contributors to the regulation of angular momentum. However, it is not clear which muscles are the primary contributors to the regulation of angular momentum in post-stroke hemiparetic subjects.

Paretic leg plantarflexor weakness has been reported as the primary impairment in post-stroke walking (e.g., Nadeau et al., 1999), which can affect the regulation of angular momentum in both the sagittal and frontal planes. Also, previous simulation analyses of post-stoke limited community walkers (average walking speed = 0.55m/s) have shown that the nonparetic leg rectus femoris (RF) and HAMS increased their contributions to the anterior-posterior (A/P) GRF impulses to compensate for the lack of plantarflexor output (Hall et al., 2011). However, it is not clear if these muscles also contribute to the regulation of angular momentum in post-stoke subjects. Although rehabilitation therapy aims to improve functional balance and motor recovery (Barbeau and Visintin, 2003), it is still not clear whether therapy influences the individual muscle contributions to the regulation of angular momentum. Such insight may assist clinicians in designing exercises that improve balance by targeting specific muscle groups. The purpose of this study was to perform a case study and identify the primary contributors to the regulation of whole-body angular momentum during post-stroke hemiparetic walking and to identify how therapy influenced these individual muscle contributions in a subject with improved dynamic balance post-therapy.

Methods

Data for Simulations

Details regarding the locomotor therapy and experimental data collection and processing were described in Chapter 4. A representative subject with improved dynamic balance (i.e., smaller range of angular momentum post-therapy) and clean (e.g., dynamically consistent) experimental data was selected (subject *A* in Appendix A). The subject (gender: male, age: 56, months since stroke: 12) had a Fugl-Meyer lower extremity assessment score of 24 and 29 pre- and post-therapy, respectively. The self-selected walking speeds in the pre- and post-therapy trials were 0.3 m/s and 0.7 m/s, respectively. Also, the fastest-comfortable walking speed pre-therapy was 0.8 m/s. The experimental data were averaged across the fastest-comfortable speed walking trials pre- and post-therapy (speed-matched trials).

Musculoskeletal Model

A 3D musculoskeletal model (Peterson et al., 2010b) with 23 degrees-of-freedom was used to generate forward dynamics walking simulations of a hemiparetic subject pre- and post-therapy. The model was developed using SIMM (MusculoGraphics, Inc., Santa Rosa, CA) and included rigid segments representing the HAT (head, arms and trunk), pelvis and two legs (femur, tibia, talus, calcaneus and toes). The pelvis had 6 degrees of freedom (3 translations and 3 rotations) with trunk and hip joints modeled as spherical joints. The knee, ankle, subtalar and metatarsophalangeal joints were modeled as single degree of freedom revolute joints. Musculoskeletal geometry was based on a previous study (Delp et al., 1990). The foot-ground contact was modeled using 31 visco-elastic elements with coulomb friction attached to each foot (Neptune et al., 2000). Passive torques were applied at each joint representing the forces applied by the ligaments,

passive tissues and joint structures (Anderson, 1999; Davy and Audu, 1987). The equations of motion were generated using SD/FAST (PTC, Needham, MA) and the forward dynamics simulation framework was produced using Dynamics Pipeline (MusculoGraphics, Inc., Santa Rosa, CA).

Each leg included 38 Hill-type muscle actuators (Table B.1, Appendix B). Given the complex neural control in hemiparetic subjects, a total of 34 independent excitations were used for each leg. Muscle excitations were defined using modified Gaussian patterns in the following form:

$$\mathrm{e(t)} = \mathrm{M}e^{-0.5}\left[\frac{\|x - x_0\|}{\sigma}\right]^n \tag{5.1}$$

where e(t) is the excitation value at time t. M, x_0, σ and n are the amplitude, center point, width and curvature, respectively. The Hill-type muscle model consists of a contractile element (CE) representing muscle fiber force generation, a parallel elastic element (PEE) representing the passive stiffness of the muscle fibers and a series elastic element (SEE) representing the tendon (Fig. 5.1). The total musculotendon actuator length (l^{MT}) depends on the pennation angle (α), the muscle fiber length (l^{M}) and the tendon length (l^{T}).

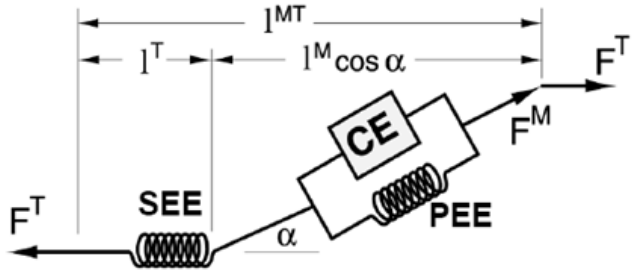

Figure 5.1. Hill-type muscle model, consisting of the series elastic element (SEE), parallel elastic element (PEE) and contractile element (CE). Total musculotendon length (l^{MT}), tendon length (l^T), muscle length (l^M), pennation angle (α), muscle force (F^M) and tendon force (F^T) are shown.

Muscle contraction dynamics are governed by force-length, force-velocity, and tendon force-strain relationships (Fig. 5.2). These relationships were scaled by individual muscle parameters including maximum isometric force (F_o^M), optimal fiber length (l_o^M), tendon slack length (l_s^T), and pennation angle (α). The activation dynamics was modeled using a first-order differential equation (Raasch et al., 1997). The muscle-specific parameters and activation-deactivation constants (Winters and Stark, 1988) are provided in Table B.1 in Appendix B.

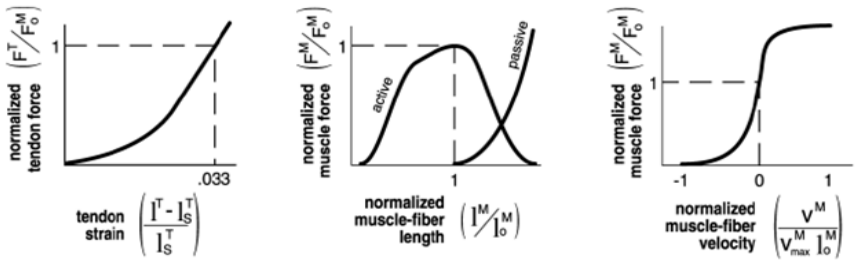

Figure 5.2. Muscle contraction dynamics are governed by tendon force-strain (left), muscle force-length (middle) and muscle force-velocity (right) relationships (Zajac, 1989).

Optimization Framework

Two forward dynamic simulations of walking over a full gait cycle were generated using dynamic optimization to emulate the experimental data for a hemiparetic subject pre- and post-therapy. The muscle excitation patterns (amplitude and timing) and the initial joint angular velocities were optimized using a simulated annealing algorithm (Corana et al., 1987). The following objective function was used to minimize differences between the simulation output and the experimental data while minimizing muscle stress.

$$J = \sum_{i=1}^{n}\left[\sum_{j=1}^{m} w_j \frac{\left(Y_{ij} - \hat{Y}_{ij}\right)^2}{SD_j^2} + w\sum_{k=1}^{p}\frac{F_{ik}}{A_{ik}}\right] \tag{5.2}$$

where w_j is the weighting factor of a variable j, Y_{ij} is the experimental value of a variable j at time step i, $\hat{Y}_{ij}$ is the simulation value for that variable at time step i, and SD_j^2 is the average variability of variable j across trials. The Y quantities in the cost function included joint angles (ankle, knee and 3D hip), 3D trunk rotations, 3D pelvis translations and rotations and 3D GRFs. The second term in the cost function corresponds to muscle stress where w is the weighting factor, F_{ik} is the force and A_{ik} is the corresponding cross section area of muscle k at time step i. Muscle stress is included in the cost function to minimize co-contractions. An initial guess of the muscle excitation parameters and initial joint velocities were defined based on previous simulations of hemiparetic walking. The corresponding simulation values were compared (using the objective function, Eq. 5.2) with the experimental data over a full gait cycle. The muscle excitation parameters were modified until the objective function was minimized (Fig. 5.3).

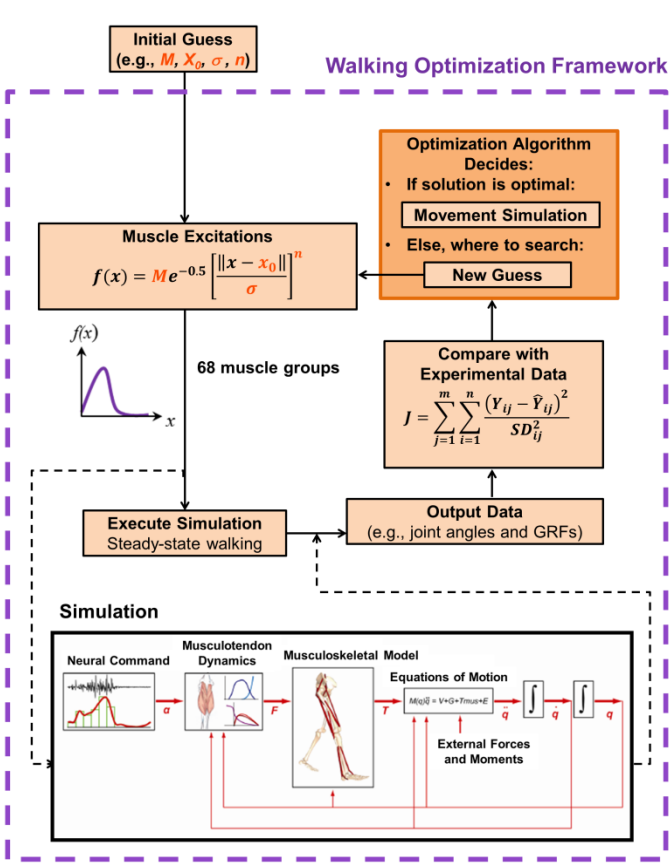

Figure 5.3. Dynamic optimization framework for generating hemiparetic walking simulations.

GRF Decomposition and Contributions to the Net External Moment

In order to identify the contributions of individual muscles to the regulation of angular momentum in 3D, the contributions to the external moments were determined as described in Eq. (4.2) of Chapter 4 as:

$$\vec{M}_{ext} = \vec{r} \times \overrightarrow{GRF} \tag{5.3}$$

The external moment about the body CoM equals the time rate of change of angular momentum and is calculated using the cross product of the moment arm vector from body CoM to CoP and the GRFs vector. To identify the contributions of individual muscles to the GRFs, a ground reaction force decomposition technique was used (Neptune et al., 2004). In short, the state of the system at time step *i* was determined. Then, at time step *i-1* all muscle forces were applied to the system except that of the muscle of interest. The equations of motions were then integrated from step *i-1* to step *i*. The difference between the original GRFs (when all muscle forces were applied) and the new GRFs (excluding the muscle of interest) was considered the contribution of the muscle of interest. This process was repeated for each muscle over the entire gait cycle. The contribution of gravity to external moments was also determined using a similar procedure while setting the gravitational acceleration equal to zero.

Results

The optimized 3D simulations of the hemiparetic gait reproduced kinematics and GRFs similar to those from the experimental data (Appendix C). Simulation results tracked the experimental data within +/-2 standard deviations except for the left hip abduction and part of the ankle angle. Also, the pelvic rotations in the post-therapy simulation were not within the error margin. However, these angles were very small compared to the sagittal-plane joint angles. The average root mean square difference between the experimental data and simulated results for the joint angles were 5.2 degrees (6.4 degrees, post-therapy) and for the normalized GRFs were 6.2% BW (7.0% BW, post-therapy) pre-therapy. The muscle and gravity contributions to the regulation of angular momentum were analyzed based the optimized simulations. The results

corresponding to average healthy control subjects were from a previous study (Neptune et al., 2011) and used for comparison.

Frontal Plane

In the frontal plane, a positive moment corresponds to a clockwise direction. The data for the healthy control subjects and the nonparetic leg corresponds to the left leg. Thus a positive moment for the healthy control data and the nonparetic leg indicates rotation towards the contralateral leg and for the paretic leg indicates rotation towards the ipsilateral leg. Overall, the external moment generation patterns were similar between pre- and post-therapy (Figs. 5.4 and 5.5).

During the nonparetic leg stance, angular momentum was primarily regulated by the VAS, GMED, GAS and SOL muscles (Figs. 5.4 and 5.5). Overall, VAS, GAS and SOL acted to rotate the body towards the paretic leg while GMED acted to rotate the body towards the nonparetic leg. Also, during the late stance, the paretic leg muscles contributed to rotating the body towards the paretic leg (Fig. 5.6). These contributions were mainly from the paretic leg AM, gluteus maximus (GMAX) and HAMS (Figs. D.1 and D.2).

During the paretic leg stance, the external moments were much smaller than those during the nonparetic leg stance (Figs. 5.4 and 5.5). During early stance, AM, GMAX, HAMS and tibialis anterior (TA) acted to rotate the body towards the nonparetic leg while RF and GMED acted to rotate the body towards the paretic leg. Also, the nonparetic leg SOL and GAS acted to rotate the body towards the paretic leg (Fig. D.2) while the gravity acted to rotate the body towards the nonparetic leg (Fig. 5.7). During mid-stance there were small contributions from the nonparetic leg HAMS and GMAX acting to rotate the body towards the nonparetic leg (Fig. D.2). During late stance, there

were small contributions from SOL and GAS acting to rotate the body towards paretic and nonparetic legs, respectively.

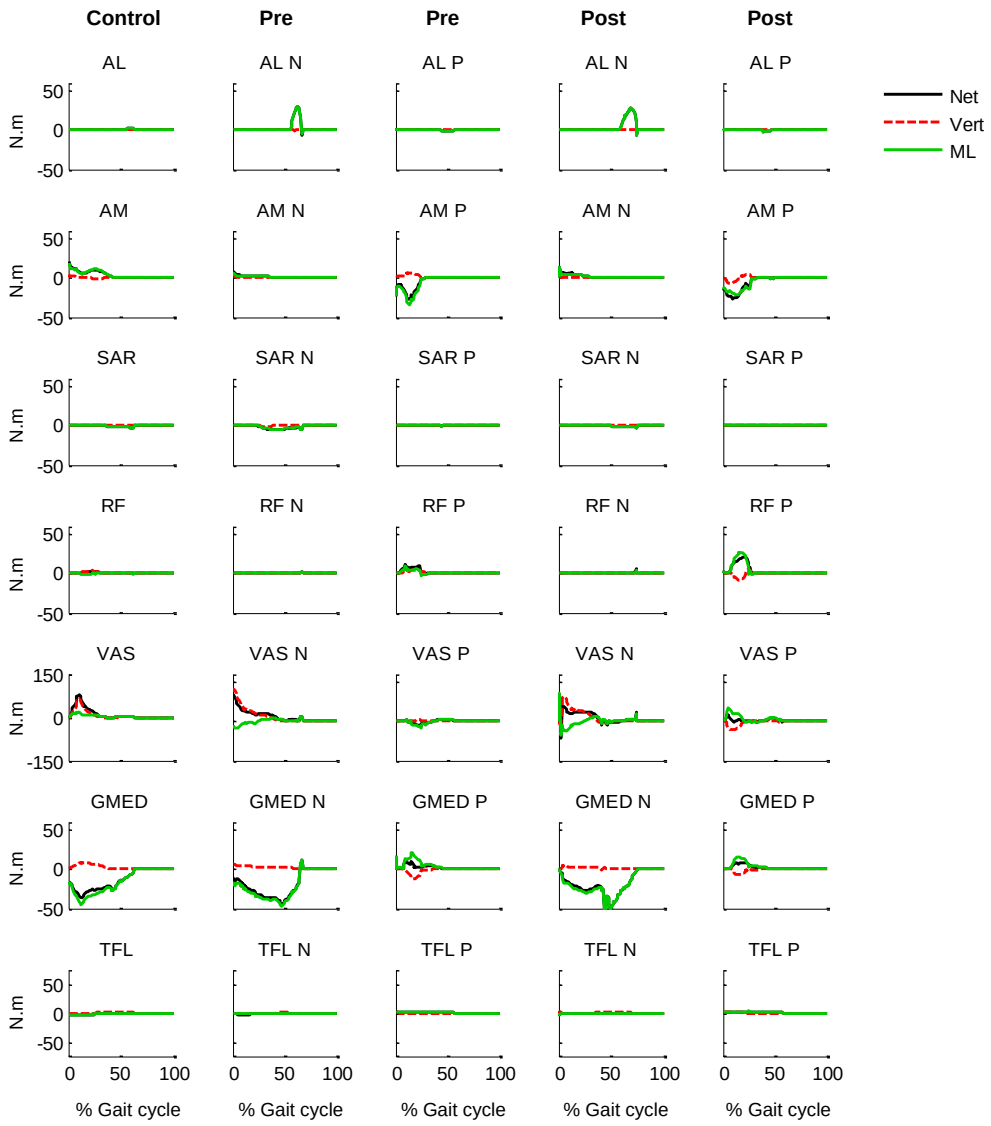

Figure 5.4. Individual muscle contributions to the regulation of angular momentum in the frontal plane for healthy control subjects and the hemiparetic subject pre- and post-therapy. '*N*' and '*P*' indicate nonparetic and paretic legs, respectively. All plots are in the ipsilateral leg reference frame. The muscle contributions to each external moment component as well as the net moment are shown. '*Vert*' corresponds to the moment generated by the mediolateral moment arm and the muscle contributions to the vertical GRF. '*ML*' corresponds to the moment generated by the vertical moment arm and the muscle contributions to the mediolateral GRF. Positive values indicate clockwise moment (left leg: healthy control and the nonparetic leg).

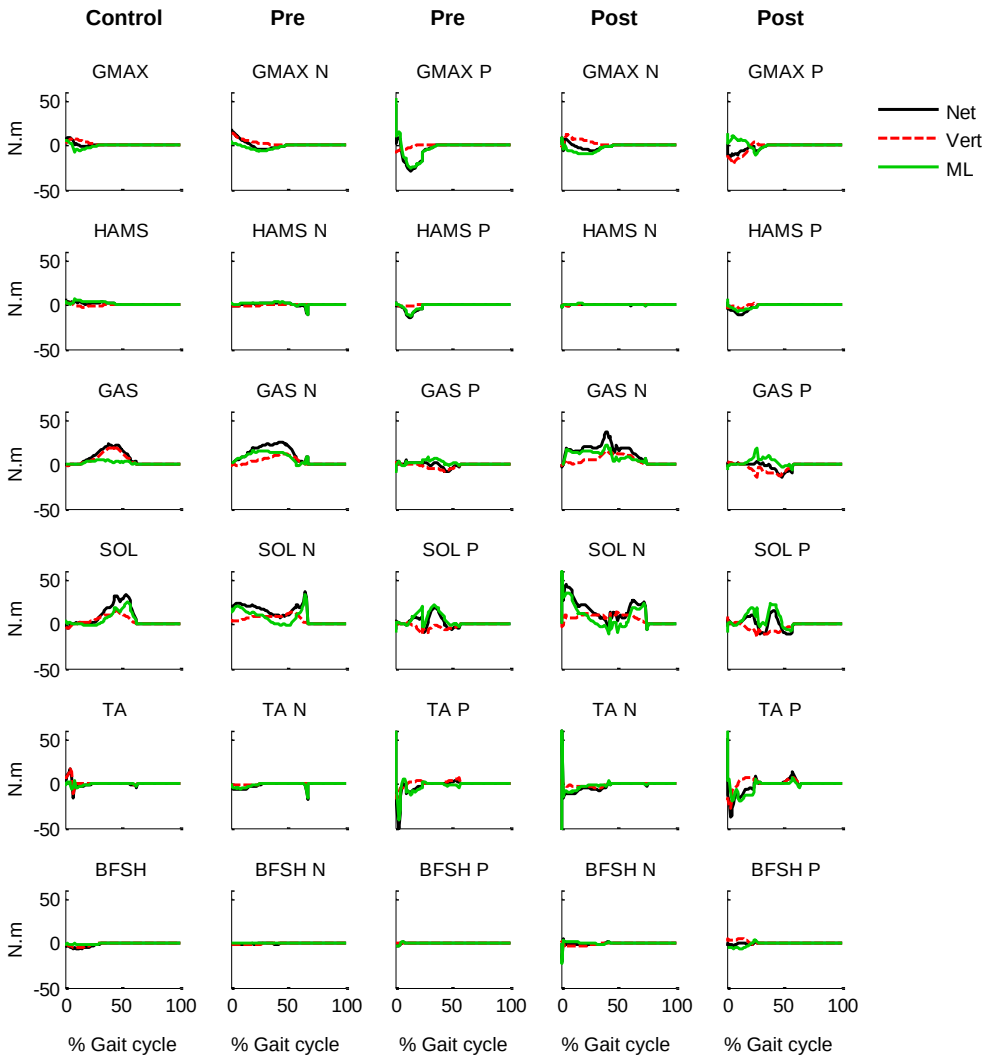

Figure 5.5. Individual muscle contributions to the regulation of angular momentum in the frontal plane for healthy control subjects and the hemiparetic subject pre- and post-therapy. '*N*' and '*P*' indicate nonparetic and paretic legs, respectively. All plots are in the ipsilateral leg reference frame. The muscle contributions to each external moment component as well as the net moment are shown. '*Vert*' corresponds to the moment generated by the mediolateral moment arm and the muscle contributions to the vertical GRF. '*ML*' corresponds to the moment generated by the vertical moment arm and the muscle contributions to the mediolateral GRF. Positive values indicate clockwise moment (left leg: healthy control and the nonparetic leg).

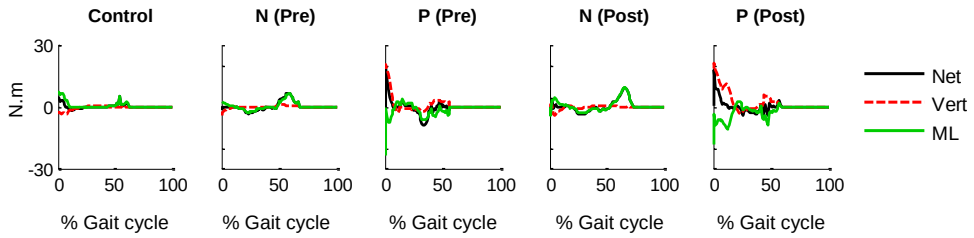

Figure 5.6. Sum of the contralateral leg muscle contributions to the regulation of angular momentum in the frontal plane for healthy control subjects and the hemiparetic subject pre- and post-therapy. '*N*' and '*P*' indicate nonparetic and paretic legs, respectively. All plots are in the ipsilateral leg reference frame. '*Vert*' corresponds to the moment generated by the mediolateral moment arm and the contralateral leg muscle contributions to the vertical GRF. '*ML*' corresponds to the moment generated by the vertical moment arm and the contralateral leg muscle contributions to the mediolateral GRF. Positive values indicate clockwise moment (left leg: healthy control and the nonparetic leg).

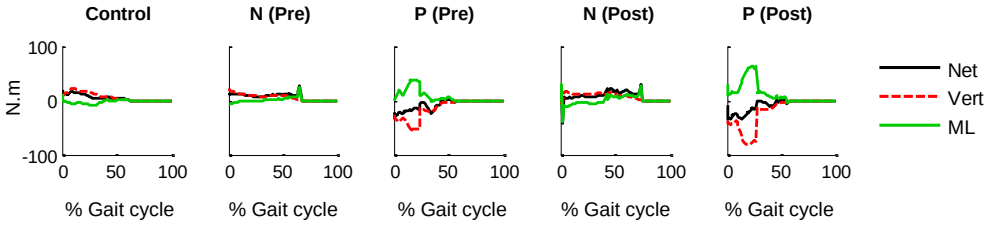

Figure 5.7. Gravity contributions to the regulation of angular momentum in the frontal plane for healthy control subjects and the hemiparetic subject pre- and post-therapy. '*N*' and '*P*' indicate nonparetic and paretic legs, respectively. All plots are in the ipsilateral leg reference frame. '*Vert*' corresponds to the moment generated by the mediolateral moment arm and the gravity contributions to the vertical GRF. '*ML*' corresponds to the moment generated by the vertical moment arm and the gravity contributions to the mediolateral GRF. Positive values indicate clockwise moment (left leg: healthy control and the nonparetic leg).

Sagittal Plane

In the sagittal plane, a positive moment corresponds to a backward rotation. Overall, the external moment generation was similar between pre- and post-therapy (Figs. 5.8 and 5.9). During the nonparetic leg stance, angular momentum was primarily regulated by the VAS, GMED, RF, GMAX, HAMS, GAS, SOL and TA. During early stance, VAS, GAS and SOL acted to rotate the body forward while GMED, GMAX, HAMS, TA and gravity acted to rotate the body backward (Figs. 5.8, 5.9 and 5.11). During late stance, VAS and SOL continued to generate a forward moment along with gravity while GMED, GAS and to some extend HAMS generated a backward moment.

During the paretic leg stance, the moment generations were similar to those during the nonparetic leg stance, except that both the magnitude and duration of moment generation were reduced, particularly for VAS, HAMS, SOL and GAS. Also, GAS only generated a forward moment during mid to late paretic stance and RF generated a forward moment during the early paretic leg stance. In addition, the contributions of the nonparetic leg to the regulation of angular momentum during the paretic leg stance were higher than those from the paretic leg during the nonparetic leg stance (Fig. 5.10). However, there were no clear patterns in the nonparetic muscle contributions between pre- and post- therapy conditions.

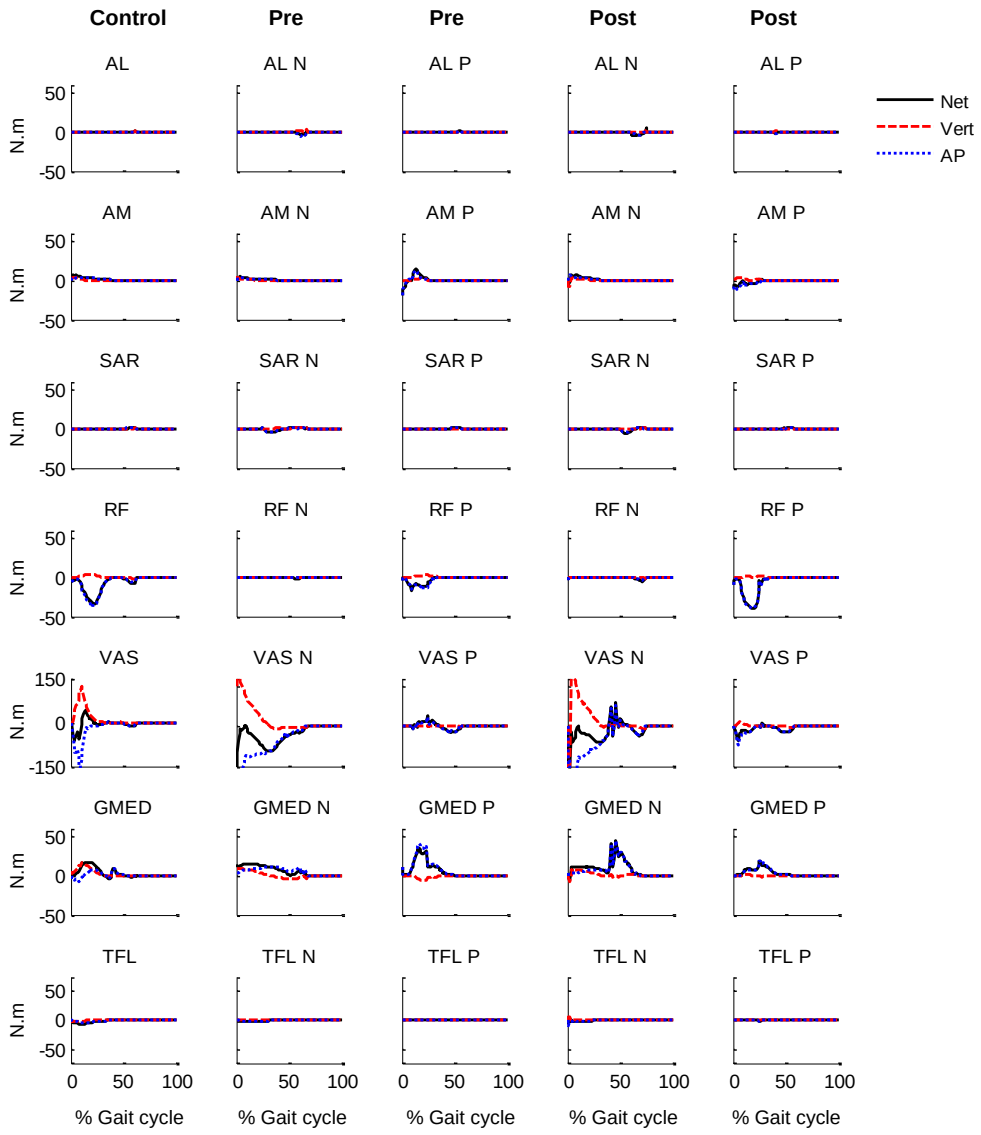

Figure 5.8. Individual muscle contributions to the regulation of angular momentum in the sagittal plane for healthy control subjects and the hemiparetic subject pre- and post-therapy. '*N*' and '*P*' indicate nonparetic and paretic legs, respectively. All plots are in the ipsilateral leg reference frame. The muscle contributions to each external moment component as well as the net moment are shown. '*Vert*' corresponds to the moment generated by the anterior-posterior moment arm and the muscle contributions to the vertical GRF. '*AP*' corresponds to the moment generated by the vertical moment arm and the muscle contributions to the anterior-posterior GRF. Positive (negative) values indicate moment acting to rotate the body backward (forward).

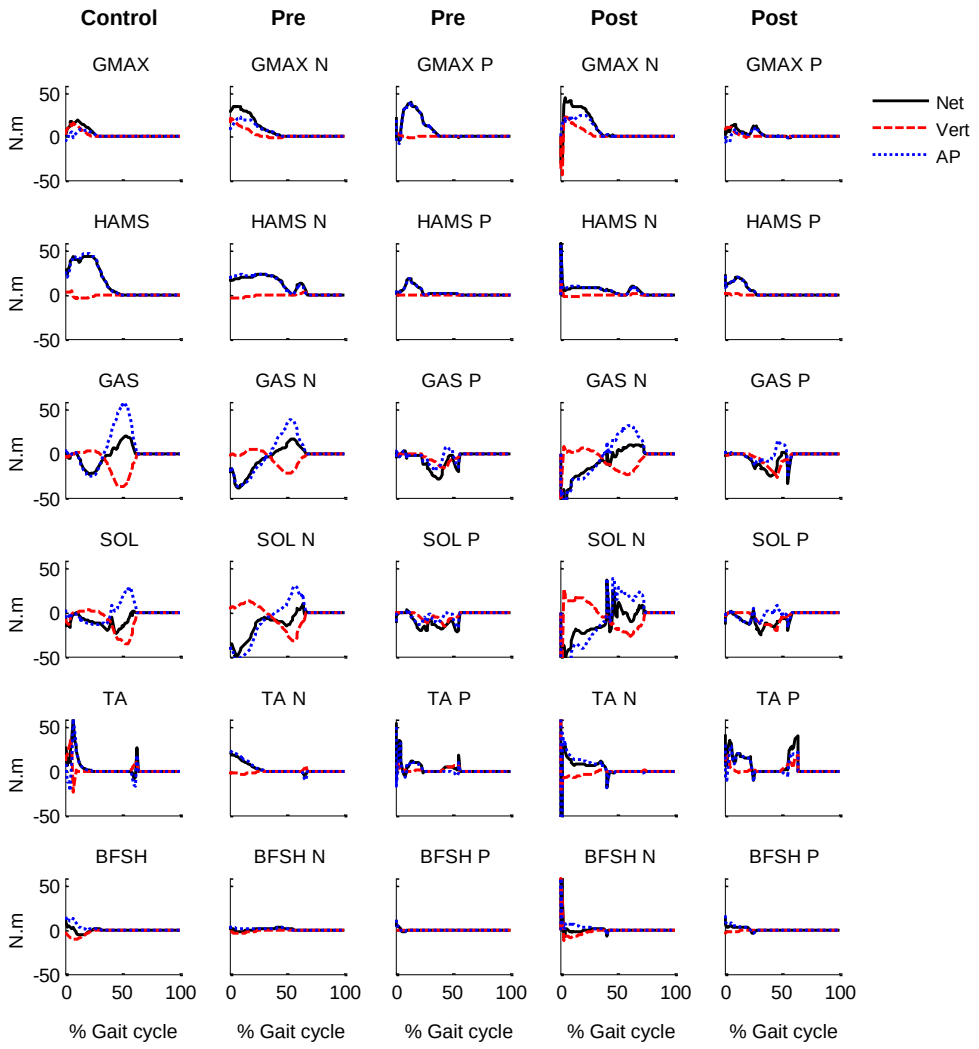

Figure 5.9. Individual muscle contributions to the regulation of angular momentum in the sagittal plane for healthy control subjects and the hemiparetic subject pre- and post-therapy. '*N*' and '*P*' indicate nonparetic and paretic legs, respectively. All plots are in the ipsilateral leg reference frame. The muscle contributions to each external moment component as well as the net moment are shown. '*Vert*' corresponds to the moment generated by the anterior-posterior moment arm and the muscle contributions to the vertical GRF. '*AP*' corresponds to the moment generated by the vertical moment arm and the muscle contributions to the anterior-posterior GRF. Positive (negative) values indicate moment acting to rotate the body backward (forward).

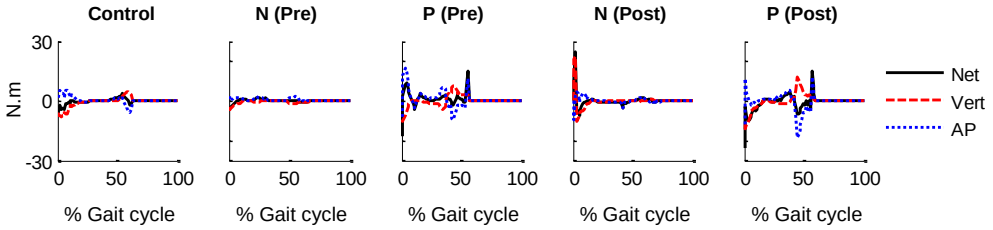

Figure 5.10. Sum of the contralateral leg muscle contributions to the regulation of angular momentum in the sagittal plane for healthy control subjects and the hemiparetic subject pre- and post-therapy. '*N*' and '*P*' indicate nonparetic and paretic legs, respectively. All plots are in the ipsilateral leg reference frame. '*Vert*' corresponds to the moment generated by the anterior-posterior moment arm and the contralateral leg muscle contributions to the vertical GRF. '*AP*' corresponds to the moment generated by the vertical moment arm and the contralateral leg muscle contributions to the anterior-posterior GRF. Positive (negative) values indicate moment acting to rotate the body backward (forward).

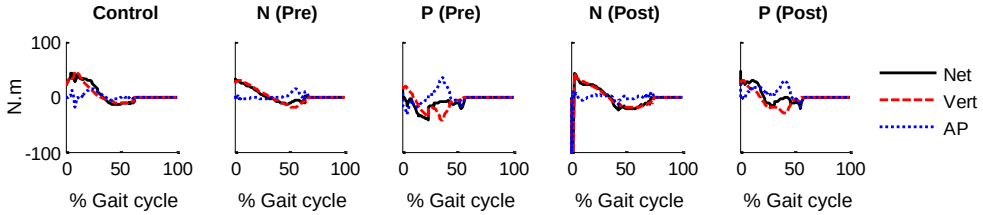

Figure 5.11. Gravity contributions to the regulation of angular momentum in the sagittal plane for healthy control subjects and the hemiparetic subject pre- and post-therapy. '*N*' and '*P*' indicate nonparetic and paretic legs, respectively. All plots are in the ipsilateral leg reference frame. '*Vert*' corresponds to the moment generated by the anterior-posterior moment arm and the gravity contributions to the vertical GRF. '*AP*' corresponds to the moment generated by the vertical moment arm and the gravity contributions to the anterior-posterior GRF. Positive (negative) values indicate moment acting to rotate the body backward (forward).

Discussion

The purpose of this study was to perform a case study and identify the primary contributors to the regulation of whole-body angular momentum during post-stroke hemiparetic walking and to investigate if locomotor therapy influenced these contributions. Overall, the muscle contributions to the regulation of angular momentum were similar between pre- and post-therapy. Although significant differences were observed in the peak external moment arms and GRFs from the experimental data (Appendix A), these small but significant differences were not reflected in the analysis of the individual muscle contributions to the external moments. A potential contributing factor to this lack of difference could be that the simulations were tracking the experimental data within +/-2 standard deviations and not strictly the mean values. Given the complex neural control post-stroke and the asymmetric excitation patterns, it is extremely challenging and computationally expensive to produce hemiparetic walking simulations that emulate the average experimental data. In an effort to accelerate the optimization convergence, alternative optimization algorithms have been tested for other movement tasks that may be applied to walking in the future (Appendix E). However, the simulations in this case study reflected well the characteristics of hemiparetic gait and the analysis provided insight into the primary muscles that contributed to the regulation of angular momentum.

In the frontal plane, during the nonparetic leg stance the primary muscles that contributed to the regulation of whole-body angular momentum were similar to those in healthy control subjects (Figs. 5.4 and 5.5). Overall, VAS, SOL and GAS as well as gravity acted to rotate the body towards the contralateral (paretic) leg, while GMED acted to rotate the body towards the ipsilateral (nonparetic) leg. These findings are consistent with muscle and gravity contributions to the regulation of angular momentum during

healthy walking (Neptune et al., 2011). The major difference between the nonparetic leg muscle contributions and those from healthy control subjects were in the increased contributions from SOL during early nonparetic leg stance. A previous study has shown that during hemiparetic walking, plantarflexor output increased in the nonparetic leg (during the early nonparetic leg stance) to compensate for the reduced propulsion from the paretic leg (Raja et al., 2012).

During the paretic leg stance, the overall paretic leg muscle contributions to the regulation of angular momentum were smaller while the gravity and contralateral leg muscle contributions were larger than those during the nonparetic leg stance as well as in healthy walking (Figs. 5.4-5.7). Of the muscles that contributed to rotating the body towards the contralateral leg, the plantarflexors and VAS in the paretic leg had reduced contributions compared to the healthy controls and the nonparetic leg. Instead, there were increased contributions from gravity and the paretic leg AM, GMAX and to a lesser extent HAMS and TA, all of which contributed to rotating the body towards the contralateral (nonparetic) leg. Previous studies have suggested that the paretic leg hip flexors may compensate for the lack of plantarflexor output (e.g., Nadeau et al., 1999). Thus, it is possible that increased contributions from GMAX were related to the lack of SOL and GAS output in the paretic leg. Of the muscles that contributed to rotating the body towards the ipsilateral leg, paretic leg GMED had reduced contributions compared to healthy controls and the nonparetic leg. Interestingly, SOL and to a lesser extent RF in the paretic leg contributed to rotating the body towards the ipsilateral (paretic) leg. In addition, SOL and GAS from the contralateral (nonparetic) leg contributed to rotating the body towards the paretic leg (Figs. 5.6 and D.2). This is consistent with previous studies suggesting that altered nonparetic leg output may be a compensatory mechanism due to the paretic leg muscle weakness (e.g., Raja et al., 2012).

In the sagittal plane, during the nonparetic leg stance, the primary muscles that contributed to the regulation of whole-body angular momentum were similar to those in healthy control subjects (Figs. 5.8 and 5.9). Overall, GMAX, HAMS, GAS (late stance), TA and GMED as well as gravity (early stance) acted to rotate the body backward, while SOL, GAS (early stance), RF, VAS as well as gravity (late stance) acted to rotate the body forward (Figs. 5.8, 5.9, 5.11). These findings were consistent with those from simulation analyses of healthy walking (Neptune and McGowan, 2011). Also, the contributions from the contralateral (paretic) leg muscles to the nonparetic leg moment generation were small and similar to those from the contralateral leg in healthy walking (Fig. 5.10).

During the paretic leg stance, of the muscles that acted to rotate the body backward, HAMS and GAS (late stance) had reduced contributions compared to those in healthy controls and the nonparetic leg. In contrary to nonparetic leg late stance where GAS acted to rotate the body backward, in paretic leg stance it only acted to rotate the body forward. Instead, to a small extent TA contributed to the backward moment during late stance. Of the muscles that acted to rotate the body forward, SOL (early stance) and VAS in the paretic leg had reduced contributions compared to those in healthy controls and the nonparetic leg. Instead, RF contributed to a forward moment.

In summary, this case study highlighted interesting findings regarding the regulation of angular momentum during post-stroke hemiparetic gait. The primary muscle contributors to the regulation of angular momentum during nonparetic leg stance were similar to those identified during healthy control walking. Although the simulations were not of high enough fidelity to detect differences between pre- and post-therapy, the consistent results between the nonparetic leg and the healthy control walking suggest robustness of the optimized simulations and the analysis in identifying the primary

contributors to the regulation of angular momentum in both healthy and post-stroke populations. Also, the results confirm findings from previous studies regarding the existence of compensatory mechanisms due to the paretic leg muscle weakness (e.g., Raja et al., 2012).

Another interesting finding from this study was the insight into the mechanisms used for regulating angular momentum in the frontal plane. During the nonparetic leg stance, angular momentum was mainly regulated by the nonparetic leg muscles (SOL, GAS and VAS) and gravity acting to rotate the body towards the paretic leg, while GMED acted to rotate the body towards the nonparetic leg. However, during the paretic leg stance, angular momentum was partially regulated by the paretic leg muscles (GMAX, AM and TA) but mainly by gravity acting to rotate the body towards the nonparetic leg, and the nonparetic leg muscles SOL and GAS acting to rotate the body towards the paretic leg. Further, this study highlighted again the importance of plantarflexors in regulating whole-body angular momentum both in the frontal and sagittal planes. Previously, simulation analyses of healthy walking have identified the plantarflexors as the primary contributors to the external moments in the frontal (Neptune et al., 2011) and sagittal (Neptune and McGowan, 2011) planes. Also, a previous study of below-knee amputees suggested the importance of the missing ankle plantarflexors in regulating angular momentum during walking (Silverman and Neptune, 2011). Further, restricting the ankle plantarflexors by wearing a rigid AFO during healthy walking resulted in decreased propulsive impulse (i.e., the time integral of anterior GRFs) generation and poor regulation of angular momentum (Vistamehr et al., 2014). In hemiparetic gait, during the nonparetic leg stance, plantarflexors were still primary contributors to the regulation of angular momentum. However, during the paretic leg stance, due to the paretic ankle muscle weakness, their contributions were reduced.

Although other muscles in both the paretic and nonparetic legs may have partially compensated for this lack of contribution, the compensations alone were not adequate for the proper regulation of angular momentum, resulting in a higher range compared to the healthy control subjects (Fig. A.1, Appendix A). Thus, improving ankle muscle output can potentially improve dynamic balance in post-stroke subjects.

Chapter 6: Conclusions

The overall goal of this research was to understand the walking mechanisms and adaptations used to maintain dynamic balance by analyzing whole-body angular momentum in populations that are susceptible to falls including older adults and post-stroke subjects. This research has provided insight into the underlying mechanisms for maintaining dynamic balance.

In Chapter 2, dynamic balance was analyzed in healthy younger and older adults while walking at self-selected and fastest-comfortable walking speeds. The older adults had a significantly higher range of frontal-plane angular momentum compared to the younger adults at both speeds. This difference was related to the increased step width in the older adults, which when combined with the dominant vertical ground reaction force, created a higher destabilizing external moment during single-leg stance that acted to rotate the body towards the contralateral leg and increased the range of frontal-plane angular momentum. There were no differences in the range of sagittal-plane angular momentum between age groups at either speed. These results suggest that maintaining mediolateral balance may be more challenging than sagittal-plane balance for older adults with a slow self-selected walking speed. The results also highlight the importance of proper foot placement and sufficient muscle strength to generate the ground reaction forces needed to regulate angular momentum and maintain dynamic balance.

In Chapter 3, the influence of a unilateral solid ankle-foot-orthosis on dynamic balance and the generation of forward propulsion during walking were investigated. The results showed that the propulsive impulses decreased in the leg with ankle-foot-orthosis compared to the contralateral leg and no ankle-foot-orthosis condition. Further, the ankle-foot-orthosis resulted in a greater range of angular momentum in both the frontal and sagittal planes, which were correlated with the reduced peak hip abduction and reduced ankle plantarflexor moments, respectively. Thus, solid ankle-foot-orthoses limit the

successful execution of important mobility subtasks in healthy adults and that the prescription of ankle-foot-orthosis should be carefully considered.

In Chapter 4, the influence of locomotor rehabilitation therapy on dynamic balance during post-stroke hemiparetic gait was investigated. Overall, the specific locomotor training used did not improve dynamic balance in the post-stroke subjects. However, for those subjects who achieved a clinically meaningful improvement in their self-selected walking speed, their change in speed was correlated with improved dynamic balance. Further, improved dynamic balance was associated with narrower mediolateral paretic foot placement, longer anterior nonparetic steps, higher braking ground-reaction-force peaks and impulses, higher (lower) propulsive ground-reaction-force peaks and impulses from the paretic (nonparetic) leg, and higher vertical ground-reaction-force impulses from both legs during the late stance. Targeting these biomechanical quantities may assist clinicians with designing effective locomotor therapies for improving dynamic balance in post-stroke subjects.

In Chapter 5, individual muscle contributions to the regulation of angular momentum during post-stroke gait (pre- and post-therapy) were identified through musculoskeletal modeling and forward dynamics simulations. Overall, the muscle contributions to the regulation of angular momentum were similar between pre- and post-therapy. The primary muscle contributors to the regulation of angular momentum during the nonparetic leg stance were similar to those identified during healthy control walking, with the ankle plantarflexors contributing to both the frontal- and sagittal-plane angular momentum. However, during the paretic leg stance phase, due to paretic leg muscle weakness, there were decreased contributions from the paretic muscles and increased compensations from the nonparetic leg muscles as well as gravity. This study highlighted the importance of ankle plantarflexors, knee extensors and hip abductors in regulating

whole-body angular momentum. Thus, exercise programs that target improving the output from these muscles in the paretic leg can potentially improve dynamic balance in post-stroke subjects.

Publications from this research

Vistamehr, A., Kautz, S.A. and Neptune, R.R. (2014). **The influence of solid ankle-foot orthoses on forward propulsion and dynamic balance in healthy adults during walking.** *Clinical Biomechanics* (in press)

Vistamehr, A., Kautz, S.A., Bowden, M. and Neptune, R.R. (2014). **The influence of locomotor training on dynamic balance and its relation with increased walking speed in post-stoke hemiparetic subjects.** *Journal of Biomechanics* (in preparation)

Chapter 7: Future Work

The overall goal of this work was to understand mechanisms for maintaining dynamic balance in both the older adults and post-stroke hemiparetic subjects. The results provided rationale for improving current rehabilitation therapies by improving the output of specific lower-extremity muscles and proper foot placement and carefully considering the prescription of ankle-foot orthoses. This work can be expanded in several areas.

In Chapter 2, poor balance control in older adults was associated with a wider mediolateral step and a lower hip abductor moment. However, the influence of wider steps on dynamic balance of the older adults during perturbed walking should be further investigated. For example, subjects can walk with controlled step widths (narrow and wide) while external lateral perturbations are applied. Such a study would identify whether wider or narrower step widths can assist older adults with successfully recovering from similar perturbations.

In Chapter 3, the results showed that widely prescribed solid ankle-foot-orthoses can limit the successful execution of important mobility subtasks in healthy adults. The next step would be to investigate the influence of solid AFOs in post-stroke hemiparetic walking. Further, future studies should aim at identifying biomechanical measures that can distinguish which post-stroke subjects (depending on severity of stroke) can benefit from specific types of AFOs. For example, in cases where an AFO is needed to compensate for foot drop, perhaps more advanced AFOs that promote plantarflexion can be used. Also, forward dynamic simulations of both healthy and post-stroke subjects walking with and without an AFO would provide insight into the functional roles of AFOs during walking and the influence of AFOs on individual muscle contributions to mobility subtasks.

In Chapters 4 and 5, dynamic balance was analyzed in post-stroke hemiparetic subjects. Important biomechanical quantities pertaining to foot placement and GRF

generation were identified for potentially improving dynamic balance. Future work should target these quantities in locomotor therapy and re-evaluate the effectiveness of balance training in the current rehabilitation programs. Also, simulation analyses of hemiparetic walking can provide a powerful tool for evaluating the effectiveness of rehabilitation therapy. Thus, developing an optimization framework that can produce quickly simulations of hemiparetic walking that accurately emulate the experimental data can indeed be a valuable contribution to the field. We have developed and implemented an alternative optimization algorithm for producing simulations of pedaling movement (Appendix E). Future work should investigate if this method can also accelerate the optimization convergence for walking simulations.

Appendix A: Dynamic Balance Analysis for Two Post-stroke Hemiparetic Subjects

Whole-body angular momentum and peak external moment components were analyzed for two representative subjects (*A,* improved dynamic balance post-therapy; *B,* did not improve dynamic balance post-therapy) in Chapter 4. Also, in Chapter 5, forward dynamics simulations of walking pre- and post-therapy were generated for Subject *A* with improved balance.

The angular momentum profiles and peak-to-peak ranges pre- and post-therapy are presented here for subjects *A* and *B* (Fig. A.1). In Subject *A*, the range of angular momentum in the frontal and sagittal (2^{nd} half of the gait cycle) planes decreased post-therapy, whereas in Subject *B* the range of angular momentum in the sagittal plane increased post-therapy. Assessments of the biomechanical quantities for subjects *A* and *B* show that the two subjects used different adaptations in their external moment components to regulate their whole-body angular momentum.

In the frontal plane for Subject *A,* step width, peak M/L moment arm and peak vertical GRF (generated by the nonparetic leg) decreased post-therapy (Fig. A.2). These adaptations were correlated with a decreased range of angular momentum (Table A.1). However, in Subject *B*, both step width and peak vertical GRF (generated by the nonparetic leg) increased post-therapy (Fig. A.3). In the sagittal plane for both subjects, the peak vertical GRF in the nonparetic leg during late stance was positively correlated with the range of angular momentum (Tables A.1 and A.2). Contrary to Subject *A*, the peak vertical GRF in the nonparetic leg (during early and late stance) increased in Subject *B*. Also, in the other moment component (i.e., the vertical moment arm and A/P GRF) the vertical moment arm in the paretic leg was negatively correlated with the range of angular momentum in both subjects. However, contrary to Subject *A* this quantity decreased in Subject *B*. Lastly, the peak braking GRF in the paretic leg, which was positively correlated with the range of angular momentum in both subjects, decreased in

Subject *A* but increased in Subject *B*. More importantly, the peak propulsive GRF in the paretic leg, which was negatively correlated with the range of angular momentum in both subjects, increased in Subject *A* but decreased in Subject *B* (Figs. A.2 and A.3). Further, the propulsive GRF impulses in the paretic leg were nearly zero in Subject *B*, suggesting they had poor plantarflexor output. Previous simulation analyses of post-stroke walking have shown that deficits in paretic leg muscle contributions to forward propulsion were directly related to a poor functional walking status (Hall et al., 2011). This finding holds true in both subjects. Subject *A* with improved paretic leg propulsive impulse was classified as community walker with overground walking speeds of 0.76 m/s and 1.08 m/s pre- and post-therapy, indicating improved functional walking status. In contrast, Subject *B* with poor paretic plantarflexor output was classified as limited community walker with overground walking speeds of 0.43 m/s and 0.59 m/s pre- and post-therapy, indicating poor functional walking status.

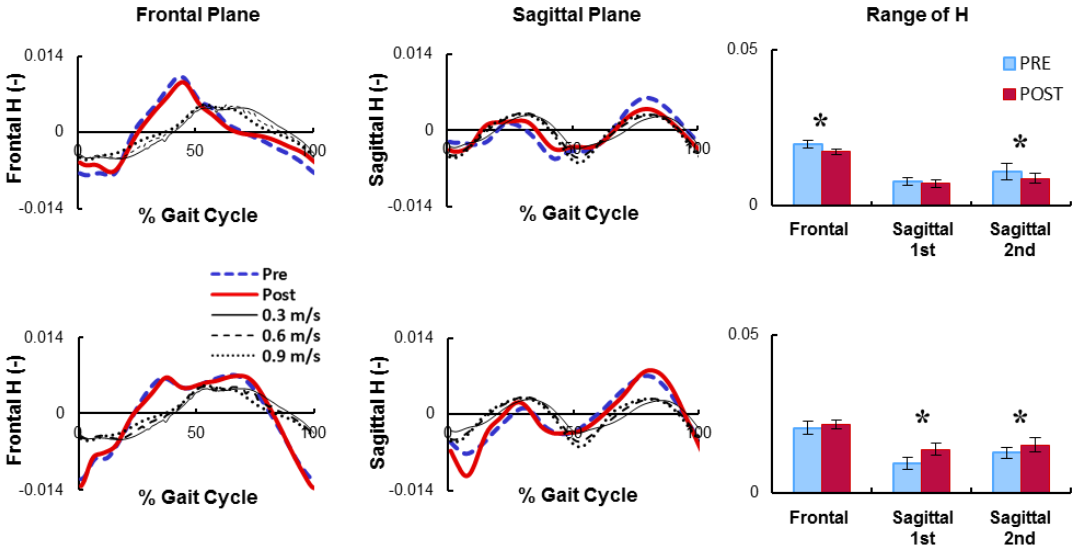

Figure A.1. Normalized, mean angular momentum (*H*) in the frontal and sagittal planes during the fastest-comfortable (FC) walking condition pre- and (speed-matched) post-therapy. Top and bottom rows correspond to Subject *A* (improved balanced post-therapy, FC speed: 0.8 m/s) and Subject *B* (did not improve balance post-therapy, FC speed: 0.4 m/s), respectively. Normalized, mean *H* is also shown for healthy control subjects when walking at 0.3 m/s, 0.6 m/s and 0.9 m/s speeds. The mean (± SD) range of *H* in the frontal plane and sagittal plane during the 1st and 2nd halves of the gait cycle is shown on the right. Statistically significant differences in each subject between pre- and post-therapy are indicated with '*' ($p < 0.05$).

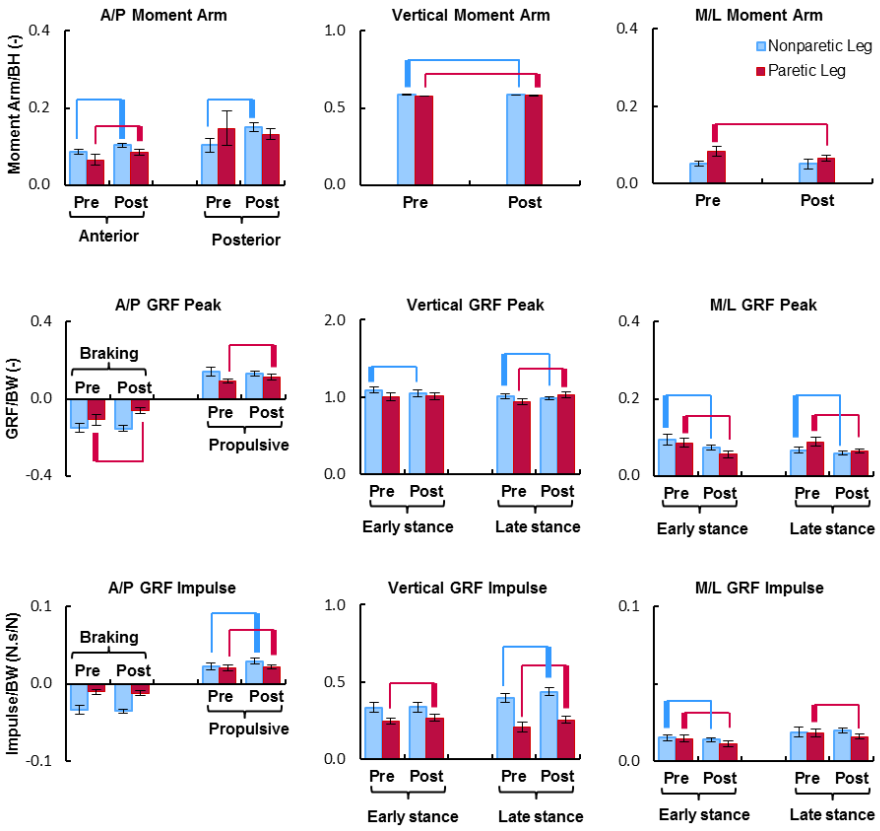

Figure A.2. Biomechanical quantities for Subject *A* (with improved balance post-therapy) during the fastest-comfortable walking speed (0.8 m/s) condition pre- and post-therapy. Top row shows the body-height normalized, mean (± SD) moment arms. Middle row shows the body weight-normalized, mean (± SD) peak *GRFs*. Bottom row shows the body weight-normalized, mean (± SD) *GRF* impulses during early and late stance. Significant differences pre- and post-therapy are shown with brackets. Thicker side of the bracket corresponds to a higher value.

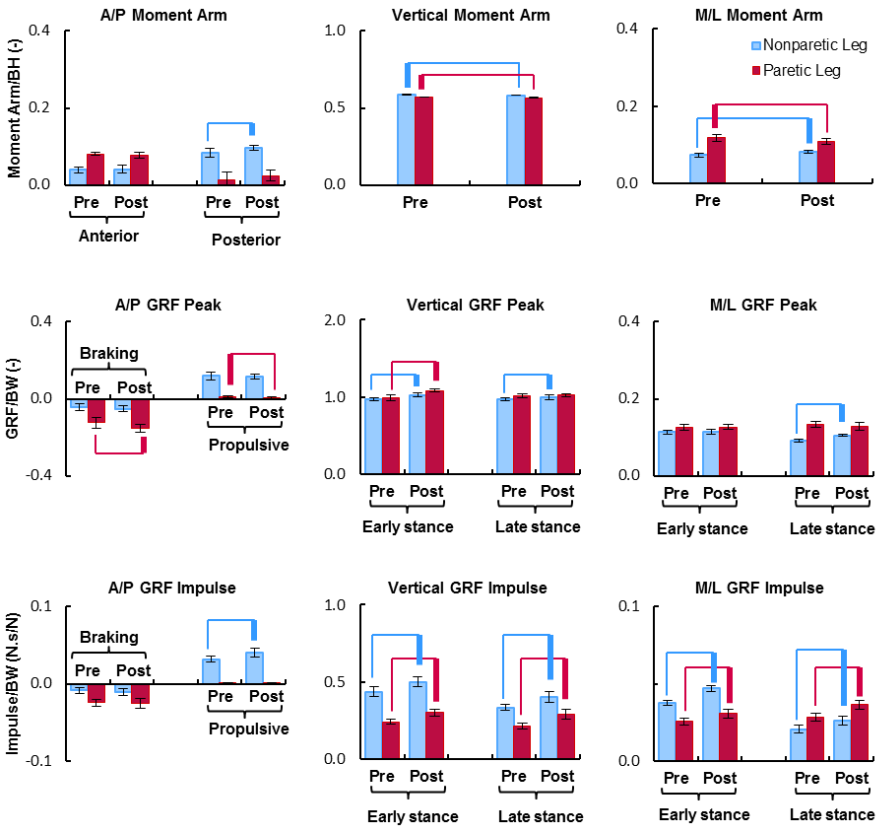

Figure A.3. Biomechanical quantities for Subject *B* (with no improvement in balance post-therapy) during the fastest-comfortable walking speed (0.4 m/s) condition pre- and post-therapy. Top row shows the body-height normalized, mean (± SD) moment arms. Middle row shows the body weight-normalized, mean (± SD) peak *GRFs*. Bottom row shows the body weight-normalized, mean (± SD) *GRF* impulses during early and late stance. Significant differences pre- and post-therapy are shown with brackets. Thicker side of the bracket corresponds to a higher value.

Table A.1. Significant Pearson correlations 'r (p-value)' between biomechanical quantities and the range of angular momentum (*H*) in the frontal and sagittal planes during fastest-comfortable walking speed (0.8 m/s) condition. '1st' and '2nd' represent the 1st and 2nd halves of the gait cycle. Correlations are shown for biomechanical quantities from '*Paretic*' and '*Nonparetic*' legs. Data corresponds to Subject ***A*** with improved balance post-therapy.

	H (frontal plane)		H (sagittal plane 1st)		H (sagittal plane 2nd)	
	Paretic	***Nonparetic***	***Paretic***	***Nonparetic***	***Paretic***	***Nonparetic***
Biomechanical quantity						
Peak anterior moment arm	-0.45 (0.002)	-0.41 (0.005)			-0.37 (0.013)	
Peak posterior moment arm		-0.60 (0.000)				-0.42 (0.005)
Peak vertical moment arm		0.36 (0.015)	-0.30 (0.046)		-0.45 (0.002)	0.35 (0.020)
Peak M/L moment arm	0.54 (0.000)					
Peak braking GRF	0.52 (0.000)				0.42 (0.004)	
Peak propulsive GRF	-0.33 (0.028)	0.36 (0.017)			-0.37 (0.014)	
Peak vertical GRF (early stance)	-0.34 (0.025)					
Peak vertical GRF (late stance)	-0.62 (0.000)	0.42 (0.004)				0.54 (0.000)
Peak M/L GRF (early stance)	0.69 (0.000)	0.62 (0.000)				
Peak M/L GRF (late stance)	0.63 (0.000)	0.33 (0.029)				
Braking GRF impulse			-0.31 (0.042)			
Propulsive GRF impulse		-0.48 (0.001)				-0.31 (0.041)
Vertical GRF impulse (early stance)	-0.46 (0.002)					
Vertical GRF impulse (late stance)	-0.48 (0.001)	-0.45 (0.002)				
M/L GRF impulse (early stance)	0.50 (0.001)	0.31 (0.041)				
M/L GRF impulse (late stance)	0.37 (0.013)				0.47 (0.001)	

Table A.2. Significant Pearson correlations 'r (p-value)' between biomechanical quantities and the range of angular momentum (*H*) in the frontal and sagittal planes during fastest-comfortable walking speed (0.4 m/s) condition. '1st' and '2nd' represent the 1st and 2nd halves of the gait cycle. Correlations are shown for biomechanical quantities from '*Paretic*' and '*Nonparetic*' legs. Data corresponds to Subject ***B*** with no improvement in balance post-therapy.

	H (frontal plane)		H (sagittal plane 1st)		H (sagittal plane 2nd)	
	Paretic	***Nonparetic***	***Paretic***	***Nonparetic***	***Paretic***	***Nonparetic***
Biomechanical quantity						
Peak anterior moment arm			-0.41 (0.023)			
Peak posterior moment arm	0.40 (0.026)		0.40 (0.025)			
Peak vertical moment arm		0.40 (0.027)	-0.59 (0.000)	-0.56 (0.001)		
Peak M/L moment arm			-0.50 (0.004)	0.66 (0.000)		0.43 (0.016)
Peak braking GRF			0.55 (0.001)			
Peak propulsive GRF		0.48 (0.006)	-0.32 (0.078)		-0.47 (0.007)	
Peak vertical GRF (early stance)			0.81 (0.000)	0.55 (0.001)	0.51 (0.004)	0.58 (0.001)
Peak vertical GRF (late stance)						
Peak M/L GRF (early stance)						
Peak M/L GRF (late stance)				0.77 (0.000)		0.48 (0.006)
Braking GRF impulse				0.36 (0.043)	0.39 (0.028)	
Propulsive GRF impulse				0.38 (0.034)		0.46 (0.010)
Vertical GRF impulse (early stance)	0.37 (0.042)		0.74 (0.000)	0.59 (0.000)	0.52 (0.002)	0.51 (0.004)
Vertical GRF impulse (late stance)			0.69 (0.000)	0.63 (0.000)	0.51 (0.003)	0.54 (0.002)
M/L GRF impulse (early stance)			0.66 (0.000)	0.83 (0.000)	0.43 (0.017)	0.40 (0.027)
M/L GRF impulse (late stance)			0.71 (0.000)	0.57 (0.001)	0.40 (0.026)	0.53 (0.002)

Appendix B: Muscle Parameters

Table B.1. Muscles included in the musculoskeletal model and their parameters including maximum isometric force (F_o^M), optimal fiber length (l_o^M), tendon slack length (l_s^T), pennation angle (α) and activation (τ_{act}) and deactivation (τ_{deact}) time constants.

Muscle name	Analysis group	F_O^M (N)	l_O^M (cm)	l_S^T (cm)	α (°)	τ_{act} (ms)	τ_{deact} (ms)
Iliacus	IL	429	10	9	7	12	48
Psoas	IL	371	10.4	13	8	12	48
Adductor Longus	AL	418	13.8	11	6	12	48
Adductor Brevis	AL	286	11.3	2	0	12	48
Pectineus	AL	177	13.3	0.1	0	12	48
Quadratus Femoris	QF	254	5.4	2.4	0	12	48
Superior Adductor Magnus	AM	346	8.7	6	5	12	48
Middle Adductor Magnus	AM	312	12.1	13	3	12	48
Inferior Adductor Magnus	AM	444	13.1	26	5	12	48
Sartorius	SAR	104	57.9	4	0	9	43
Rectus Femoris	RF	779	8.4	34.6	5	9	39
Vastus Medialis	VAS	1294	8.9	12.6	5	17	61
Vastus Lateralis	VAS	1871	8.4	15.7	5	16	58
Vastus Intermedius	VAS	1365	8.7	13.6	3	13	50
Anterior Gluteus Medius	GMED	546	5.35	7.8	8	12	48
Middle Gluteus Medius	GMED	382	8.45	5.3	0	12	48
Posterior Gluteus Medius	GMED	435	6.46	5.3	19	12	48
Piriformis	PIRI	296	2.6	11.5	10	12	48
Gemellus	GEM	109	2.4	3.9	0	12	48
Anterior Gluteus Minimus	GMIN	180	6.8	1.6	10	12	48
Middle Gluteus Minimus	GMIN	190	5.6	2.6	0	12	48
Posterior Gluteus Minimus	GMIN	215	3.8	5.1	21	12	48
Tensor Fascia Lata	TFL	155	9.5	42.5	3	12	48
Anterior Gluteus Maximus	GMAX	382	14.2	12.5	5	12	48
Middle Gluteus Maximus	GMAX	546	14.7	12.7	0	12	48
Posterior Gluteus Maximus	GMAX	368	14.4	14.5	5	12	48
Semitendinosus	HAM	328	20.1	26.2	5	12	48
Semimembranosus	HAM	1030	8	35.9	15	17	59
Gracilis	HAM	108	35.2	14	3	12	48
Biceps Femoris Long Head	HAM	717	10.9	34.1	0	17	60
Biceps Femoris Short Head	BFSH	402	17.3	10	23	11	45
Medial Gastrocnemius	GAS	1113	4.5	40.8	17	11	45
Lateral Gastrocnemius	GAS	488	6.4	38.5	8	9	38
Soleus	SOL	2839	3	26.8	25	31	111
Tibialis Posterior	SOL	1270	3.1	31	12	10	43
Flexor Digitorum Longus	SOL	310	3.4	40	7	9	39
Tibialis Anterior	TA	603	9.8	22.3	5	15	55

Appendix C: Simulated and Experimental Data Comparisons

The experimental data for subject *A*, used in dynamic optimizations in Chapter 5 are shown in Figs. C.1-C.3 (pre-therapy) and Figs. C.4-C.6 (post-therapy). Also, the optimized simulated GRFs and kinematics are shown in blue (--).

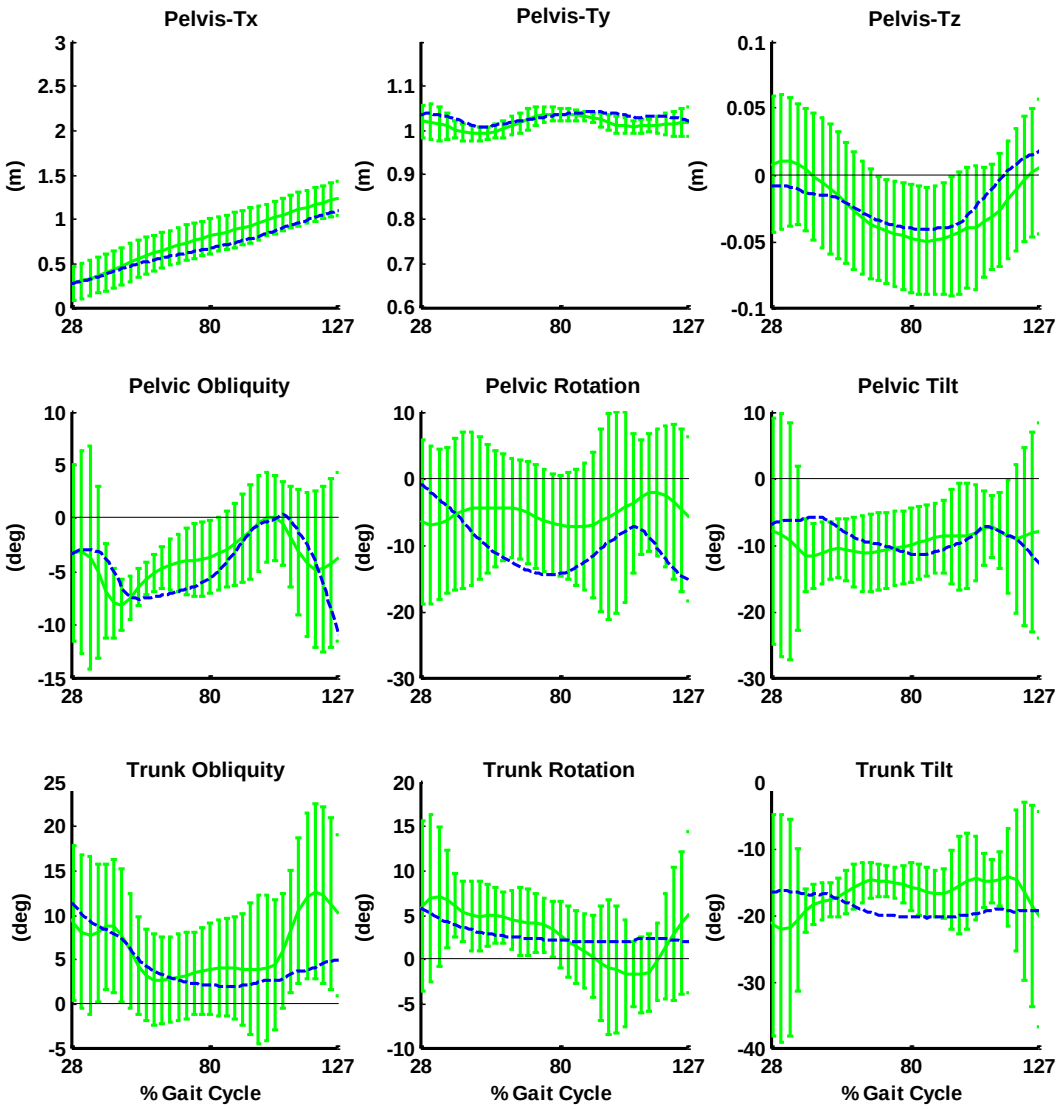

Figure C.1. Simulated and experimental kinematic data for subject *A* (in Appendix A and Chapter 5) walking at 0.8 m/s, pre-therapy. Data is shown in the right (paretic) leg reference frame, 28% after right heel strike. The experimental data average (+/- 2 standard deviations) across trials is shown in green (bars).

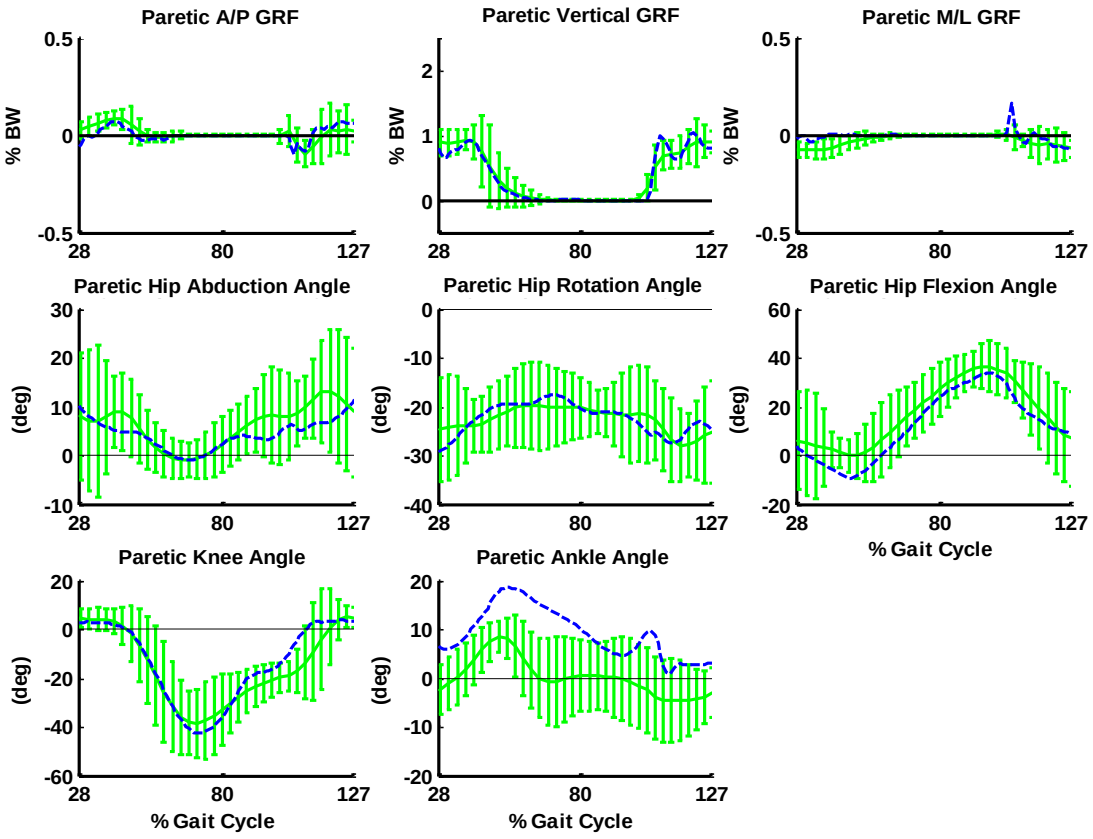

Figure C.2. Simulated and experimental GRF and kinematic data for subject *A* (in Appendix A and Chapter 5) walking at 0.8 m/s, pre-therapy. Data is shown in the right (paretic) leg reference frame, 28% after right heel strike. The experimental data average (+/- 2 standard deviations) across trials is shown in green (bars).

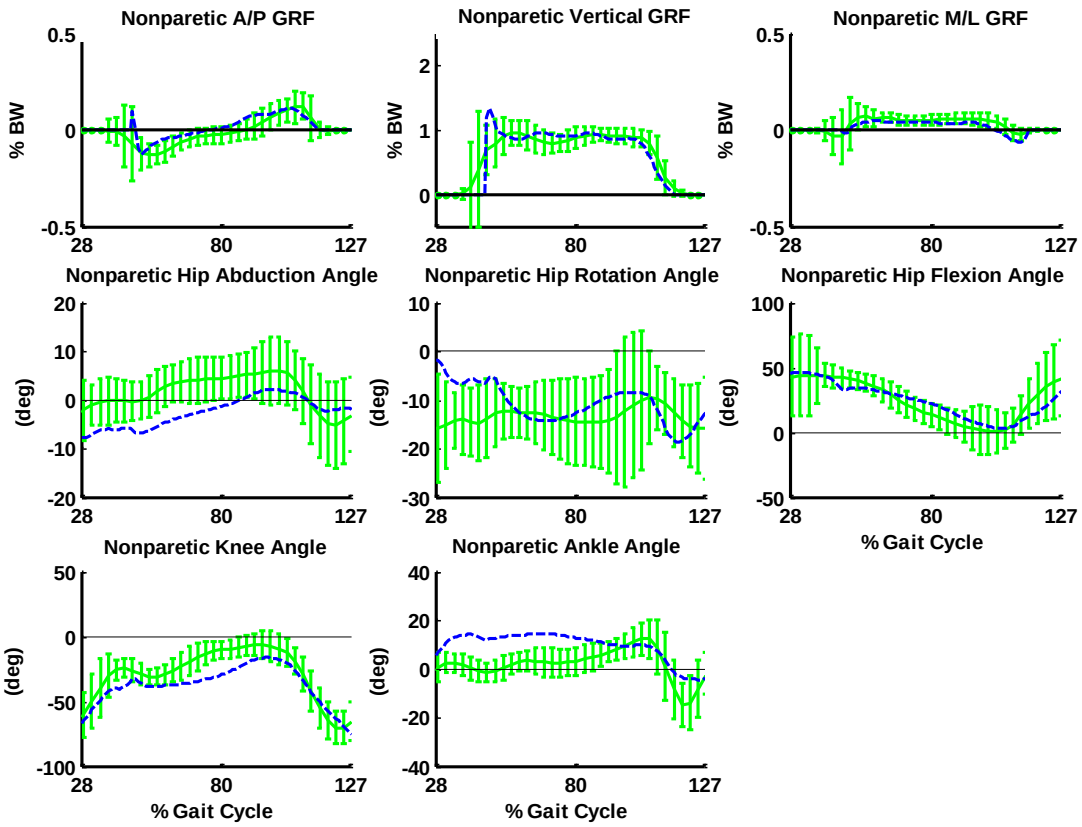

Figure C.3. Simulated and experimental GRF and kinematic data for subject *A* (in Appendix A and Chapter 5) walking at 0.8 m/s, pre-therapy. Data is shown in the right (paretic) leg reference frame, 28% after right heel strike. The experimental data average (+/- 2 standard deviations) across trials is shown in green (bars).

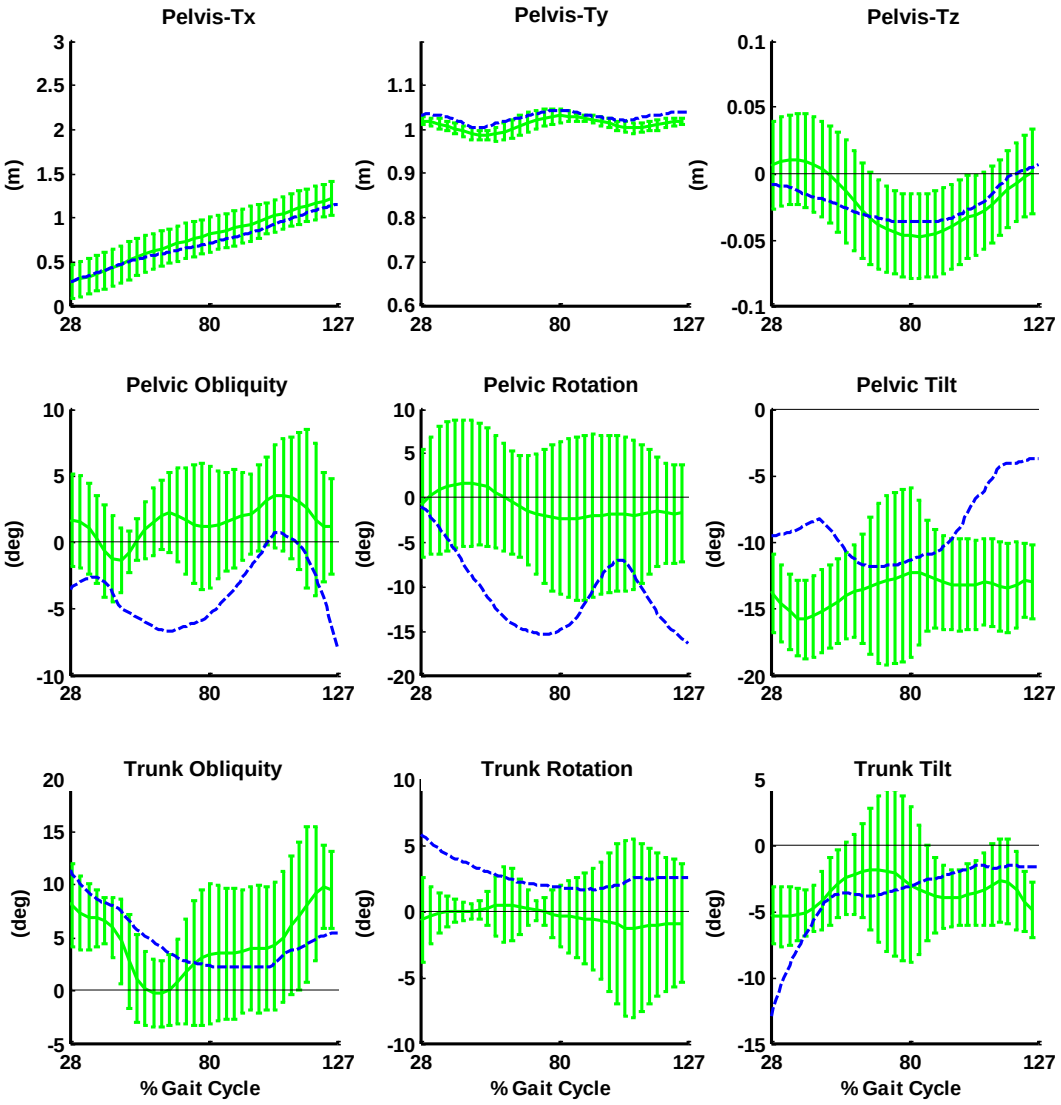

Figure C.4. Simulated and experimental kinematic data for subject *A* (in Appendix A and Chapter 5) walking at 0.8 m/s, post-therapy. Data is shown in the right (paretic) leg reference frame, 28% after right heel strike. The experimental data average (+/- 2 standard deviations) across trials is shown in green (bars).

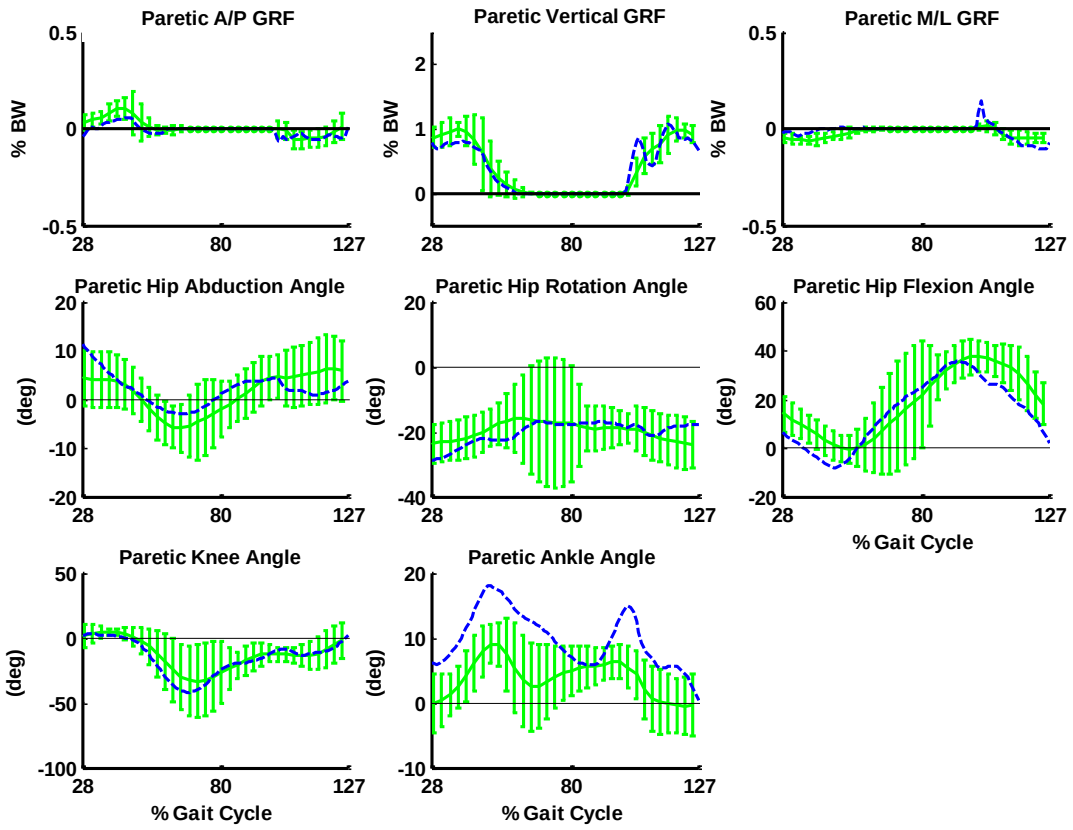

Figure C.5. Simulated and experimental GRF and kinematic data for subject *A* (in Appendix A and Chapter 5) walking at 0.8 m/s, post-therapy. Data is shown in the right (paretic) leg reference frame, 28% after right heel strike. The experimental data average (+/- 2 standard deviations) across trials is shown in green (bars).

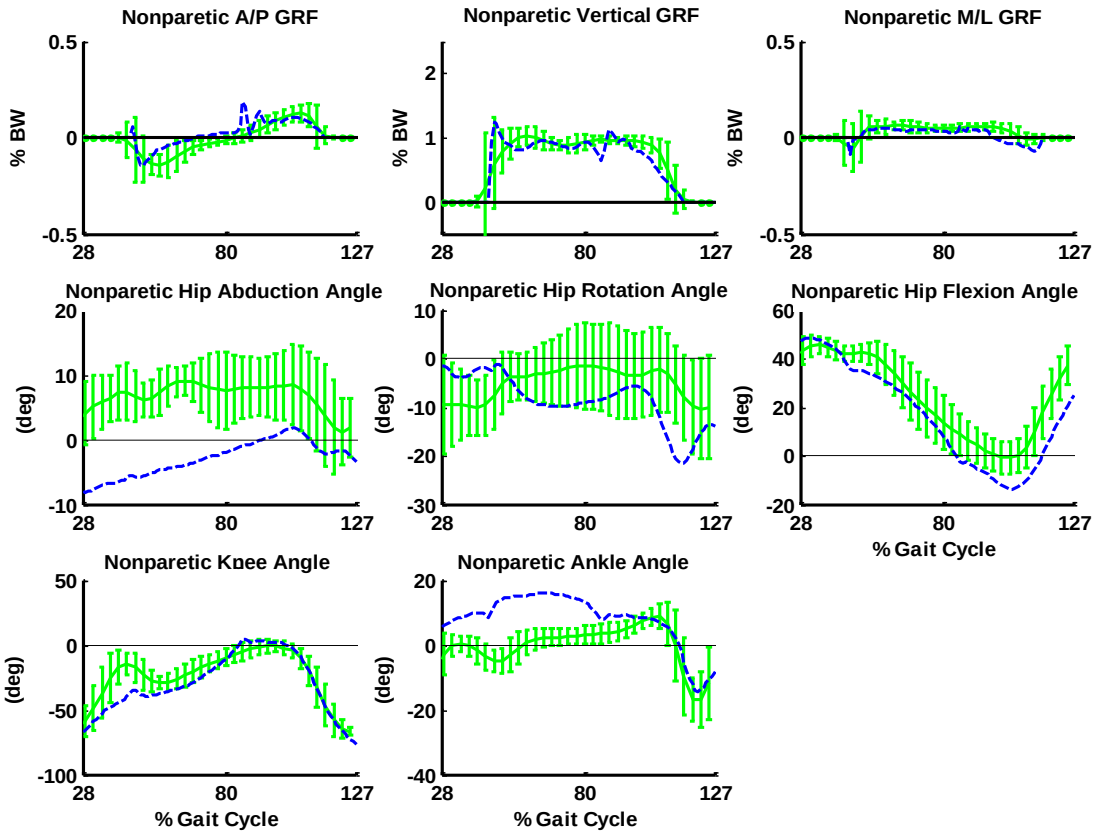

Figure C.6. Simulated and experimental GRF and kinematic data for subject *A* (in Appendix A and Chapter 5) walking at 0.8 m/s, post-therapy. Data is shown in the right (paretic) leg reference frame, 28% after right heel strike. The experimental data average (+/- 2 standard deviations) across trials is shown in green (bars).

Appendix D: Contralateral Leg Muscle Contributions

The sum of all contralateral leg muscle contributions to the regulation of whole-body angular momentum was presented in Chapter 5. For more detail, the contralateral leg individual muscle contributions to the regulation of angular momentum in the frontal and sagittal planes are shown in Figs. D.1-D.4.

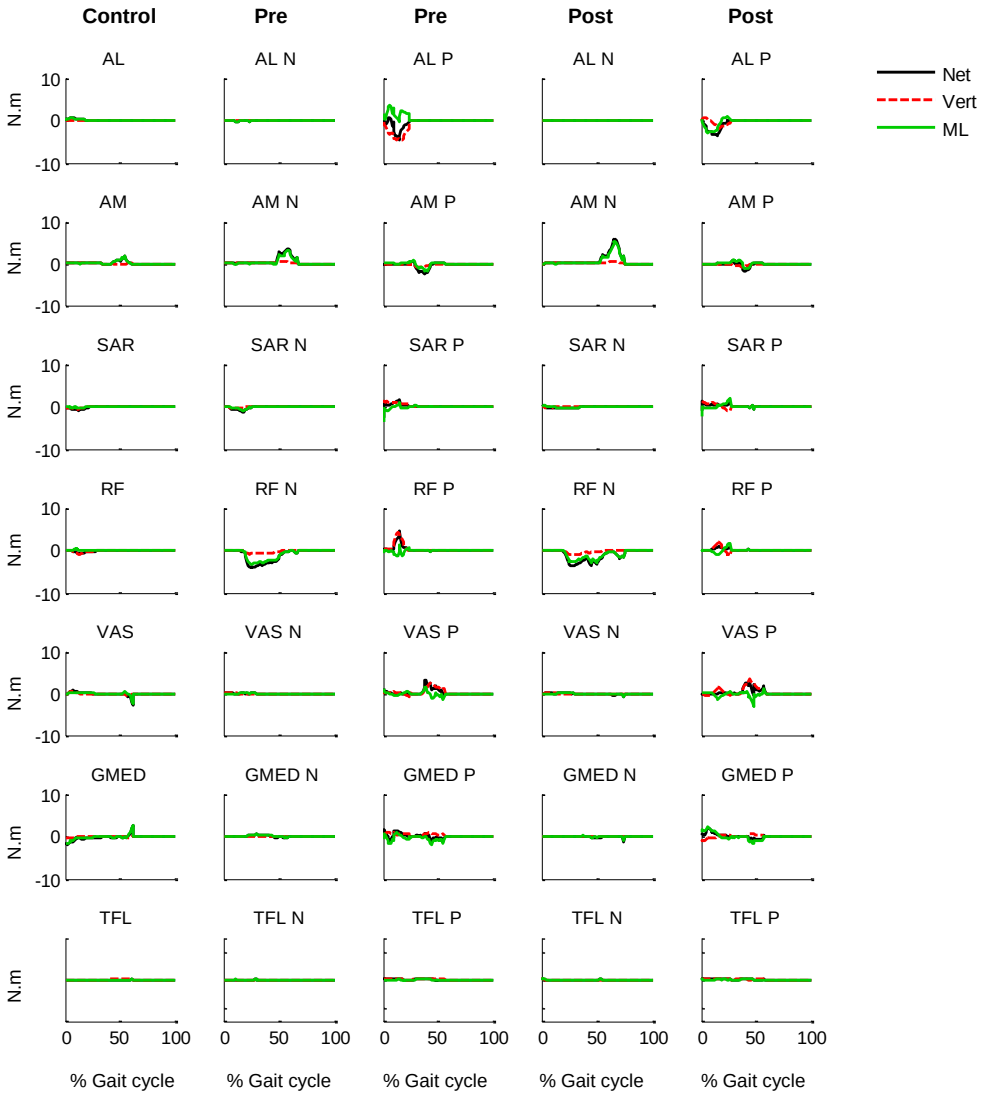

Figure D.1. Contralateral leg muscle contributions to the regulation of angular momentum in the frontal plane for healthy control subjects and a hemiparetic subject pre- and post-therapy. '*N*' and '*P*' indicate nonparetic and paretic legs, respectively. All plots are in the ipsilateral leg reference frame. '*Vert*' corresponds to the moment generated by the mediolateral moment arm and the contralateral leg muscle contributions to the vertical GRF. '*ML*' corresponds to the moment generated by the vertical moment arm and the contralateral leg muscle contributions to the mediolateral GRF. Positive values indicate clockwise moment (left leg: healthy control and the nonparetic leg).

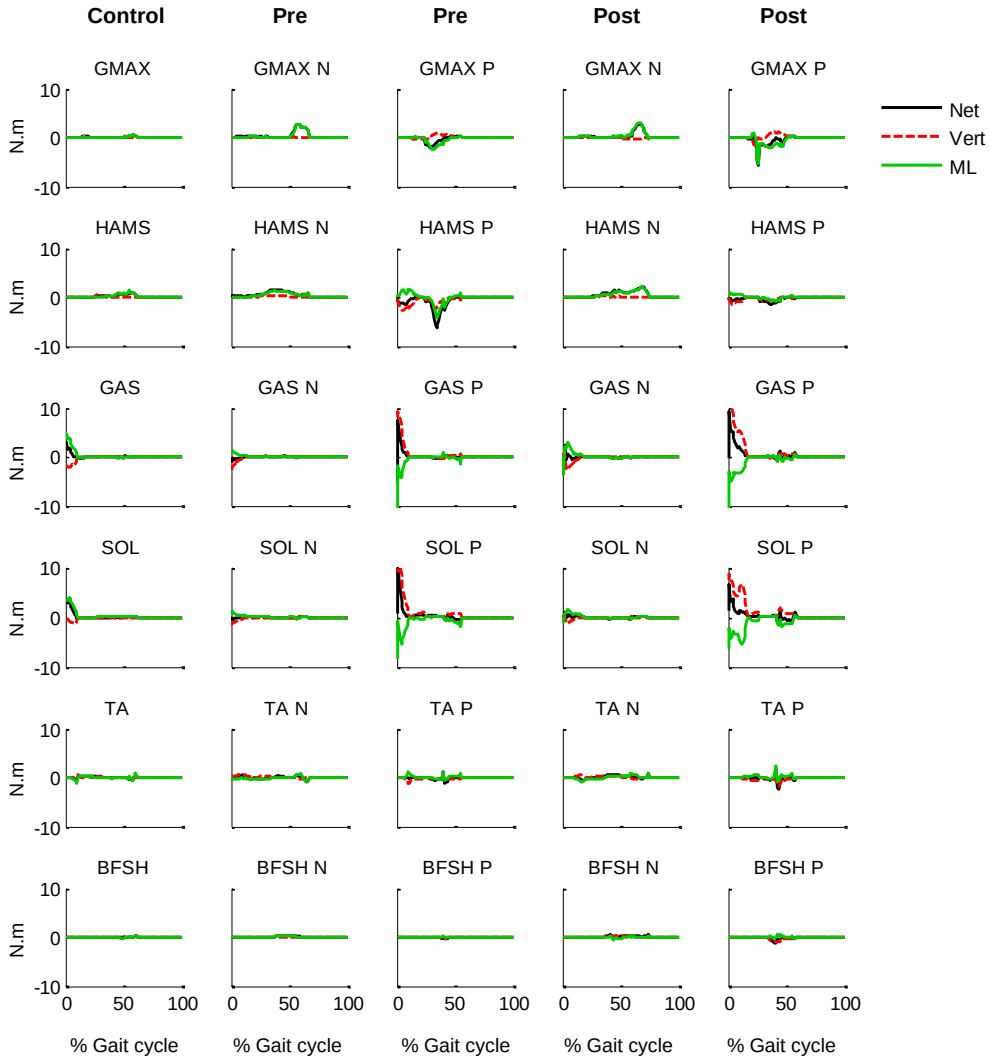

Figure D.2. Contralateral leg muscle contributions to the regulation of angular momentum in the frontal plane for healthy control subjects and a hemiparetic subject pre- and post-therapy. '*N*' and '*P*' indicate nonparetic and paretic legs, respectively. All plots are in the ipsilateral leg reference frame. '*Vert*' corresponds to the moment generated by the mediolateral moment arm and the contralateral leg muscle contributions to the vertical GRF. '*ML*' corresponds to the moment generated by the vertical moment arm and the contralateral leg muscle contributions to the mediolateral GRF. Positive values indicate clockwise moment (left leg: healthy control and the nonparetic leg).

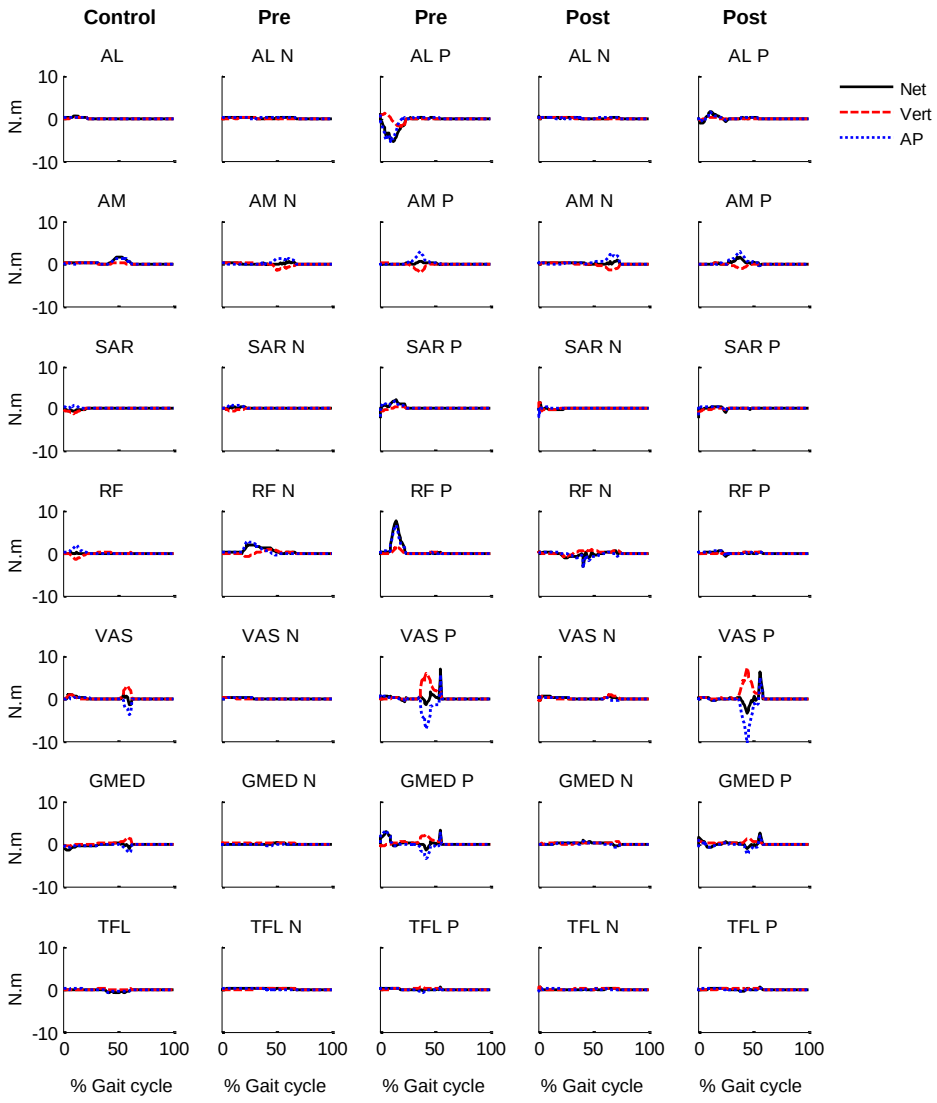

Figure D.3. Contralateral leg muscle contributions to the regulation of angular momentum in the sagittal plane for healthy control subjects and a hemiparetic subject pre- and post-therapy. '*N*' and '*P*' indicate nonparetic and paretic legs, respectively. All plots are in the ipsilateral leg reference frame. '*Vert*' corresponds to the moment generated by the anterior-posterior moment arm and the contralateral leg muscle contributions to the vertical GRF. '*AP*' corresponds to the moment generated by the vertical moment arm and the contralateral leg muscle contributions to the anterior-posterior GRF. Positive (negative) values indicate moment acting to rotate the body backward (forward).

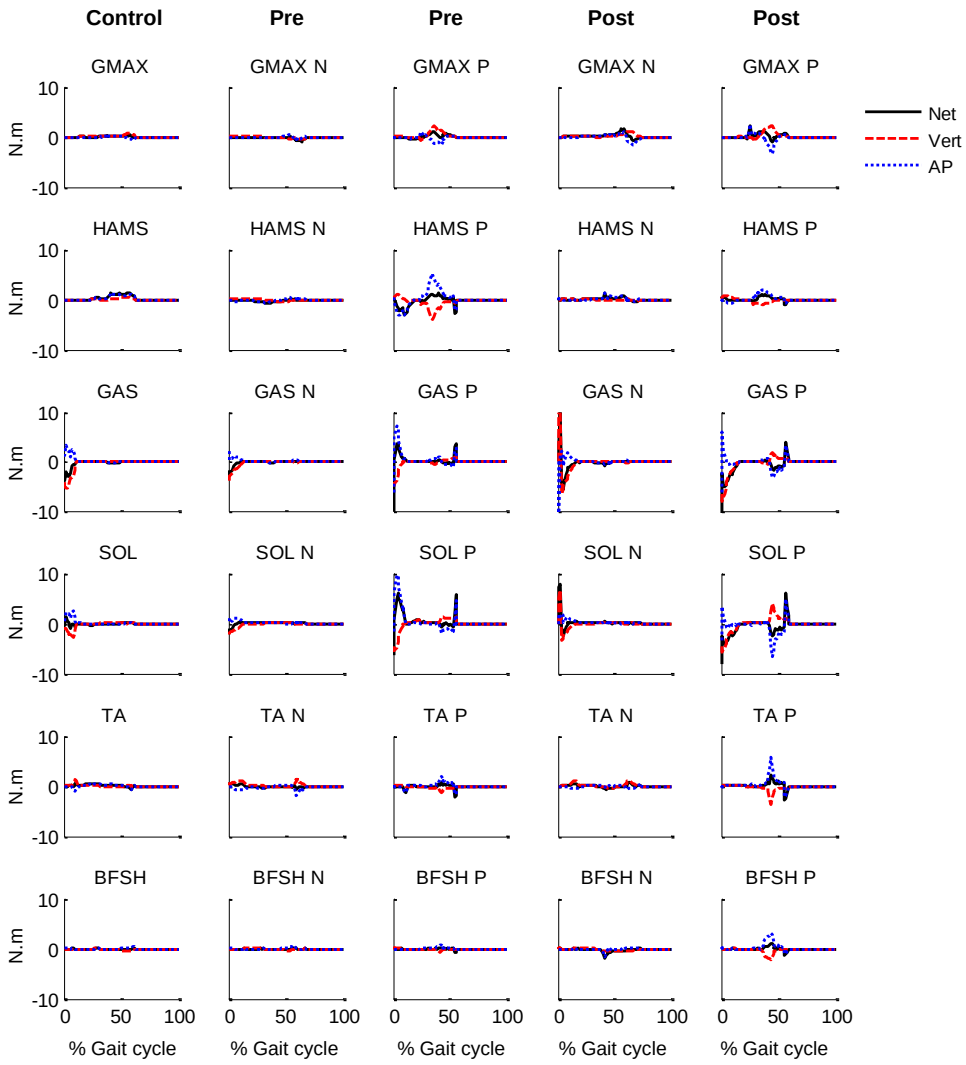

Figure D.4. Contralateral leg muscle contributions to the regulation of angular momentum in the sagittal plane for healthy control subjects and a hemiparetic subject pre- and post-therapy. '*N*' and '*P*' indicate nonparetic and paretic legs, respectively. All plots are in the ipsilateral leg reference frame. '*Vert*' corresponds to the moment generated by the anterior-posterior moment arm and the contralateral leg muscle contributions to the vertical GRF. '*AP*' corresponds to the moment generated by the vertical moment arm and the contralateral leg muscle contributions to the anterior-posterior GRF. Positive (negative) values indicate moment acting to rotate the body backward (forward).

Appendix E: An Adaptive TABU Search Optimization Algorithm for Generating Forward Dynamics Simulations of Human Movement

Introduction

Forward dynamics simulations have become a valuable tool for gaining insight into the biomechanics and neuromotor control of human movement. Quantities that are difficult or impossible to measure, such as individual muscle forces and their contributions to specific movement subtasks, can be estimated using muscle-driven forward dynamics simulations that emulate experimentally collected kinetic and kinematic data (Neptune and Hull, 1998). To generate the simulations, dynamic optimization is often used to fine-tune the muscle excitation patterns using an iterative process to produce the desired movement. Typically, an optimal tracking objective function is used to minimize the RMS difference between the simulations and corresponding experimental data. The performance of the optimization algorithm depends on the rate of convergence and how well the objective function is minimized.

The performance of various optimization algorithms (e.g., simulated annealing (SA), gradient-based sequential quadratic programming, and simplex methods) was previously evaluated in solving a pedaling optimal tracking problem, where SA was found to outperform the other algorithms (Neptune, 1999). In the last few decades, tabu search (TS), a metaheuristic memory-based algorithm, has been found to have superior performance in solving combinatorial optimization problems in a number of research domains such as operations research, telecommunications and financial analysis (Glover and Laguna, 1997). The purpose of this study was to implement an adaptive TS algorithm to solve a pedaling optimal tracking problem and to compare its performance with a widely used SA algorithm.

Methods

A previously described musculoskeletal pedaling model was used in the analysis (Neptune and Hull, 1998). The two-legged three degree-of-freedom (crank and two pedal angles) model was driven by 10 muscle groups per leg. Muscle excitations were defined using a modified Gaussian pattern (4 parameters per muscle group). Parameters included amplitude, center point, width and curvature, each referred to as a parameter category in the tabu search. A pedaling simulation of 90 rpm and 265 Watts was generated.

In order to implement the adaptive TS algorithm, the parameter space was discretized within the given bounds of each parameter. Four neighborhood categories were defined each corresponding to a parameter category. Neighborhoods were generated by perturbing a parameter category in all muscles (± one step size), one muscle at a time. For instance, in neighborhood category one, the amplitude of muscle excitations was perturbed in each muscle. The neighborhood minimum was then calculated and compared to the cost of the incumbent solution. If the cost improved, the solution was accepted and the search was intensified by decreasing the grid size of all the parameters. However, if the cost was not improved, before an uphill solution was accepted, the rest of the parameter categories were perturbed and the neighborhood minimum was accepted as a downhill or uphill solution. In the case of an uphill (poorer) solution acceptance, the search space was expanded within the specified grid size bounds.

Upon solution acceptance, the parameter associated with the accepted move was stored in the tabu memory and was prohibited from repetition for a duration specified by the tabu tenure (i.e., tabu list size). Similar to the parameter grid size, tabu tenure was also restricted between specified bounds and was used for the search intensification and expansion. If the optimal solution did not improve over five consecutive neighborhoods, as an escape strategy the incumbent solution was replaced with the last optimal solution

found. However, to avoid a repeated search, the escape strategy could be used only once after each optimal improvement.

The performance of the TS algorithm was compared to that of SA. The SA algorithm (Corana et al., 1987) perturbed the parameters randomly, thus a priori insight into the problem was not necessary. Both methods used an identical objective function and initial guess for the excitation parameters. Since TS is deterministic and SA includes stochasticity, the average results from 16 SA optimizations were used for comparison to TS.

Results and Discussion

In the early stages of the search, TS had a superior performance over SA, improving the solution by over 60% in the first hour (Fig. E.1). Despite the initial fast decrease in the cost using TS, both methods converged to similar cost values after 8 hours of search. A similar performance pattern was observed using different starting solutions, except for the case where the starting solution was completely random and the pedaling motion was not completed, in which case the stochasticity in SA was more beneficial in the early stages of the search. The quality of the solution obtained by TS after one hour of search was compared to the best SA solution obtained after 49 hours (Fig. E.2). The resulting pedal angle, tangential pedal reaction force, crank and joint moments were similar between the different algorithms and were within ±2 SD of the experimental data (Fig. E.2).

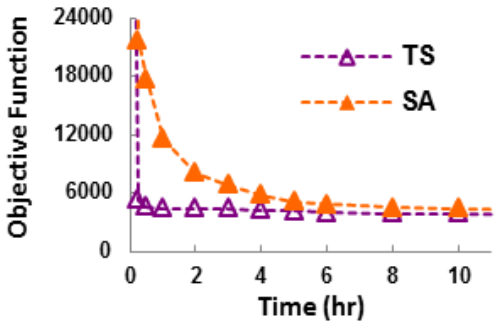

Figure E.1. Objective function value versus elapsed search time. The initial cost (79,500) is not shown.

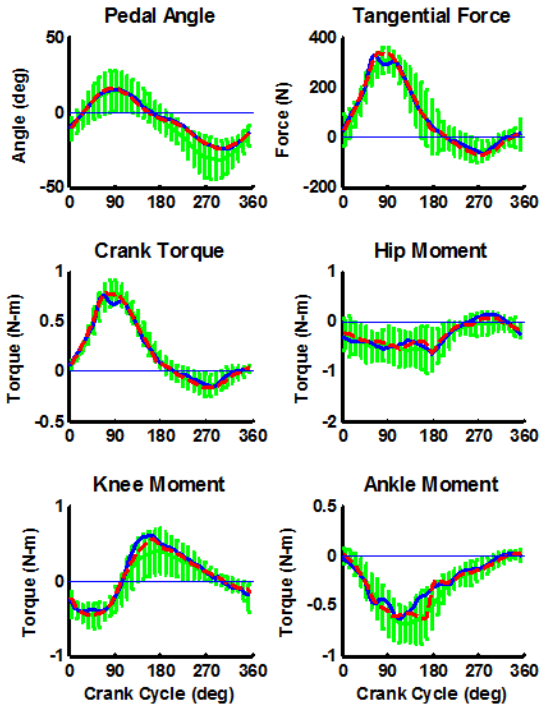

Figure E.2. Experimental data (with error bars representing ±2SD) and simulation data: (--) best optimal solution obtained by SA in 49 hours (cost= 3,150); (—) solution obtained by TS in 1 hour (cost=4,430).

In summary, an adaptive TS optimization algorithm was designed and implemented in a forward dynamics simulation of pedaling. TS had a superior performance over the SA algorithm in the early stages of the search, although the TS performance was sensitive to appropriate neighborhood and parameter grid size selection. The solution obtained using TS in the first hour of the search tracked well the experimental data. Thus, the TS algorithm is initially computationally more efficient compared to SA, although it is sensitive to the initial parameters and a priori insight into the problem and the parameter space. The performance may improve by using a hybrid SA-TS algorithm and/or implementing a reactive TS algorithm (Glover and Laguna, 1997). Briefly, a reactive TS algorithm monitors the search and reacts to the occurrence of cycles by adjusting the tabu tenure. Future work is needed to assess whether an adaptive TS algorithm will accelerate the optimization convergence for other tasks such as walking, which is dynamically more unstable and computationally more intensive than pedaling.

References

Abe, H., Michimata, A., Sugawara, K., Sugaya, N., Izumi, S., 2009. Improving gait stability in stroke hemiplegic patients with a plastic ankle-foot orthosis. *Tohoku J Exp Med* 218 (3), 193-9.

Anderson, F. C., 1999. A dynamic optimization solution for a complete cycle of normal gait. Doctoral Dissertation, Austin, TX, The University of Texas at Austin.

Anderson, F. C., Pandy, M. G., 2003. Individual muscle contributions to support in normal walking. *Gait Posture* 17 (2), 159-69.

Ashburn, A., Hyndman, D., Pickering, R., Yardley, L., Harris, S., 2008. Predicting people with stroke at risk of falls. *Age Ageing* 37 (3), 270-6.

Balasubramanian, C. K., Bowden, M. G., Neptune, R. R., Kautz, S. A., 2007. Relationship between step length asymmetry and walking performance in subjects with chronic hemiparesis. *Arch Phys Med Rehabil* 88 (1), 43-9.

Balasubramanian, C. K., Neptune, R. R., Kautz, S. A., 2010. Foot placement in a body reference frame during walking and its relationship to hemiparetic walking performance. *Clin Biomech (Bristol, Avon)* 25 (5), 483-90.

Barak, Y., Wagenaar, R. C., Holt, K. G., 2006. Gait characteristics of elderly people with a history of falls: a dynamic approach. *Phys Ther* 86 (11), 1501-10.

Barbeau, H., Visintin, M., 2003. Optimal outcomes obtained with body-weight support combined with treadmill training in stroke subjects. *Arch Phys Med Rehabil* 84 (10), 1458-65.

Bartonek, A., Eriksson, M., Gutierrez-Farewik, E. M., 2007. Effects of carbon fibre spring orthoses on gait in ambulatory children with motor disorders and plantarflexor weakness. *Dev Med Child Neurol* 49 (8), 615-20.

Bauby, C. E., Kuo, A. D., 2000. Active control of lateral balance in human walking. *J Biomech* 33 (11), 1433-40.

Bennett, B. C., Russell, S. D., Sheth, P., Abel, M. F., 2010. Angular momentum of walking at different speeds. *Hum Mov Sci* 29 (1), 114-24.

Berg, K., Wood-Dauphinee, S., Williams, J. I., 1995. The Balance Scale: reliability assessment with elderly residents and patients with an acute stroke. *Scand J Rehabil Med* 27 (1), 27-36.

Bowden, M. G., Behrman, A. L., Neptune, R. R., Gregory, C. M., Kautz, S. A., 2013. Locomotor rehabilitation of individuals with chronic stroke: difference between responders and nonresponders. *Arch Phys Med Rehabil* 94 (5), 856-62.

Bregman, D. J., De Groot, V., Van Diggele, P., Meulman, H., Houdijk, H., Harlaar, J., 2010. Polypropylene ankle foot orthoses to overcome drop-foot gait in central neurological patients: a mechanical and functional evaluation. *Prosthet Orthot Int* 34 (3), 293-304.

Bruijn, S. M., Meyns, P., Jonkers, I., Kaat, D., Duysens, J., 2011. Control of angular momentum during walking in children with cerebral palsy. *Res Dev Disabil* 32 (6), 2860-6.

Cakar, E., Durmus, O., Tekin, L., Dincer, U., Kiralp, M. Z., 2010. The ankle-foot orthosis improves balance and reduces fall risk of chronic spastic hemiparetic patients. *Eur J Phys Rehabil Med* 46 (3), 363-8.

Centers for Disease Control and Prevention (CDC), 2008. Self-reported falls and fall-related injuries among persons aged > or = 65 years-United States, 2006. Morbidity and Mortality Weekly Report, 57, 225-229.

Corana, A., Marchesi, M., Martini, C., Ridella, S., 1987. Minimizing Multimodal Functions of Continuous-Variables with the Simulated Annealing Algorithm. *Acm Transactions on Mathematical Software* 13 (3), 262-280.

Crabtree, C. A., Higginson, J. S., 2009. Modeling neuromuscular effects of ankle foot orthoses (AFOs) in computer simulations of gait. *Gait Posture* 29 (1), 65-70.

Czernuszenko, A., 2007. Risk factors for falls in post-stroke patients treated in a neurorehabilitation ward. *Neurol Neurochir Pol* 41 (1), 28-35.

Davy, D. T., Audu, M. L., 1987. A dynamic optimization technique for predicting muscle forces in the swing phase of gait. *J Biomech* 20 (2), 187-201.

Dean, J. C., Alexander, N. B., Kuo, A. D., 2007. The effect of lateral stabilization on walking in young and old adults. *IEEE Trans Biomed Eng* 54 (11), 1919-26.

Delp, S. L., Loan, J. P., Hoy, M. G., Zajac, F. E., Topp, E. L., Rosen, J. M., 1990. An interactive graphics-based model of the lower extremity to study orthopaedic surgical procedures. *IEEE Trans Biomed Eng* 37 (8), 757-67.

Deprey, S. M., 2009. Descriptive analysis of fatal falls of older adults in a Midwestern county in the year 2005. *J Geriatr Phys Ther* 32 (2), 67-72.

Desloovere, K., Molenaers, G., Van Gestel, L., Huenaerts, C., Van Campenhout, A., Callewaert, B., Van de Walle, P., Seyler, J., 2006. How can push-off be preserved during use of an ankle foot orthosis in children with hemiplegia? A prospective controlled study. *Gait Posture* 24 (2), 142-51.

Donelan, J. M., Shipman, D. W., Kram, R., Kuo, A. D., 2004. Mechanical and metabolic requirements for active lateral stabilization in human walking. *J Biomech* 37 (6), 827-35.

Duncan, P. W., Sullivan, K. J., Behrman, A. L., Azen, S. P., Wu, S. S., Nadeau, S. E., Dobkin, B. H., Rose, D. K., Tilson, J. K., Cen, S., et al., 2011. Body-weight-supported treadmill rehabilitation after stroke. *N Engl J Med* 364 (21), 2026-36.

Gabell, A., Nayak, U. S., 1984. The effect of age on variability in gait. *J Gerontol* 39 (6), 662-6.

Gehlsen, G. M., Whaley, M. H., 1990. Falls in the elderly: Part I, Gait. *Arch Phys Med Rehabil* 71 (10), 735-8.

Geurts, A. C., de Haart, M., van Nes, I. J., Duysens, J., 2005. A review of standing balance recovery from stroke. *Gait Posture* 22 (3), 267-81.

Glover, F., Laguna, M., 1997. Tabu Search. Kluwer Academic Publishers.

Greenspan, S. L., Myers, E. R., Kiel, D. P., Parker, R. A., Hayes, W. C., Resnick, N. M., 1998. Fall direction, bone mineral density, and function: risk factors for hip fracture in frail nursing home elderly. *Am J Med* 104 (6), 539-45.

Guerra Padilla, M., Molina Rueda, F., Alguacil Diego, I. M., 2011. Effect of ankle-foot orthosis in postural control after stroke: a systematic review. *Neurologia*

Guimaraes, R. M., Isaacs, B., 1980. Characteristics of the gait in old people who fall. *Int Rehabil Med* 2 (4), 177-80.

Hall, A. L., Peterson, C. L., Kautz, S. A., Neptune, R. R., 2011. Relationships between muscle contributions to walking subtasks and functional walking status in persons with post-stroke hemiparesis. *Clin Biomech (Bristol, Avon)* 26 (5), 509-15.

Herr, H., Popovic, M., 2008. Angular momentum in human walking. *J Exp Biol* 211 (Pt 4), 467-81.

Hesse, S., 2008. Treadmill training with partial body weight support after stroke: a review. *NeuroRehabilitation* 23 (1), 55-65.

Hesse, S., Bertelt, C., Schaffrin, A., Malezic, M., Mauritz, K. H., 1994. Restoration of gait in nonambulatory hemiparetic patients by treadmill training with partial body-weight support. *Arch Phys Med Rehabil* 75 (10), 1087-93.

Hof, A. L., Vermerris, S. M., Gjaltema, W. A., 2010. Balance responses to lateral perturbations in human treadmill walking. *J Exp Biol* 213 (Pt 15), 2655-64.

Hollands, K. L., Pelton, T. A., Tyson, S. F., Hollands, M. A., van Vliet, P. M., 2012. Interventions for coordination of walking following stroke: systematic review. *Gait Posture* 35 (3), 349-59.

Kaya, B. K., Krebs, D. E., Riley, P. O., 1998. Dynamic stability in elders: momentum control in locomotor ADL. *J Gerontol A Biol Sci Med Sci* 53 (2), M126-34.

Kirker, S. G. B., Simpson, D. S., Jenner, J. R., Wing, A. M., 2000. Stepping before standing: hip muscle function in stepping and standing balance after stroke. *Journal of Neurology Neurosurgery and Psychiatry* 68 (4), 458-464.

Knutsson, E., Richards, C., 1979. Different types of disturbed motor control in gait of hemiparetic patients. *Brain* 102 (2), 405-30.

Kung, H. C., Hoyert, D. L., Xu, J., Murphy, S. L., 2008. Deaths: final data for 2005. *Natl Vital Stat Rep* 56 (10), 1-120.

Kuo, A. D., 1999. Stabilization of lateral motion in passive dynamic walking. *International Journal of Robotics Research* 18 (9), 917-930.

Liu, M. Q., Anderson, F. C., Pandy, M. G., Delp, S. L., 2006. Muscles that support the body also modulate forward progression during walking. *J Biomech* 39 (14), 2623-30.

Liu, M. Q., Anderson, F. C., Schwartz, M. H., Delp, S. L., 2008. Muscle contributions to support and progression over a range of walking speeds. *J Biomech* 41 (15), 3243-52.

Luukinen, H., Koski, K., Laippala, P., Kivela, S. L., 1995. Risk factors for recurrent falls in the elderly in long-term institutional care. *Public Health* 109 (1), 57-65.

MacKinnon, C. D., Winter, D. A., 1993. Control of whole body balance in the frontal plane during human walking. *J Biomech* 26 (6), 633-44.

Maki, B. E., 1997. Gait changes in older adults: predictors of falls or indicators of fear. *J Am Geriatr Soc* 45 (3), 313-20.

Martelli, D., Monaco, V., Bassi Luciani, L., Micera, S., 2013. Angular momentum during unexpected multidirectional perturbations delivered while walking. *IEEE Trans Biomed Eng* 60 (7), 1785-95.

McAndrew Young, P. M., Dingwell, J. B., 2012. Voluntarily changing step length or step width affects dynamic stability of human walking. *Gait Posture* 35 (3), 472-7.

Mercer, V. S., Chang, S. H., Williams, C. D., Noble, K., Vance, A. W., 2009. Effects of an exercise program to increase hip abductor muscle strength and improve lateral stability following stroke: a single subject design. *J Geriatr Phys Ther* 32 (2), 50-9.

Moe-Nilssen, R., Helbostad, J. L., 2005. Interstride trunk acceleration variability but not step width variability can differentiate between fit and frail older adults. *Gait Posture* 21 (2), 164-70.

Nadeau, S., Gravel, D., Arsenault, A. B., Bourbonnais, D., 1999. Plantarflexor weakness as a limiting factor of gait speed in stroke subjects and the compensating role of hip flexors. *Clin Biomech (Bristol, Avon)* 14 (2), 125-35.

Nair, P. M., Rooney, K. L., Kautz, S. A., Behrman, A. L., 2010. Stepping with an ankle foot orthosis re-examined: a mechanical perspective for clinical decision making. *Clin Biomech (Bristol, Avon)* 25 (6), 618-22.

Nelson, A. J., Certo, L. J., Lembo, L. S., Lopez, D. A., Manfredonia, E. F., Vanichpong, S. K., Zwick, D., 1999. The functional ambulation performance of elderly fallers and non-fallers walking at their preferred velocity. *NeuroRehabilitation* 13 (3), 141-146.

Neptune, R. R., 1999. Optimization algorithm performance in determining optimal controls in human movement analyses. *J Biomech Eng* 121 (2), 249-52.

Neptune, R. R., Hull, M. L., 1998. Evaluation of performance criteria for simulation of submaximal steady-state cycling using a forward dynamic model. *J Biomech Eng* 120 (3), 334-41.

Neptune, R. R., Kautz, S. A., Zajac, F. E., 2001. Contributions of the individual ankle plantar flexors to support, forward progression and swing initiation during walking. *J Biomech* 34 (11), 1387-98.

Neptune, R. R., McGowan, C. P., 2011. Muscle contributions to whole-body sagittal plane angular momentum during walking. *J Biomech* 44 (1), 6-12.

Neptune, R. R., McGowan, C. P., 2013. Muscle contributions to three-dimensional whole-body angular momentum during human walking. *J Biomech* (in review)

Neptune, R. R., McGowan, C. P., Hall, A. L., 2011. Muscle contributions to frontal and transverse plane whole-body angular momentum during walking. Proceedings of the International Society of Biomechanics **129**.

Neptune, R. R., Sasaki, K., Kautz, S. A., 2008. The effect of walking speed on muscle function and mechanical energetics. *Gait Posture* 28 (1), 135-43.

Neptune, R. R., Wright, I. C., Van Den Bogert, A. J., 2000. A Method for Numerical Simulation of Single Limb Ground Contact Events: Application to Heel-Toe Running. *Comput Methods Biomech Biomed Engin* 3 (4), 321-334.

Neptune, R. R., Zajac, F. E., Kautz, S. A., 2004. Muscle force redistributes segmental power for body progression during walking. *Gait Posture* 19 (2), 194-205.

Nott, C. R., Neptune, R. R., Kautz, S. A., 2013. Relationships between frontal-plane angular momentum and clinical balance measures during post-stroke hemiparetic walking. *Gait Posture* (in press)

Olney, S. J., Richards, C., 1996. Hemiparetic gait following stroke. Part I: characteristics. *Gait Posture* 4 (2), 136-148.

Park, J. H., Chun, M. H., Ahn, J. S., Yu, J. Y., Kang, S. H., 2009. Comparison of gait analysis between anterior and posterior ankle foot orthosis in hemiplegic patients. *Am J Phys Med Rehabil* 88 (8), 630-4.

Peterson, C. L., Cheng, J., Kautz, S. A., Neptune, R. R., 2010a. Leg extension is an important predictor of paretic leg propulsion in hemiparetic walking. *Gait Posture* 32 (4), 451-6.

Peterson, C. L., Hall, A. L., Kautz, S. A., Neptune, R. R., 2010b. Pre-swing deficits in forward propulsion, swing initiation and power generation by individual muscles during hemiparetic walking. *J Biomech* 43 (12), 2348-55.

Peterson, C. L., Kautz, S. A., Neptune, R. R., 2011. Braking and propulsive impulses increase with speed during accelerated and decelerated walking. *Gait Posture* 33 (4), 562-7.

Peurala, S. H., Tarkka, I. M., Pitkanen, K., Sivenius, J., 2005. The effectiveness of body weight-supported gait training and floor walking in patients with chronic stroke. *Arch Phys Med Rehabil* 86 (8), 1557-64.

Pijnappels, M., Bobbert, M. F., van Dieen, J. H., 2004. Contribution of the support limb in control of angular momentum after tripping. *J Biomech* 37 (12), 1811-8.

Pijnappels, M., Bobbert, M. F., van Dieen, J. H., 2005a. How early reactions in the support limb contribute to balance recovery after tripping. *J Biomech* 38 (3), 627-34.

Pijnappels, M., Bobbert, M. F., van Dieen, J. H., 2005b. Push-off reactions in recovery after tripping discriminate young subjects, older non-fallers and older fallers. *Gait Posture* 21 (4), 388-94.

Pijnappels, M., Van der Burg, J. C. E., Reeves, N. D., van Dieen, J. H., 2008. Identification of elderly fallers by muscle strength measures. *European Journal of Applied Physiology* 102 (5), 585-592.

Prinsen, E. C., Nederhand, M. J., Rietman, J. S., 2011. Adaptation strategies of the lower extremities of patients with a transtibial or transfemoral amputation during level walking: a systematic review. *Arch Phys Med Rehabil* 92 (8), 1311-25.

Raasch, C. C., Zajac, F. E., Ma, B., Levine, W. S., 1997. Muscle coordination of maximum-speed pedaling. *J Biomech* 30 (6), 595-602.

Raja, B., Neptune, R. R., Kautz, S. A., 2012. Coordination of the non-paretic leg during hemiparetic gait: expected and novel compensatory patterns. *Clin Biomech (Bristol, Avon)* 27 (10), 1023-30.

Robert, T., Bennett, B. C., Russell, S. D., Zirker, C. A., Abel, M. F., 2009. Angular momentum synergies during walking. *Exp Brain Res* 197 (2), 185-97.

Sackley, C., Brittle, N., Patel, S., Ellins, J., Scott, M., Wright, C., Dewey, M. E., 2008. The prevalence of joint contractures, pressure sores, painful shoulder, other pain, falls, and depression in the year after a severely disabling stroke. *Stroke* 39 (12), 3329-34.

Savitzky, A., Golay, M. J. E., 1964. Smoothing and differentiation of data by simplified least squares procedures. *Anal. Chem.* 36 1627-1639.

Schmid, A. A., Acuff, M., Doster, K., Gwaltney-Duiser, A., Whitaker, A., Damush, T., Williams, L., Hendrie, H., 2009. Poststroke fear of falling in the hospital setting. *Top Stroke Rehabil* 16 (5), 357-66.

Shumway-Cook, A., Baldwin, M., Polissar, N. L., Gruber, W., 1997. Predicting the probability for falls in community-dwelling older adults. *Phys Ther* 77 (8), 812-9.

Shumway-Cook, A., Woollocott, M. H., 2001. Motor control theory and practical applications. Philadelphia, Lippincott Williams & Wilkins.

Silverman, A. K., Neptune, R. R., 2011. Differences in whole-body angular momentum between below-knee amputees and non-amputees across walking speeds. *J Biomech* 44 (3), 379-85.

Silverman, A. K., Neptune, R. R., 2012. Muscle and prosthesis contributions to amputee walking mechanics: a modeling study. *J Biomech* 45 (13), 2271-8.

Silverman, A. K., Neptune, R. R., Sinitski, E. H., Wilken, J. M., 2014. Whole-body angular momentum during stair ascent and descent. *Gait Posture* 39 (4), 1109-14.

Silverman, A. K., Wilken, J. M., Sinitski, E. H., Neptune, R. R., 2012. Whole-body angular momentum in incline and decline walking. *J Biomech* 45 (6), 965-71.

Simons, C. D., van Asseldonk, E. H., van der Kooij, H., Geurts, A. C., Buurke, J. H., 2009. Ankle-foot orthoses in stroke: effects on functional balance, weight-bearing asymmetry and the contribution of each lower limb to balance control. *Clin Biomech (Bristol, Avon)* 24 (9), 769-75.

Tyson, S. F., Thornton, H. A., 2001. The effect of a hinged ankle foot orthosis on hemiplegic gait: objective measures and users' opinions. *Clin Rehabil* 15 (1), 53-8.

Verghese, J., Holtzer, R., Lipton, R. B., Wang, C., 2009. Quantitative gait markers and incident fall risk in older adults. *J Gerontol A Biol Sci Med Sci* 64 (8), 896-901.

Visintin, M., Barbeau, H., Korner-Bitensky, N., Mayo, N. E., 1998. A new approach to retrain gait in stroke patients through body weight support and treadmill stimulation. *Stroke* 29 (6), 1122-8.

Vistamehr, A., Kautz, S. A., Neptune, R. R., 2014. The influence of solid ankle-foot-orthoses on forward propulsion and dynamic balance in healthy adults during walking. *Clin Biomech (Bristol, Avon)*

Wang, R. Y., Lin, P. Y., Lee, C. C., Yang, Y. R., 2007. Gait and balance performance improvements attributable to ankle-foot orthosis in subjects with hemiparesis. *Am J Phys Med Rehabil* 86 (7), 556-62.

Wang, R. Y., Yen, L., Lee, C. C., Lin, P. Y., Wang, M. F., Yang, Y. R., 2005. Effects of an ankle-foot orthosis on balance performance in patients with hemiparesis of different durations. *Clin Rehabil* 19 (1), 37-44.

Winters, J. M., Stark, L., 1988. Estimated mechanical properties of synergistic muscles involved in movements of a variety of human joints. *J Biomech* 21 (12), 1027-41.

Vita

Arian Vistamehr attended Montgomery College in Rockville, Maryland where she received her Associate of Science degree in 2004. In 2007 she received her Bachelor of Science degree in Mechanical Engineering from Texas A&M University in College Station, Texas. She continued her education at Texas A&M University and in 2009 she received her Master of Science degree in Mechanical Engineering with a focus in Rotordynamics. Finally, in 2014 she received her Doctor of Philosophy degree with a focus in Biomechanics from The University of Texas at Austin.

Permanent email address: arian.vistamehr@gmail.com
This dissertation was typed by the author.